UNIVERSITY OF SOUTHAMPTON

FACULTY OF ENGINEERING AND THE ENVIRONMENT

Aeronautics, Astronautics and Computational Engineering

Improving the Perching Capability of a Vertical Take-off and Landing Unmanned Aerial Vehicle through Reconfiguration

Mehmet Ali Erbil

Thesis for the degree of Doctor of Philosophy

July 2016

UNIVERSITY OF SOUTHAMPTON

Abstract

Landing on lighting columns like nature's birds is a desirable capability which can only extend the uses of unmanned aerial systems. This thesis investigates what the most effective form of perching on existing street furniture with a VTOL UAV and how the perch site can be recognised using low cost off the shelf sensors. Additionally to this, the UAV in question will have to execute the perch without relying on GPS data. The work conducted here covers an extensive design review which selects a bird claw like gripper to sustain the perch. In order for the UAV to know where it is in relation to the perch site without relying on GPS data, a Raspberry Pi and PiCamera were used to detect common features which are found on top of a lighting column. Using a search and perch algorithm which was developed specifically for the task of perching on lamp post projection brackets, the on-board microprocessor controlled the UAV over the perch site and gradually descended into the perch position. The perched position and approach was also tested to ensure the perching element could cope with various weather conditions. The testing was conducted in a wind tunnel with the UAV mounted in various perched positions and the moment the UAV would slip, the wind speed were measured and analysed which highlighted an interesting prediction method. During the perching development the addition of a gantry style test-rig was also developed to ease the algorithm development with minimal incidents. The final result is a search and perch algorithm which is initiated when the VTOL UAV is within the vicinity of a lamp post at which point the on-board vision processing and control system takes over, removing the burden from the UAV operator to ensure a collision free perch.

Table of Contents

List of Tables

List of Figures

Declaration of Authorship

I, Mehmet Ali Erbil declare that this thesis and the work presented in it are my own and has been generated by me as the result of my own original research.

Design Optimisation of a Reconfigurable Perching Element for Vertical Take-Off and Landing Unmanned Aerial Vehicles

1. This work was done wholly or mainly while in candidature for a research degree at this University;
2. Where any part of this thesis has previously been submitted for a degree or any other qualification at this University or any other institution, this has been clearly stated;
3. Where I have consulted the published work of others, this is always clearly attributed;
4. Where I have quoted from the work of others, the source is always given. With the exception of such quotations, this thesis is entirely my own work;
5. I have acknowledged all main sources of help;
6. Where the thesis is based on work done by myself jointly with others, I have made clear exactly what was done by others and what I have contributed myself;
7. Parts of this work have been published as:
    - M.A. Erbil, S.D. Prior, A.J. Keane; 2013; Design Optimisation of a Reconfigurable Perching Element for Vertical Take-Off and Landing Unmanned Aerial Vehicles; International Journal of Micro Air Vehicles, 5(3), Multi Science Publishing, ISSN: 1756-829, pp 207-228. DOI: 10.1260/1756-8293.5.3.207
    - Prior, S.D.; Shen, S-T.; Erbil, M.A.; Brazinskas, M.; Mielniczek, W.; 2013; HALO the Winning Entry to the DARPA UAVForge Challenge 2012; Proceedings of the 15th HCI International Conference, 21-26 July; Mirage Hotel, Las Vegas, Nevada, USA. DOI:10.1007/978-3-642-39238-2_20
    - Bell, J., Brazinskas, M., Prior, S.D., Barlow, C., Erbil, M.A., and Karamanoglu, M.; 2010; Development of a Test-Rig for Exploring Optimal Conditions of Small Unmanned Aerial Vehicle Co-Axial Rotor Systems; Proceedings of the International Conference on

Manufacturing Engineering Systems, 16-18 December; Southern Taiwan University, Tainan, Taiwan. pp. 439-444. ISSN: 2152-1522.

- M.A. Erbil, S.D. Prior, M. Karamanoglu, S. Odedra, C. Barlow, D. Lewis; 2009; Reconfigurable Unmanned Aerial Vehicles; Proceedings of the International Conference on Manufacturing Engineering Systems, 17-19 December; National Formosa University, Huwei, Yunlin, Taiwan. pp.392-396. ISSN: 2152-1522

Signed: .....

Date: .....

Acknowledgements

I'd like to say a massive thank you to Dr. Stephen Prior for guiding me throughout my research. He has been there to push me through tough times and help me achieve my goals. His dedication to my cause is much appreciated. I'd also like to thank Prof. Andy Keane who I refer to as Yoda, as his grand knowledge which was acquired through his many years as a PhD supervisor has often inspired me to drive through the scary and unknown parts of my PhD.

I'd like to say a special thank you to my family which have been so understanding and supportive of my work. They have been my biggest fans and have always been there for me whenever I needed them. My sister who was always at the end of the phone telling me 'I can do this' and my parents who always encouraged me to be the best I can be.

Definitions and Abbreviations

ADC	-	Analogue to Digital Converter
AGL	-	Above Ground Level
APC	-	Armoured Personnel Carrier
AUV	-	Autonomous Underwater Vehicles
CAA	-	Civil Aviation Authority
CAD	-	Computer Aided Design
CCTV	-	Closed Circuit Television
CF	-	Carbon Fibre
CNC	-	Computer Numerical Control
DARPA	-	Defense Advanced Research Projects Agency
DC	-	Direct Current
DoD	-	Department of Defense
Dstl	-	Defence Science & Technology Laboratory
ESC	-	Electronic Speed Controller
FAA	-	Federal Aviation Administration
FCS	-	Flight Control System
GB	-	Gigabyte
GPS	-	Global Positioning System
Hz	-	Hertz
IR	-	Infra Red
LED	-	Light Emitting Diode
Li-Po	-	Lithium Polymer
MAS	-	Morphing Aircraft Structures
MAV	-	Micro Air Vehicle
MK	-	MikroKopter
MMALV	-	Morphing Micro Air-Land Vehicle
MoD	-	Ministry of Defence
MPUAV	-	Multi-purpose UAV
MTOW	-	Maximum Take-off Weight
PCB	-	Printed Circuit Board
PDS	-	Product Design Specification
PID	-	Proportional-Integral-Derivative
POV	-	Point of View
PSU	-	Power Supply Unit

PWM	-	Pulse Width Modulation
RAM	-	Random Access Memory
RC	-	Remote Control
ROV	-	Remotely Operated Vehicles
RPAS	-	Remotely Piloted Aircraft System
UAS	-	Unmanned Aerial System
UAV	-	Unmanned Aerial Vehicle
UGV	-	Unmanned Ground Vehicle
USV	-	Unmanned Surface Vehicle
UUV	-	Unmanned Underwater Vehicle
VTOL	-	Vertical Take-Off and Landing

1. Introduction

Vertical Take-off and Landing (VTOL) rotary-winged vehicles face many challenges such as harsh weather conditions and low endurance which affect their overall performance and usability. The current usage of these types of small Unmanned Aerial Vehicles (UAVs) has changed to an urban and cluttered environment, which the larger fixed-wing UAVs cannot access to gain the required data. With interesting flight regimes such as perching, small man-portable UAVs have found their way into the military and the ever growing civilian sector.

1.1 Motivation

According to recent reports, the worldwide UAV production will total £70[1] billion and an additional £22.9[1] billion on Military UAV research funding in the next 10 years. The current £3[1] billion UAV market will grow to £10.7[1] billion by the end of the decade. This is all driven by future combat systems along with civilian and consumer UAVs. The report includes consumer UAVs for the first time due to their rapid growth over the years and the comparison of their capabilities over the commercial systems (Finnegan, 2015). The 2015 market profile of the 'World Unmanned Arial Vehicle Systems' analyses the world wide requirement for UAV from their payloads to the companies which produce them by country, region and class of UAV.

A forecast report by the Federal Aviation Administration (FAA) estimates that the hobbyist model aircraft sales will go up from £1.9[2] million in 2016 to £4.3[2] million in 2020. Whereas the commercial market sales will grow from £600,000[2] to £2.7[2] million. As the FAA is in control of airspace over the US, they have granted the Secretary of Transportation the authority to determine whether a system is airworthy or not. They grant flight exemptions and therefore have mapped the use of UAV systems according to the submitted applications. Figure 1.1 shows the top 5 markets for small UAVs (FAA, 2016).

[1] Currency conversion date: July 2016
[2] Currency conversion date: July 2016

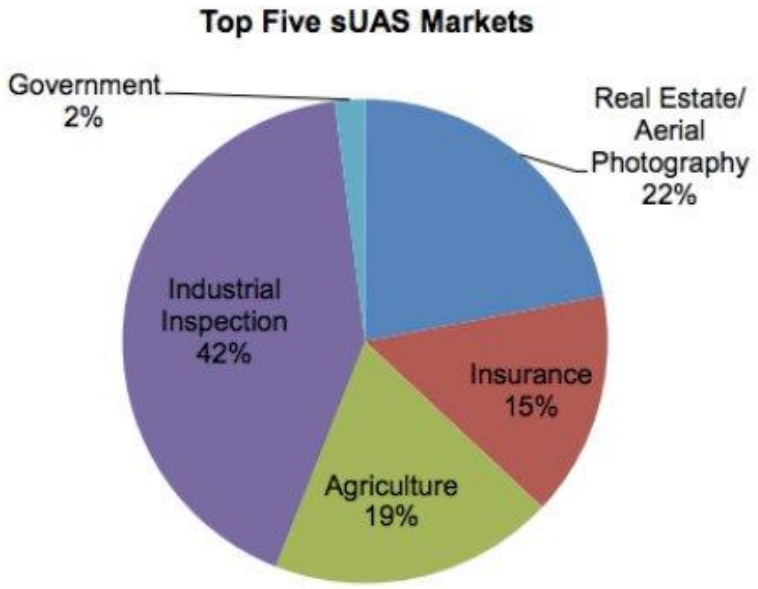

Figure 1.1 - Pie chart highlighting the top 5 sectors of small UAVs (FAA, 2016).

In addition, they also anticipate that 90% of sales would have an average sale price of £1900[2] and the higher end 10% would be in the £30,500[2] mark. This means that low cost systems are much more in demand and would be more successful. Looking at the markets, inspection systems are dominating the UAV sector with 42% of the market profile. This highlights a good area for UAV development as the demand is higher. However, the common problem with current systems is that they are unable fit into more than one type of market sector i.e. long range (agricultural) and high endurance (inspection). The solution could be offered from a reconfigurable system approach which would be able to bridge the gap between two flight regimes which are not possible with current UAVs.

1.2 Background

A small man portable surveillance UAV's typical mission consists of flying to the target area and hovering for extended periods to survey the target which is not possible with a fixed wing UAV but is with a VTOL system. Hovering for extended periods seriously affects the endurance of UAV. Unmanned systems of this size exhibit a peak in efficient flight time during a particular flight regime. Cruising at a certain speed depending on the UAV setup will increase the UAV's endurance (Cetinsoy et al., 2012, Scillitoe, 2011). By allowing the system to perch, the UAV

Figure 1.2 - Back-packable system from team HALO during the DARPA UAVforge competition 2012 GA. Fort Stewart.

will be using less energy to perform the same surveillance task. The key to this operation is to execute a perching manoeuvre automatically when required. Defense Advanced Research Projects Agency (DARPA) and Naval Warfare Systems Center Atlantic (SSC Atlantic) collaborated together to create a crowd sourcing competition called UAVForge 2012 which pushed companies, hobbyists, students and all other members of the public to take part in creating a UAS which can perform a long distance perch and stare mission. The thought process behind the competition begun back in 2008 when DARPA awarded AeroVironment £3.5 m to upgrade their current UAV inventory to be able to "hover/perch and stare" (Page, 2008). After this initial investment from DARPA, UAVForge was created in 2011. The challenge which concluded in the summer of 2012 was looking for a back packable solution which had to be a man portable UAV system capable of operating in harsh urban environment (see Figure 1.2). Each system had to execute difficult manoeuvres autonomously with very little user input. The systems had to demonstrate its capability of flying over to a target which was 2 miles away whilst avoiding obstacles and then perch on top

of a building whilst not being detected and relay live video footage of the mission back to the ground station (see Figure 1.3) (UAVforge, 2011).

Along with UAVForge 2012, other challenges have been arising in order to tackle the difficult task of perch and stare. The Ministry of Defence's – Defence Science & Technology Laboratory (Dstl) had called for research proposal which was released on the 27th September 2011. The call was funded by Centre for Defence Enterprise (CDE) which was looking for the 'Next Generation Small UAS'. The motivation behind the call was:

> "UK Armed Forces need the capability to carry out Intelligence, Surveillance and Reconnaissance (ISR) missions within highly complex environments such as inside building and deep within urban canyons."
> 'Perch-and-stare on the edge of buildings, on window ledges, on telegraph wires etc.'

(MoD, 2011)

Figure 1.3 - HALO UAV at the competition in GA. Fort Stewart. HALO's specially designed legs gave it the ability to perch on rooftops simply by descending down until it wedged itself onto the angle of the roof.

This showed the demand and need for such systems in the military context. Also in 2011, the Dstl fully funded several PhD students in a four year program to focus on the technological advancements in the field of 'autonomous systems'. One key area of interest again was bringing 'perch-and-stare' capabilities to unmanned systems (Dstl, 2012).

In the civilian market, up until recently, the task of taking off and landing was conducted manually by the UAV operator. This has all changed as the latest Flight Control Systems (FCS) allow the user to execute an automatic take off and land sequence and the push of a button (DJI, 2016). The data from all the sensors on board the FCS have been carefully scripted to enable the UAV to safely ascend and descend and has taken the guess work out of the manoeuvre. From a military approach, the automatic take-off and landing not only reduces the burden on the operator but also save money in doing so (Reed, 2010). With VTOL UAVs, the affect which ground effect has on the UAV is very evident during these manoeuvres.

The next progressive stage of auto take-offs and landings is to be able to automate the perching of a UAV. Perching is very desirable capability which is why researchers have been looking into this field for some time. Because of the wide application range for perching UAVs, multiple areas of this domain has been undertaken varying from fixed wing to VTOL UAVs. Research in energy harvesting on power lines conducted at Massachusetts Institute of Technology provides a desirable capability in UAVs (Cory, 2010). Landing on moving targets is very appealing as the implications involved with manual landing have its draw backs. Roke Manor, Tubingen University, The French Aerospace Lab and Beihang University have all looked into similar landings (Wenzel et al., 2010b, Whitehouse, 2010, Herisse et al., 2010, Bi and Duan, 2013). It is the progress which has been made in these establishments that has aided the development of this work. Including research conducted in the field of computer vision which has bought the use of cameras into the 21st century (Blosch et al., 2010, Scott, 2008).

1.3 Scope and Objectives

This research seeks to increase the capability of the UAV. By enabling the UAV to conduct perch and stare missions, it will contribute to the goal of improving the mission usability of VTOL UAVs.

1.3.1 Research Questions

The research questions which were the driving factor to the rest of the research procedures were as follows:

- What is the most effective form of perching on existing street furniture?
- How can you recognise the perch site using existing low cost off the shelf sensors?
- How can the UAV know where it is in relation to the perch site without relying on GPS data?

1.4 Layout of Thesis

Below are details of this thesis structure:

Chapter 2 – Literature Review – consists of an in-depth literature review which looks at reconfigurability aspect of UAVs along with the perching and landing. It highlights what others in the field have been doing to achieve the results they were looking for.

Chapter 3 – Perching Element – presents the perching element which essentially replaces the landing gear of the test UAV which is used to conduct the perch. It shows the various stages of concept generation, development and optimisation of the chosen design.

Chapter 4 – Experimental Hardware – is a breakdown of how the test-rig was developed along with details about the platform which is used to test the perching element. The test-rig had several criteria which determined how the final test procedures took place.

Chapter 5 – Wind Tunnel Testing – This chapter goes to in-depth details about how the gripper was validated using experiments to push the capabilities of the

gripper and UAV combination. With static and dynamic testing, the results show how close the design specification came to the final prototype.

Chapter 6 – Search and Perch Algorithm – this chapter details the work which was undertaken to develop the search and perch algorithm which is what controls the UAV into the final perched position. It acquires and analyses the data from a on board vision sensors which translate the information into a UAV manoeuvre by instructing the UAV to navigate over the perch site and carefully descend onto the lighting projection bracket. The resultant manoeuvre was analysed and critiqued here which determined the effectiveness of the chosen design along with the methods used to get here.

Chapter 7 – Conclusion – finally concludes all the work undertaken including any future work and recommendations. Here the main contributions of the PhD are highlighted. Plus a new development which strengthens the research conducted here.

1.5 Contribution

The following contributions have emerged whilst investigating the research questions which are highlighted throughout this thesis. The answers have led to the following:

1 The design, selection and optimisation of a perching element which can be attached to a UAV.
2 Detailed wind tunnel results of the optimised perching element.
3 A set of data points which can predict when the perching element will slip.
4 A method by which the UAV can locate a suitable perch site on a projection bracket of a lighting column.

1.6 Publications

- M.A. Erbil, S.D. Prior, A.J. Keane; 2013; Design Optimisation of a Reconfigurable Perching Element for Vertical Take-Off and Landing Unmanned Aerial Vehicles; International Journal of Micro Air Vehicles, 5(3), Multi Science Publishing, ISSN: 1756-829, pp 207-228.
- Prior, S.D.; Shen, S-T.; Erbil, M.A.; Brazinskas, M.; Mielniczek, W.; 2013; HALO the Winning Entry to the DARPA UAVForge Challenge

2012; Proceedings of the 15th HCI International Conference, 21-26 July; Mirage Hotel, Las Vegas, Nevada, USA.

- Bell, J., Brazinskas, M., Prior, S.D., Barlow, C., Erbil, M.A., and Karamanoglu, M.; 2010; Development of a Test-Rig for Exploring Optimal Conditions of Small Unmanned Aerial Vehicle Co-Axial Rotor Systems; Proceedings of the International Conference on Manufacturing Engineering Systems, 16-18 December; Southern Taiwan University, Tainan, Taiwan. Pp. 439-444. ISSN: 2152-1522.
- M.A. Erbil, S.D. Prior, M. Karamanoglu, S. Odedra, C. Barlow, D. Lewis; 2009; Reconfigurable Unmanned Aerial Vehicles; Proceedings of the International Conference on Manufacturing Engineering Systems, 17-19 December; National Formosa University, Huwei, Yunlin, Taiwan. Pp.392-396. ISSN: 2152-1522.

2. Literature Review

This chapter reviews the literature regarding the basics of the different types of UAVs which are available down to the specifics of reconfigurable landing and perching systems.

2.1 UAV Types

UAVs come in various shapes and sizes, and are deployed depending on the purposes they are needed for. The military uses specific UAVs with certain capabilities of specific missions requiring those certain capabilities. They don't have a single UAV that is capable of being used for a verity missions i.e. long range surveillance mission and short range urban reconnaissance. For this two different UAVs will be used. So what types of UAVs are available and what are their capabilities? UAVs are categorised by their structural configuration also taking into consideration their propulsion system. It is at this point that the clarity over the terminology of these systems should be made clear. Often the non-military industry refer to these flying systems as UAVs, Remotely Piloted Aircraft Systems (RPAS) and UAS rather than drones. It is found that the word 'drone' is associated with killing flying machines with no humans in control (Wolfgang, 2013). However the use of these words broadly reference the use of an aircraft or aircraft system that is flown in remote locations without the needs of a pilot on board (ACUO, 2016).

2.1.1 Fixed Wing

The basic principle of flight is gaining lift by moving an airfoil shaped wing through air. How it achieves this depends on the structural makeup of the flying vehicle, which in this case is a fixed wing propelled through the air by a motor, engine or jet. The military uses various fixed wing UAVs for different missions.

Figure 2.1 - 'Spotter' a fixed wing UAV with 4 m wingspan and twin engine and twin autopilot design which allows for redundancy.

2.1.2 Single Rotor

To attain flight, rotorcrafts gain the required lift by rotating the wing about a central axis instead of propelling the wing through air. They can have multiple wings, which are called rotors on this type of vehicles, which can vary from two onwards typically up to six. By adjusting the pitch of the rotor the rate at which the rotorcraft ascends or descends is adjusted. Other controls include tilting the rotor head in relation to the central drive axis which controls the crafts direction and finally, due to the rotational forces which the craft experiences, these rotorcrafts tend to have tail rotors which counter act this rotational torque (see Figure 2.2). They also experience many interfering forces due to the spinning rotors which Leishman goes into detail (Leishman, 2006).

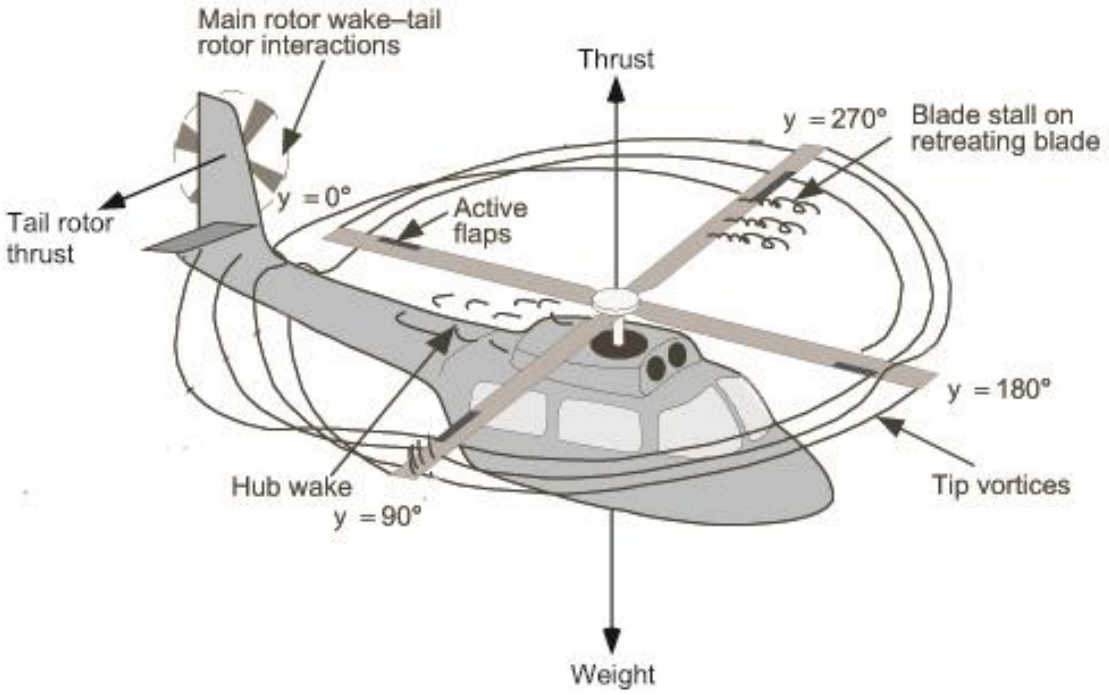

Figure 2.2 - Image showing the controls of a helicopter. Also heighted is the interfering forces which occurs when the rotors spin (Image provided by J. Gordon Leishman and Cambridge University Press, adapted from original).

2.1.3 Multi-rotor

Similar to rotorcraft vehicles, multiple rotary winged systems have more than one rotor spinning to gain lift. One axis can contain more than one rotor or it can be spread out evenly across the UAV structure. The HALO UAV (see Figure 2.3) is a Vertical Take-Off and Landing (VTOL) aerial platform capable of carrying out surveillance tasks. Its light weight design allows for just one person to transport the system to the desired location and set up ready for deployment. This type of UAV has a fixed pitch rotor. This reduces the complexity and mass of the adjustable rotor head.

Figure 2.3 - HALO UAV with three arms and each arm containing a co-axial motor and propeller configuration.

2.1.4 Lighter than Air

Balloon or blimp systems are capable of carrying very heavy payloads. The structure of these systems consists of a large balloon filled with any gas that is less dense than air (generally Hydrogen or Helium). They achieve control with a number of fixed pitch propellers directing the flow of the air around the balloon (see Figure 2.4). The advantages of this type of UAVs are the ability to reach very high altitude and remain there for long periods. But they are prone to being affected by the wind due to its very large surface area and have very slow operating speeds. They are not used for battle as they are extremely easy targets and can give positions away (Hygounenc et al., 2004).

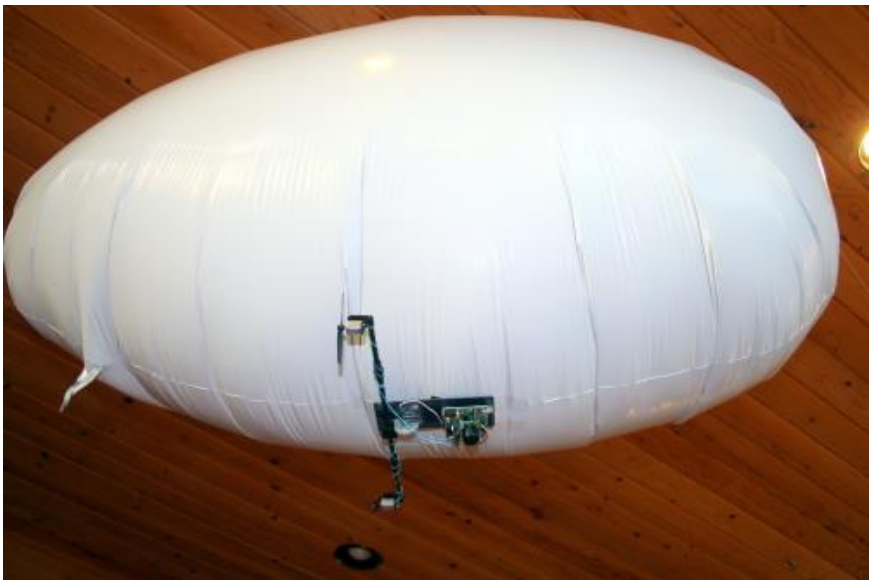

Figure 2.4 - BlimpDuino which has the control system attached below (Used with permission of Chris Anderson).

2.1.5 Paraglider

Paraglider systems are predominantly used for long endurance surveillance. They consist of a parachute and propulsion system with controls. These Paraglider UAVs can be deployed from the ground at climb to high altitudes or can be dropped off by a plane in mid-flight. Atair Aerospace Company makes a

Figure 2.5 - Leapp I, Powered Paraglider UAV (Used with permission of Atair Company).

Paraglider UAV called Leapp (Long Endurance Autonomous Powered Paraglider). Their biggest system (Leapp Type I) (see Figure 2.5) which is the size of a small car, is capable of reaching altitudes of 15,850 m for up to 55 hrs (Atair, 2014).

2.1.6 Hybrid

Often a combination of capabilities is required for specific mission where one UAV type isn't enough. The V22 (see Figure 2.6) would cover a VTOL and fast forward flight regimes from company Bell. The V22 has been in development since the early 1980s and has cost the company £20.6 bn. The two 3.05 m counter rotating propellers stay in a horizontal origination whilst trying to take off like a helicopter which then rotates 90˚ to a vertical position which converts the VTOL helicopter into a fixed wing forward flying plane. It's able to manoeuvre at slow speeds in helicopter mode for detailed reconnaissance while getting to and from its destination fast and efficiently. It was the first VTOL UAS to receive certification of airworthiness from the Federal Aviation Administration (FAA) (Rotorbreeze, 2006).

Figure 2.6 - V22 Osprey in its transition between hover to forward flight mode.

2.1.7 UAV Types Summary

The UAV market is constantly growing as there are many possible applications for these UAVs. The military has a strong influence in UAV design, as they are the largest stakeholders in the UAV sector and have the largest budgets to spend on the procurement and development of these systems. UAVs are filtering into the civilian market, as the low cost UAVs easily replace the need of a full scale helicopters or planes. UAVs tend to have high costs due to the tough military specification and undergo heavy testing. As the need for UAVs grow more from the civilian market, it will drive the cost down due to less demanding testing and certification required. Military UAVs need to be constantly improving as the demand to carry more, go faster and see more is increasing. This is mainly because the rules of engagements change with every battle or war fought which bring us to where we are now. All the UAVs which are available now have been created to meet a demand which is always changing. The need for multi-purpose UAVs is higher in demand as the way these UAV are being used changes.

2.2 Landing/Perching Systems

The available literature was explored in gain an insight into what developments have been made in the specific area of landing/perching UAVs. The developments in landing/perching systems was more heavily leaning towards the autonomous landing of VTOL UAVs, with a few projects looking specifically at perching. At the University of Illinois, a small flapping UAV, which is lacking vertical tail agility just like birds, is capable of landing/perching on a human hand (see Figure 2.7). The small flapping bird-like UAV is able to work out the best trajectory to execute the perch. It relies on the Vicon™ motion capture system to provide global reference positioning and orientation of the wings and fuselage. The Vicon™ system consists of 16 InfraRed (IR) cameras which track reflective markers attached to the articulated parts of the small flapping wing system. The setup can cost anything from £15k+ depending on the types of cameras and software used (Muir, 2011, PEPPM, 2013). The aim is to execute a perch in the gliding phase of the flight by adjusting the wings and control surfaces like a bird. The 44 g micro air vehicle (MAV, which Paranjape et al are tracking the bird to an accuracy of 1 mm at 100 Hz and controlled by closed-loop proportional-integral-derivative (PID) which is computed at 60 Hz then

transmitted at 20 Hz. The disadvantages of a this system is it's practicality in outdoor scenarios where without the Vicon™ system tracking and controlling the MAV, it would be useless as all the computation is done off-board (Paranjape et al., 2012).

Figure 2.7 - Sequential image of the flapping wing system being launched at one end and caught at another (Used with permission of Paranjape).

Stalling before perching was also implemented by Cory at Massachusetts Institute of Technology (MIT) where a larger UAV was able to perch on a typical electrical wire. Again using the Vicon™ system, Cory was able to use the flapping wing UAV to stall just before the perch (see Figure 2.8) by exploiting pressure drag on its wings and tail, but struggled outdoors (Cory, 2010).

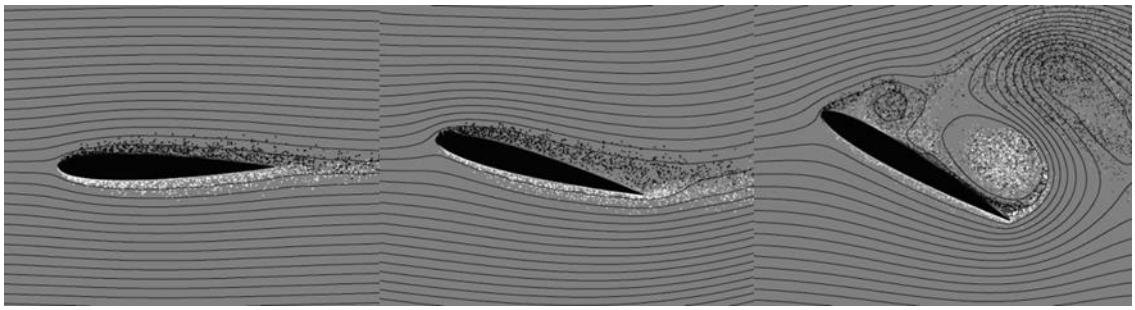

Figure 2.8 - Flow characteristics of high angle of attack (Used with permission of Cory).

Whilst work is being conducted on the dynamics of the flight for perching manoeuvres, The Computer Science and Artificial Intelligence Lab at MIT are using a similar hook setup to perch onto an electrical power line. Moore and Tedrake detects the magnetic field around the electrical power line (see Figure 2.9) using the on-board magnetometers to hone in on the electrical field to execute the perch (Moore and Tedrake, 2009). This collaboration is ideal as one group at MIT conducts work on the dynamics of the flight and the other team looks into the recognition of the perching site.

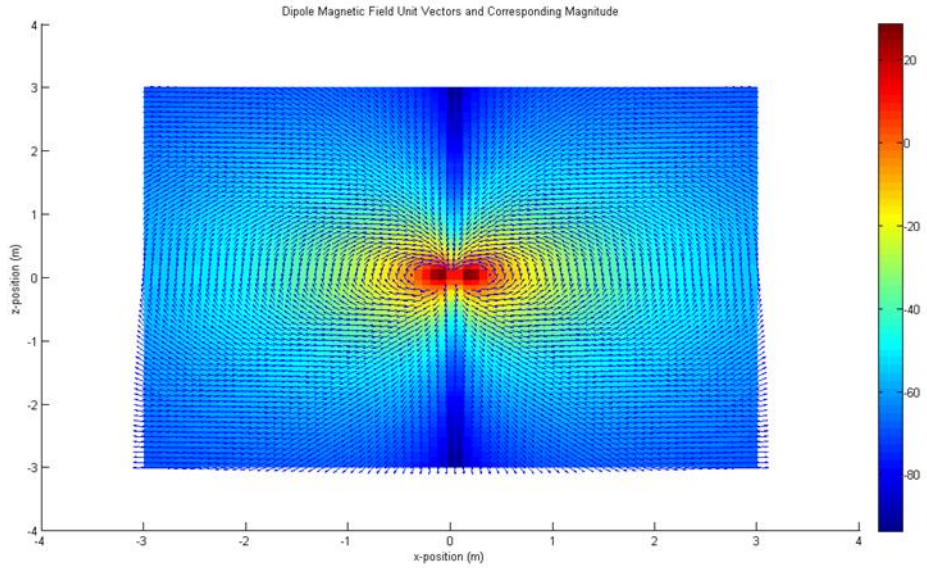

Figure 2.9 - Detection of dipole magnetic field model (Used with permission of Moore).

At Stanford University's Biomimetics and Dexterous Manipulation Laboratory, Desbiens et al have developed their own bird-like claw which grabs onto outdoor walls. The fixed wing UAV is able to fly straight towards a solid wall before manoeuvring to a vertical stall position with a high attack angle, similar to the MIT system, to slow the UAV down in order to give the claws a chance to grip the wall (see Figure 2.10). The 400 g UAV has an ultrasonic sensor mounted to the front of the fuselage which detects the wall to engage the perching manoeuvre from up to 5 m away. The ballistic motion of the plane contacts the wall between 1-3 m/s where the leg and foot suspension keeps the claw engaged whilst dissipating the kinetic energy from the flight (Desbiens et al., 2009). The disadvantage of this type of system is the UAV platform that is used which is unable of achieving zero velocity, which is crucial to perching. By achieving a state of zero velocity, it allows the UAV to make a more controlled perching manoeuvre. This system also suffers the danger of misjudging the wall surface and risk getting damaged due to crashing head first into a solid wall. They are also limited to the type of wall face they can perch onto, but do have the advantage of having on-board intelligence of conducting the perch without user input. The MIT system which not only relies on external controllers, but also only works indoors, whereas the Stanford system can work in real outdoor scenarios.

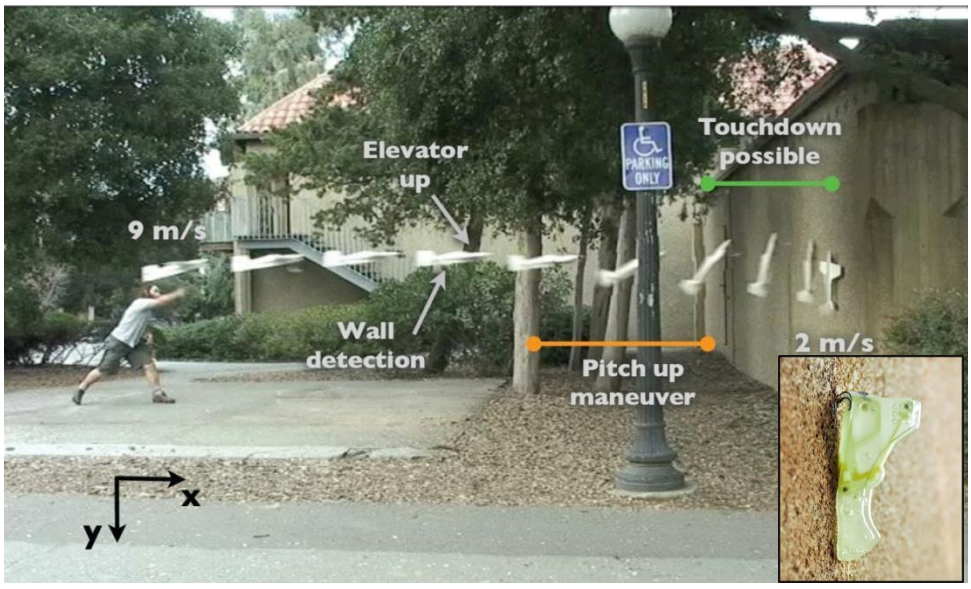

Figure 2.10 - Sequence of UAV being launched towards a wall and the UAV detecting and initiating the perch manoeuvre. Image of the claw design is also attached to the lower right hand side (Used with permission of Prof. Cutkosky).

Various undercarriage gripper arrangements were also found in the literature which was not directly linked to perching but have shared components to achieve different applications. Not all of them were used for landing/perching purposes. Some were used as manipulators such as Voyles and Jiang's force closure grasping UAV at the University of Denver. This UAV's manipulator was designed to be able to apply torque action such as that found in a wrench using thrust vectoring to achieve the grasp (see Figure 2.11) (Voyles and Jiang, 2012). Although the UAV platform is designed to allow for forced closure grasping, the manipulator is still yet to have intelligence of its own to allow for aerial manipulation.

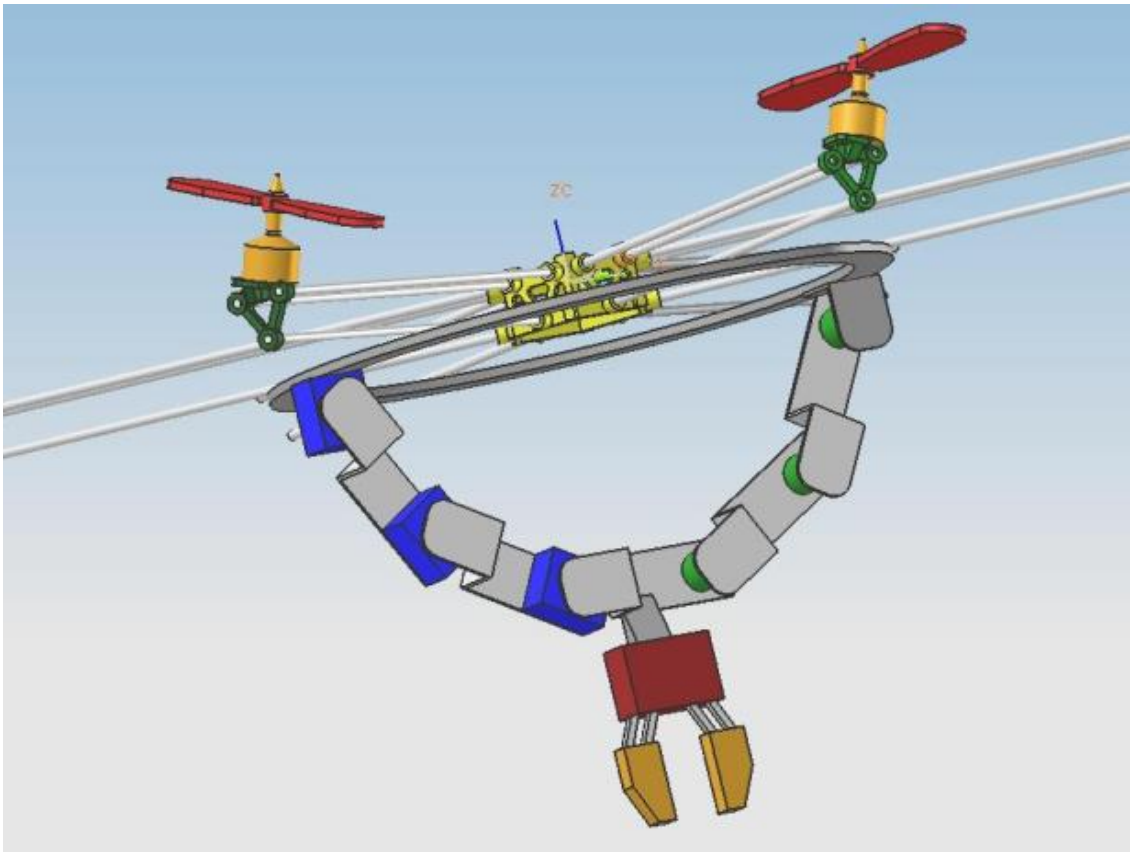

Figure 2.11 - Closed chain manipulator design (Used with permission of Voyles).

At the University of Pennsylvania, Lindsey et al are using the under-slung gripper design for an interesting application. They have the gripper system attached to the bottom of a quadrotor UAV flying in a controlled indoor environment, again relying on the Vicon™ camera motion tracking system for navigation and to stack special magnetised building blocks to create pre-programed structures (see Figure 2.12). Each building block is transported individually by a group of UAVs working together on completing the desired structure. The intelligent part is in

the algorithm instructing the UAVs in a collaborative manner to complete the task together (Lindsey et al., 2012). The drawback to this system is the accuracy of the Global Positioning System (GPS) which is within a 7.8 m radius worst case and nominally within 4 m accuracy. The horizontal error is less than 3.9 m

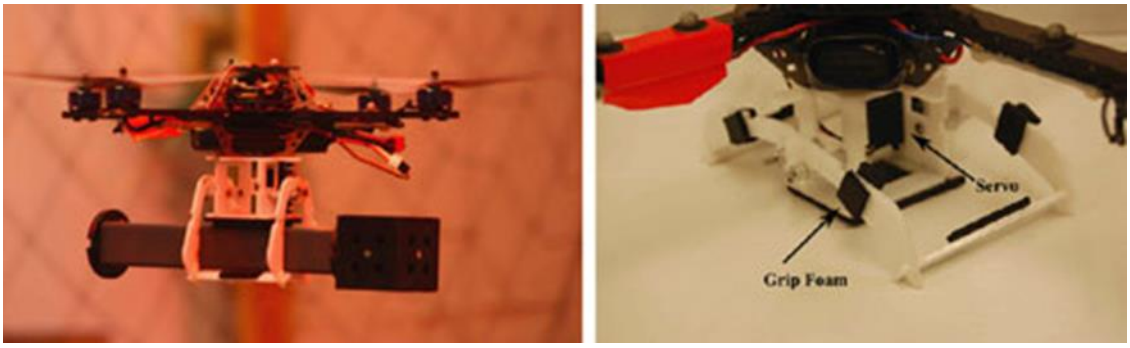

Figure 2.12 - Gripper grasping the special magnetic building blocks (Used with permission of Lindsey).

(Hughes, 2013), 95% of the time, which is not accurate enough to enable close quarter UAV collaboration without a mid-air collision. With the launch of the new Galileo satellite constellation in 2016, the accuracy should be within 100 mm (Thomas, 2011). The only advantage to these systems is that they have their own on-board controllers for the actuation of the manipulator.

The indoor aerial gripping quadrotor from Utah State University has the issue that not every graspable item has a recognisable pattern. Ghadiok is using IR Light Emitting Diodes (LEDs) as a marker and using the low cost IR camera from a Nintendo Wii Mote to track the position of the UAV for directional control. The UAV is able to track the IR LEDs at a rate of 200 Hz. Once the UAV is over the object, it then positions itself to grasp the object surrounded by the pre-placed IR LEDs. The camera can track up to 6 LED beams to gain positional information (Ghadiok, 2011).

Ghadiok has understood how aerial grasping should be conducted and highlights three major challenges that need to be overcome:

- Precise positioning of the UAV.
- Object sensing and manipulation.
- Stabilisation in the presence of disturbances.

The interaction between an object and the UAV creates instability in the flight dynamics, which must be dealt with in order to achieve aerial grasping (see

Figure 2.13) (Ghadiok et al., 2011). The system relies on off-board processing which is undesirable as it is not always possible to have an umbilical cord or reliable radio transmission. However they have underlined some key points which will be used when developing the reconfigurable perching element.

Figure 2.13 - UAV approaching stuffed panda toy (Used with permission of Ghadiok).

Similar to the building block application, Pounds et al at Yale University have used remotely operated helicopters with a gripper underneath the system to carry various payloads to see what the effects will be on the stabilisation during flight (Pounds and Dollar, 2010) and hover with an off-the-shelf autopilot with unmodified PID gains. Whilst the gripping is done under the remote instructions of the pilot, they have acknowledged that there will be disturbances to the aircraft from external forces, whether it is a perching manoeuvre or an aerial manipulation (Pounds and Dollar, 2010). By understanding the external forces, they estimate the counter-acting forces required to keep a stable flight, but with the input of an expert pilot (see Figure 2.14).

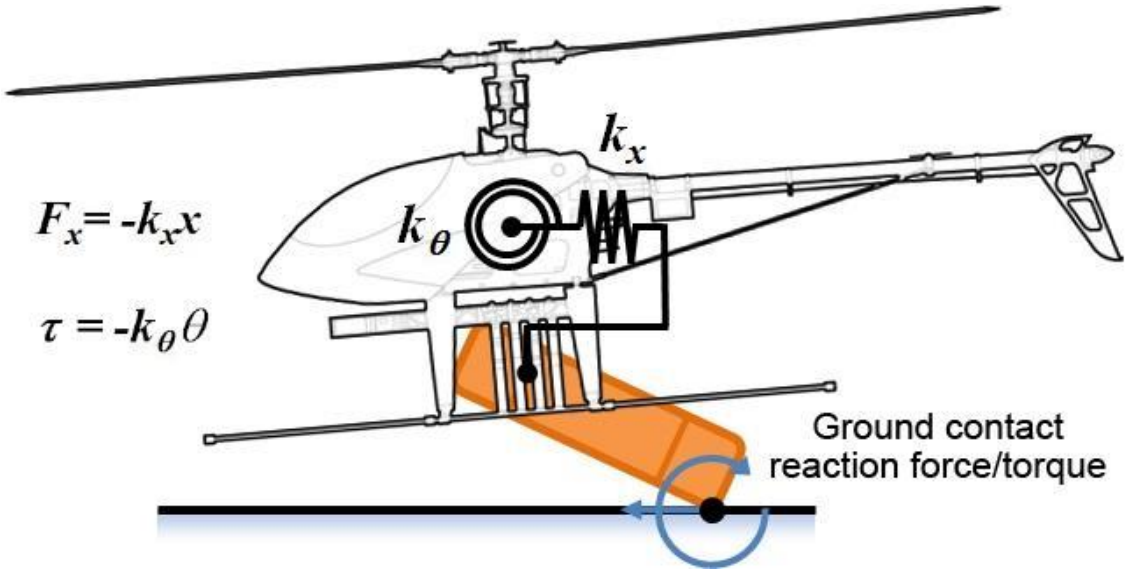

Figure 2.14 - Yale Helicopter with gripper attached and interacting with an object (Used with permission of Pounds).

Work on autonomous landing, which is closely related to perching, has also been conducted but relies on recognition of pre-placed patterns or sensors on or around the landing/perching site. At the University of Tübingen in Germany, Wenzel et al have been tracking a ground vehicle which is transmitting an IR beam to the quadrotor UAV, which is similar to the work done at Utah State University as previously mentioned. Intelligent use of low cost sensors and off the shelf components enabled the successful landing of a moving vehicle. Of

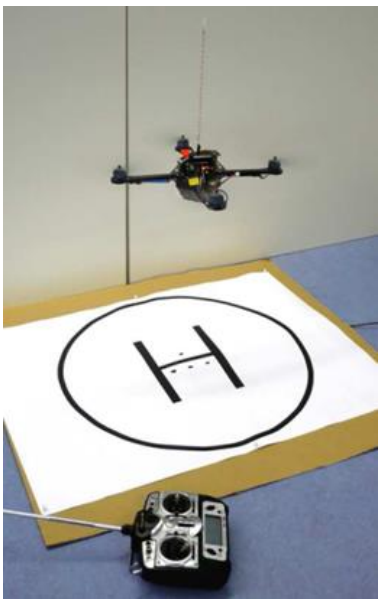

Figure 2.15 - Tracking IR LEDs incorporated into helipad (Used with permission of Wenzel, 2010).

course it all relies on the placement of the IR transmitter which might be feasible for a moving vehicle but not for an un-reachable land/perch site (see Figure 2.15) (Wenzel et al., 2010a). Roke Manor Research Limited in the south of England is also working on a recognition based landing system. Rather than relying on IR beacons surrounding the land/perch site, they use a smart recognition algorithm to locate and land on the 'H' of a helicopter pad (see Figure 2.16 & Figure 2.17) (Whitehouse, 2010).

Figure 2.16 - Image of helicopter with the autoland system being tested on moving Armoured personnel carrier (APC) (Image courtesy Chemring Technology Solutions).

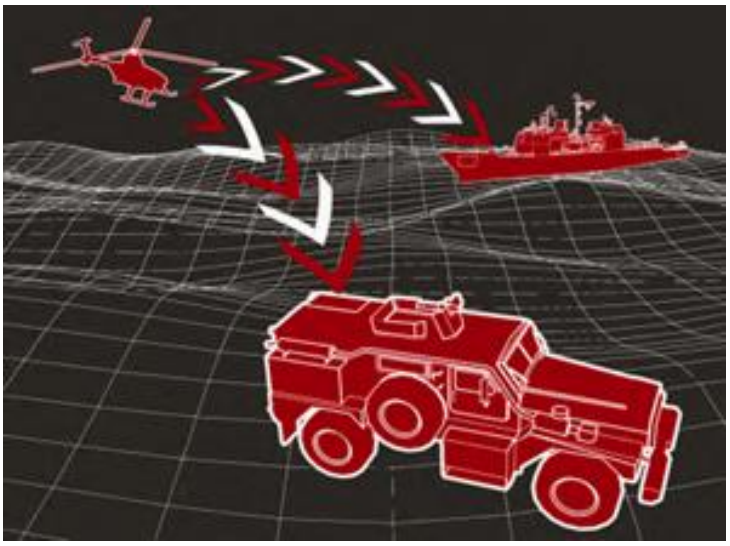

Figure 2.17 - Roke autoland system which tracks the moving landing target (Used with permission of Roke).

Doyle et al have been developing 'An Avian-Inspired Passive Mechanism for Quadrotor Perching' which is a passive system capable of maintaining a perch without the need for any additional power. It relies on the mass of the quadrotor to act as a gripping force (see Figure 2.18). Its design adopts the use of an interesting linkage system which exists in the Sorrow bird which allows the mass of the UAV to ensure the platform stays put on the perch site. However, due to the interesting design of the gripper, it easily adapts to most uniform profiles. The flexible finger joints wrap around the perchable cross section for a secure hold. Heavily inspired by nature, the gripper has no electrical parts, which simplify its operation. However, it still relies on the coordinated instructions of the pilot and is also very bulky which overshadows the UAV and affects the flight dynamics (Doyle et al., 2011, Doyle et al., 2012).

Figure 2.18 - Passive perching system which takes its inspiration from the gripping system of a Sorrow bird (Used with permission of Doyle).

A blend between the Stanford's head on approach and Doyle's avian inspired gripper, EPFL have come up with a way of perching on both natural and man-made structures such as trees and painted concrete facades of buildings (Kovac et al., 2009). The benefits of this system is that it uses zero energy to sustain the perch which means it can remain perched indefinitely. It uses a tiny motor which activated the release arm which sets the MAV free again.

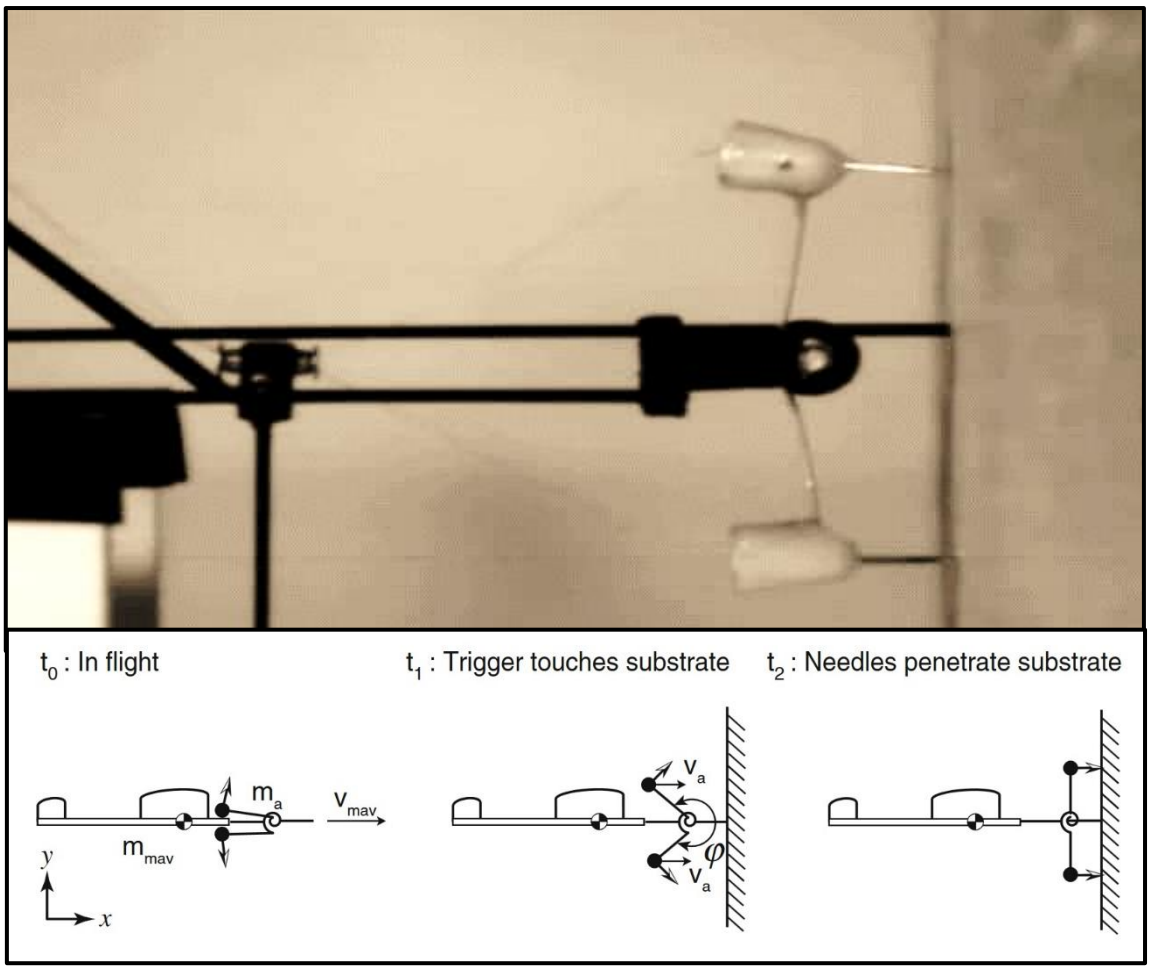

Figure 2.19 - Needle gripper deployed once made contact with wall or tree.

2.3 Summary

This area of research has already produced many interesting projects which this research will benefit from. The review heighted a possible area for development which a VTOL UAV could perch and stare. The perching and auto-landing systems provided a starting point with regards to how the work should be structured. The on-board vs off-board processing will have to be further investigated as this was an aspect which kept dividing how the work was conducted. Another point worth mentioning is the difference in the work relating to the detection of the perch site. It was noted that the selection of the perch site could be a crucial point in the research as it will direct the rest of the research.

3. Perching Element

This chapter presents the perching element which essentially replaced the landing gear of the test UAV which is used to conduct the perch. It shows the various stages of concept generation, development and optimisation of the chosen design.

3.1 Introduction

Perching is a highly complex manoeuvre which birds execute on a daily basis and can be split into two different stages: flight control planning and grasping. The flight control planning aspect is the recognition of the perch site and executing the manoeuvres required to attain the perch. The grasping aspect is the physical connection between the Unmanned Aerial Vehicle (UAV) and the perch site. A perching manoeuvre is a highly desirable capability as is it can lead to a perch-and-stare system which can conduct extended reconnaissance missions. Furthermore, a perching UAV can also harvest energy either with the use of photovoltaics (PV) or inductive charging (QinetiQ, 2008, Moore and Tedrake, 2009).

Before concepts were generated, more information was required, such as determining the perch site, identifying common features about the perch site along with further knowledge on grippers.

3.1.1 Urban Landscape

In terms of surveillance, urban cities are the most watched due to them attracting all sorts of crimes which need to be observed. In order to get the best views for surveillance, an elevated point of view (POV) is required which is able to capture a larger area of interest. The cost of installing, monitoring and servicing a fixed camera system can be high and not all areas need to be under constant surveillance. The urban environment has many perch sites to offer such as trees, sign posts and buildings. Lighting columns however offer an excellent perch site. They provide the elevated perspective whilst also offering common features to perch on whereas trees and builds may also offer a raised perspective if not better, but can vary a great deal which may make the recognition process very

difficult. Also having such varied geometries, the perching element would have to be extremely versatile which may not be possible due to weight restrictions.

3.1.2 Lighting Columns

Every country has different regulations for the different types of lighting columns which illuminates their streets. They vary from small streets with low speed limits to lighting columns which are on busy motorways and superhighways and to those which are just merely to illuminate the way for pedestrians. From lighting intensity, height of the column, the materials used and finish of the column, all are regulated (Highways Agency, 1999). Using online resources and physical measurements, data was collected and organised to gain visualise the possible land/perch sites (see Appendix A). In addition to the online and physical data, local governing authorities were contacted in order to gain access to the various types of lighting columns which were available. They also granted access to typical lighting column sections (see Figure 3.1).

To better understand the land/perch site, the information gathered was analysed which showed that there were common features which could be used for detection. The main emphasis was on lighting columns that were used in the London metropolitan area. Figure 3.2 highlights the key features of a sample lighting column along with their industry used names.

Figure 3.1 - Various lighting columns with assorted projection brackets.

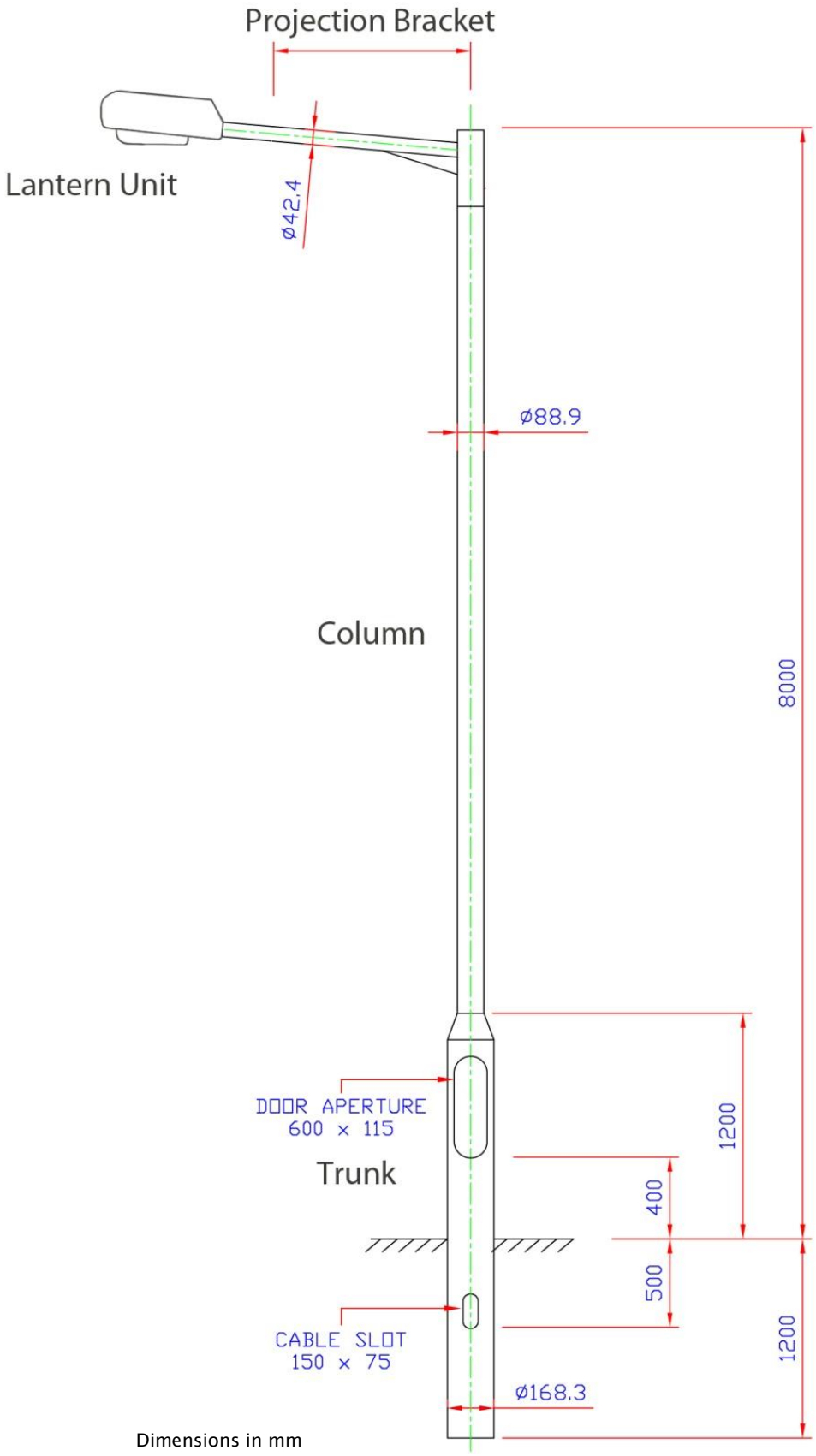

Figure 3.2 - Lamppost anatomy highlighting main features: Lantern Unit, Projection Bracket, Column and Trunk.

3.1.3 Identifying Common Features

The ideal location to perch on street furniture would be on the projection bracket of the lighting column. But more precisely in-between the lantern unit and the column itself as there would be the least amount of obstructions and this is where the most common feature is (see Figure 3.3). The benchmark looking at the different types of bracket projection profile conducted in greater London, found that the most common was the circular profile which ranged between 33.5-109 mm diameters. Twenty different types of lighting columns were identified. The median diameter of 42.5 mm sits between the first and third quartile (35-50 mm respectively) (see Figure 3.4). There are however a few outliers which are represented by the un-filled circles, which indicates a group of lighting column which has a projection bracket diameter outside the norm but are still considered. The angle at which the projection bracket exits the main column also varies between 0º to 15º. These projections have regulations which the Highway Agency states that the bracket projection cannot exceed a projection of 0.25 x the nominal height of the lighting column or less than 3 m whichever is the least. The maximum height restrictions for steel, aluminium and concrete lighting columns are <20 m or <18 m with a bracket. Glass fibre lighting columns have considerably greater height restrictions due to the structural rigidity of the glass fibre column. It must be <10 m with a bracket not

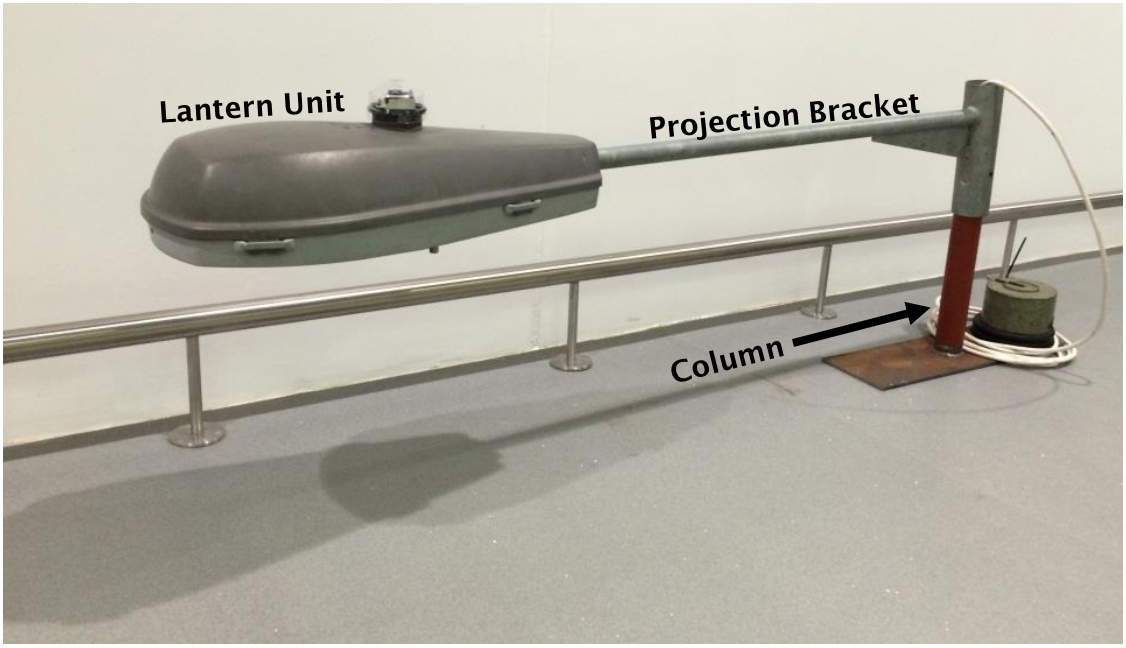

Figure 3.3 - Lighting Bracket Projection with luminaire unit attached.

exceeding 1.5 m (Highways Agency, 2004). The projection brackets also tend to be angled which does not exceed five degrees.

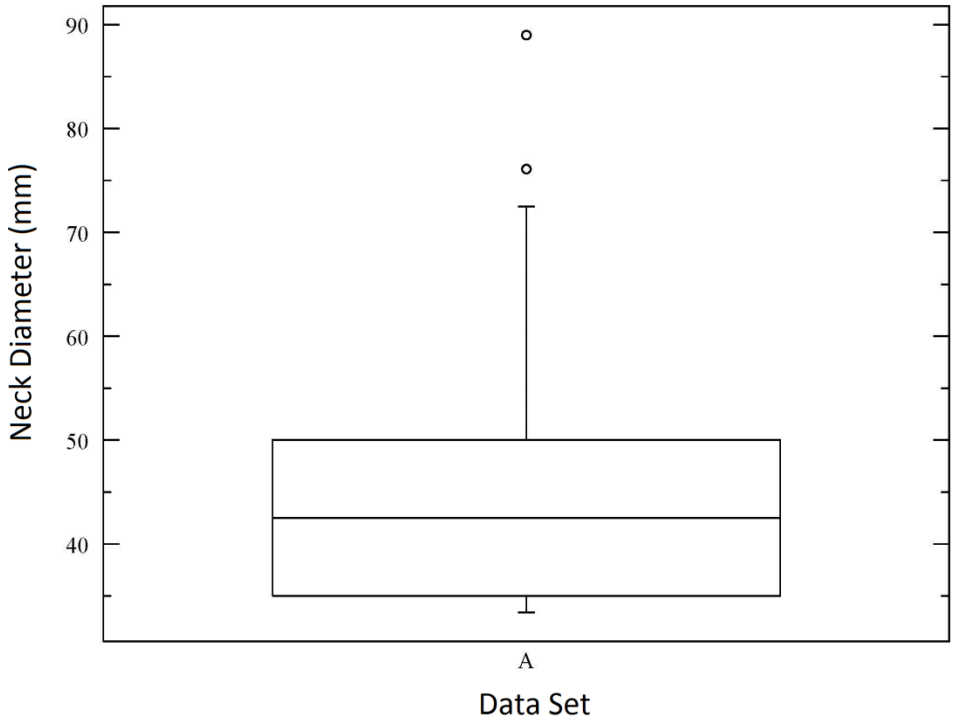

Figure 3.4 - Box plot of projection bracket neck diameter.

3.2 Grasping Types

Looking to biological inspiration, lighting columns are regularly perched on by birds. Understanding how they achieve a firm grasp was essential. Reviewing mechanical grippers, there were many ways in which a gripper could hold onto the perch site. This physical interaction between the perching element and the projection bracket are considered an active pair mating. Monkman has identified four prehension methods into the following categories: Impactive, Ingressive, Astrictive and Contigutive.

Impactive gripping is when the solid jaw of the gripper touches the objects surface to produce the necessary grasping force. Ingressive gripping is the deformation or intrusion of the surface of the gripping moving into a predefined depth of the object. Astrictive is the attraction between two surfaces through either natural properties or applied elements. Contigutive is interaction between

two surfaces. These gripper classifications are broken down further (see Table 3.1) (Monkman et al., 2006).

Table 3.1 - Gripper types broken down into four categories with brief description of how it interacts with the object being gripped and examples of the gripping type Adapted from a table by Monkman (2006).

Prehension Method	**Gripper Type**	**Typical Examples**
Impactive	-	Clamps (external fingers, internal fingers, chucks, spring clamps), tongs, (parallel, shear, angle, radial)
Ingressive	Intrusive	Pins, needles, hackles
	Non-intrusive	Hook and loop
Astrictive	Vacuum Suction	Vacuum suction cup/bellow
	Magnetoadhesion	Permanent magnet, electromagnet
	Electroadhesion	Electric field
Contigutive	Thermal	Freezing, melting
	Chemical	Permatack adhesives
	Fluid	Capillary action, surface tension

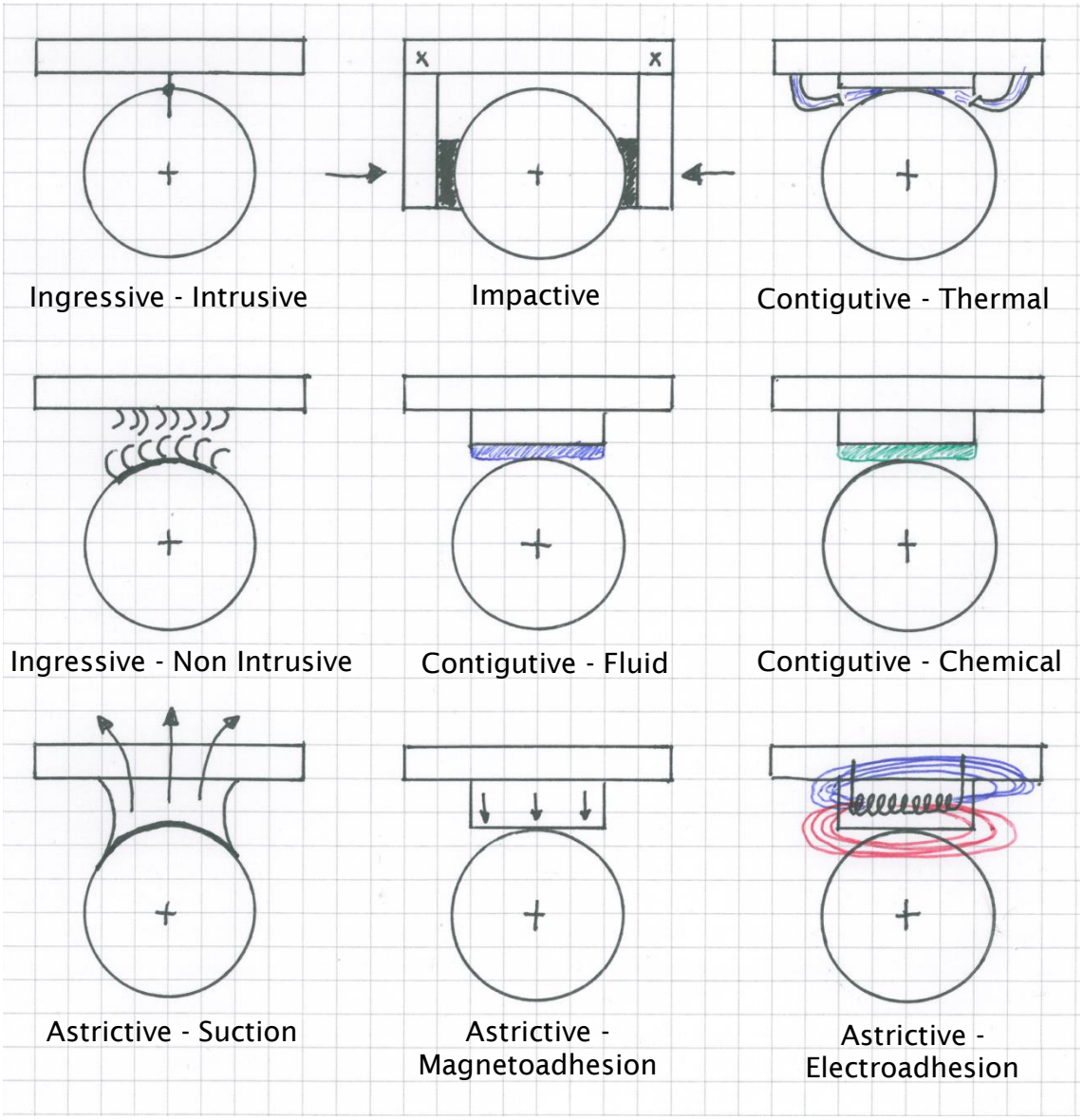

Figure 3.5 - Illustrations of Monkman's Gripper types on circular profile.

The visualisation of the gripping methods (see Figure 3.5) made clear how it could be a possible grasping a projection bracket profile. These methods were later used to develop design concepts which was then compared against each other.

3.2.1 Novel Gripping/Perching

This pneumatic gripper from the Festo Company is a three fingered gripper which is able to firmly grasp objects whilst conforming to its shape. Each finger uses two flexible bands which come together to form a triangle with struts evenly spaced out via joints which connect the two pieces (see Figure 3.6). This

combination of three fingers allows for manipulation of objects multiple types of surfaces, shapes and sizes. The only down side is the constant requirement of a compressed air supply which may be great in lab environments but not UAVs (Festo, 2014).

Figure 3.6 - Image of Festo's robotic gripper which conforms to the object's shape every time (Image courtesy of Festo Ltd).

To create a gripper using any of the methods provided in this section is possible and viable. There is one solution however which does not fall under any gripper categories and that is to simply land on the lighting column projection bracket and balance the UAV using the thrust from the propellers. This method would not only save mass by removing the existing landing gear but also have the least amount of components and therefore free to produce. The only downside is the amount of energy which would be used to sustain the balance. This would also incur an endurance limit to the whole system therefore was not included in the following design section.

3.3 Product Design Specification

These guidelines were set in order to move on to the next stage; concept generation. The fourteen criteria contain both quantitative and qualitative data sets. The PDS allows the design process to be more efficient as the concepts must stay within the set parameters. With the information gained from the literature search, gripping techniques and perching site, the PDS can be

specifically designed to meet the project parameters. The UAV test platform to be used is the MikroKopter (MK) Hexa; a multi-copter which as the name implies has six rotors on the same horizontal plane. At the tip of the equally spaced out arms, which are at 60º from each other, are the brushless out-runner motor with ten inch fixed pitch propeller combination. The advantage over a single rotor helicopter is that it has fewer moving parts and linkages which produce less vibration. It is powered by a 4 cell 14.8 Vdc lithium-polymer battery which is rated at 3300 mAh. The Hexa weighs 1480 g with the battery and 1105 g without and has a 555 mm pitch circle diameter for the centre of the motor shafts. The Hexa has also been used as a research platform by Winkvist, Peter and Lea-Cox (Winkvist and Rushforth, 2013, Peter, 2012, Lea-Cox et al., 2012).

The following are crucial attributes which helped determine the best concept:

· Multi-functional: This category rewarded any system which replaced the existing landing gear and converted it into an all-in-one system (i.e. the designed system replaces the existing 84.4 g landing legs and no longer needs them). Systems which still require the use of the original landing legs or additional support for landing were also be penalised in the mass category.

· Mass: Less than 1 kg including all elements of the landing system (due to the payload capabilities of the MK Hexa).

· Emergency Landing: In the event of a total electronics failure during landing or take-offs, the UAV must be able to land on a flat horizontal surface (i.e. landing gear always in the ready to land position). If the system required additional support for this it will be penalised in the mass category. It rewarded concepts which were ready to land as the landing gear does not have to be initialised.

· Idle/Operational Power: System must not use additional power to keep the landing system holding (i.e. no power consumption during idle state of the system). Research showed that UAVs are already power hungry. Adding more burdens on the system will reduce the UAVs capabilities. UAV has to execute the manoeuvre in a timely manner whilst consuming minimal power. No more than 45 W at 14.8 Vdc which shouldn't impede the endurance of the UAV.

· Environmental conditions: The platform must be able to operate in the following environmental conditions, based on statistics from Met Office UK and

Windfinder (Windfinder.com, 2014, Met Office, 2014): -10 to 30˚C temperature range. 10 year (2001-2011) average wind speeds in the UK of 4.6 m/s, with wind gusts up to 28 m/s.

· Perchability: All operations must be conducted in a safe manner at all times. If the system were to land below the projection bracket then the chances of survival would be less than if it were to land above the bracket. This is due to there being the column element which can get in the way.

· Centre of Gravity: The perching elements CoG must be close to the centre of the UAV's CoG.

· Complexity: The system must be able to survive the usual wear and tear. It must also be able to withstand the stresses and strains of regular UAV operations (i.e. landing, acceleration in all directions, etc.). If the system has more moving parts, then the likelihood of it affecting the flight dynamics are higher.

· Engaging/Disengaging time: The system must be able to engage and disengage in less than 6 s. The longer it takes the more power the UAV will consume. This is considered to be the time taken to initiate the contact and confirm the hold and power down.

· Volume: No bigger than 0.3 m diameter from the centre of the MK Hexa (due to airflow restrictions), and less than 0.2 m height which gives a volume of 0.014 m^3. Data taken from existing landing skids.

· Multi-purpose: This criterion rewarded concepts if it were to have the capability to be used on multiple materials and terrain types.

· Cost: The landing/perching system must cost less than £350, excluding sensors

These criteria were also used to score each concept against each other on a scale of 0 to 10 in the weighted matrix. The answer to the research question 'What factors affect a VTOL UAV ability to perch?' is presented in the 14 different criteria which when combined highlights the factors which affect the perching capabilities of a VTOL UAV see Table 3.2.

3.4 Concept Generation

Concept generation was an essential stage which needed a deeper understanding of the problem in order to solve it in the most efficient way. The main objective was to land onto a lighting column efficiently and effectively in order to preserve battery power whilst surveying an area. It became clear that the system must be able to orientate itself in relation to the lighting column so that is can land every time with the system perfectly lined up with the bracket projection. Also taking into consideration how fast the system must execute the manoeuvre, how much the system will weigh and how much power it will consume whilst executing the task. After several concept generation iterations, 53 concepts were created of which only 21 were taken to the next stage as some concepts were grouped together and/or combined (see Appendix B). The task of selecting a final concept would have been difficult without a weighted matrix to guide it.

It is also noted that a pattern emerged regarding the adhesion method. Two of the top five concepts use impactive – clamping method (overall position first and third) for adhesion between the perching element and the projection bracket of the lighting column. Two use astrictive – magnetoadhesion (overall position second and forth) and the fifth uses contigutive – chemical. A detailed description of each can be found in the section on 'The top five concepts'.

3.5 Weighted Matrix

Pahl & Beitz and Black commonly use a weighted matrix approach to evaluate each criterion to select the strongest concept, therefore this method was also used in this research (Black, 1996, Pahl et al., 2007). The top five designs which came out on top after applying the weightings to the concepts are highlighted in (Table 3.2). Each concept was given a score per criterion, which was multiplied by the criterion weighting. The sums of all the scores for each concept are added up to give a final score. The sum of all the criteria weightings is 100, which are distributed amongst the 14 different criteria.

3.6 Breakdown of the Weightings and Scores

Some of the following criteria have a quantitative number which can be easily determined or estimated using calculations, where other criteria require a slightly more elaborate approach to give it a score. Middendorf has done by grouping the design attributes into sets which are given a score (i.e. set 1 will result in a score of 10). The number of sets per criteria, are determined by the number of attributes which can be judged and vary between 2-4 sets. The score of 10 will then be divided into the number of sets available (i.e. two sets will have a score of 10 and 0 for sets 1 and 2 respectively). Each criterion was optimised to ensure the systematic approach which has been adopted for this research (Middendorf, 1986).

Emphasis on the importance of the multi-functionality was given by assigning the highest weighting along with mass as these two criteria have the greatest affect the UAV.

The percentage of the weightings for each criterion was as follows (see Figure 3.7).

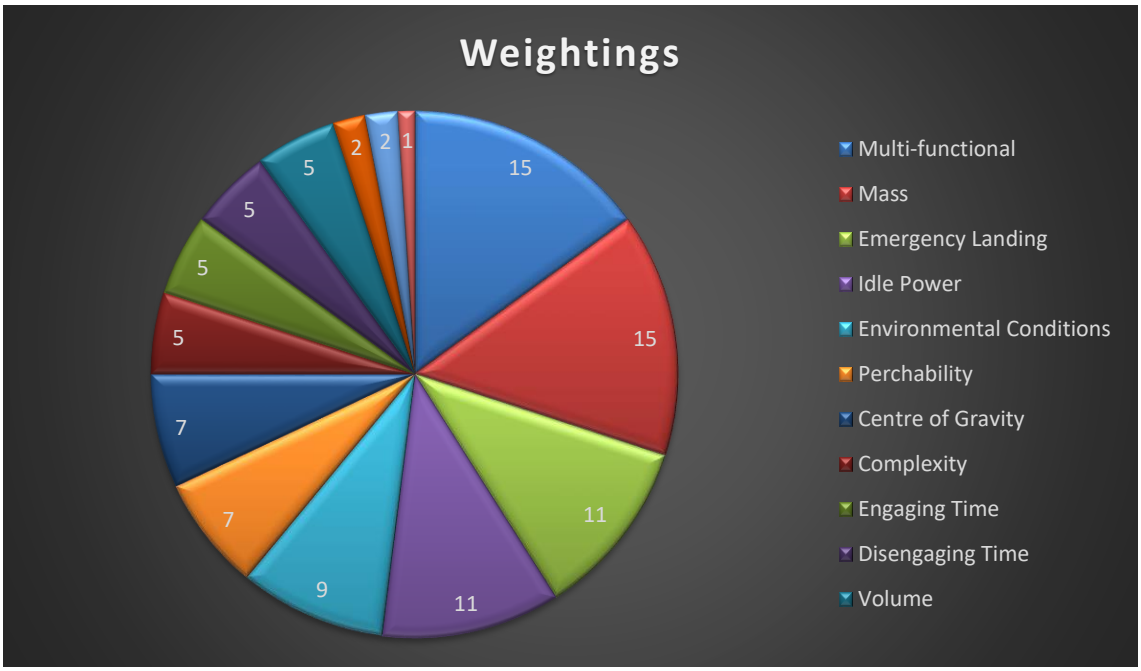

Figure 3.7 - Weightings Pie Chart

Table 3.2 - Weighted matrix showing the five highlighted concepts which scored the highest. Concepts have been ordered according to rank.

	Weighting	15	15	11	11	9	7	7	5	5	5	5	2	2	1	100	
Concept No.	Concept Name	Multi-functional	Mass	Emergency Landing	Idle Power	Environmental Conditions	Perchability	Centre of Gravity	Complexity	Engaging Time	Disengaging Time	Volume	Operational Power	Multi-purpose	Cost	Total	Gripper Classification
-	Perfect System	10	10	10	10	10	10	10	10	10	10	10	10	10	10	1000	-
-	Worst System	0	0	0	0	0	0	0	0	0	0	0	0	0	0	0	-
3	The Claw	10	3	10	10	10	10	5	7	8	8	6	6	10	2	789	Impactive - Clamp
5	Magno Screw	5	5	10	10	10	10	10	7	10	5	7	7	5	3	772	Astrictive - Magnetoadhesion
8	Slider	10	2	10	10	10	10	5	7	3	8	6	7	10	4	753	Impactive - Clamp/Tong
4	Magno Hug	10	3	10	10	10	10	5	7	8	3	6	4	5	2	750	Astrictive - Magnetoadhesion
12	Slimer	0	7	10	10	10	10	10	7	10	9	6	6	5	5	742	Contigutive - Chemical
11	The Gecko	0	7	10	10	10	10	10	7	10	3	6	6	5	5	712	Contigutive - Chemical
18	Snap On Cuffs	0	10	10	10	0	10	5	10	9	2	10	10	10	10	680	Impactive - Clamp
19	The Lock Down	0	4	10	10	10	10	10	7	5	9	7	4	5	4	672	Impactive - Clamp
14	The Jumper	0	7	10	10	5	10	10	7	10	3	6	10	0	5	665	Astrictive - Electroadhesion
6	Twister	10	1	10	10	5	10	5	7	1	2	5	4	10	1	639	Impactive - Clamp
7	The Hook	0	10	10	10	0	0	5	10	10	10	10	10	10	10	655	Impactive - Clamp
16	The Winch	0	3	10	10	10	10	10	4	0	8	6	4	5	3	606	Astrictive - Magnetoadhesion
2	The Millipede	10	4	0	0	10	10	10	4	5	5	6	4	10	1	569	Ingressive - Pins
21	Fly	0	4	10	10	0	10	10	10	2	3	7	3	5	3	549	Contigutive - Fluid
13	Tesla Grip	0	3	10	0	5	10	10	7	10	10	6	1	0	5	512	Astrictive - Electroadhesion
1	The Balloon	10	1	0	0	10	10	5	7	2	10	4	1	10	2	499	Astrictive - Vacuum Suction
20	Freezo	0	4	10	0	10	10	10	10	2	0	7	1	5	0	507	Contigutive - Thermal
10	Bat Feet	0	10	0	10	0	0	5	10	10	1	9	10	10	10	495	Impactive - Clamp
15	Shooting Gripper	0	1	10	10	10	10	0	0	0	8	4	1	10	1	478	Impactive - Clamp
9	Sucker	0	2	10	0	5	10	10	7	3	4	7	1	10	5	457	Astrictive - Vacuum Suction
17	Monkey Tail	0	3	0	0	10	10	5	4	1	5	8	2	10	1	355	Impactive - Clamp

3.6.1 Multi-Functional

This criterion has the joint highest weighting and was considered to be one of the most important attribute to the generated concepts. Weighted at 15%, this criterion had three sets which are marked as 10, 5 & 0 for sets 1, 2 & 3 respectively. The aim here is to reward any system which replaced the existing landing system as described previously in the PDS section. This multi-functional attribute was very desirable as it saved on mass and increased usability. Concepts must be able to increase the existing capabilities of the landing gear and/or outperform it.

3.6.2 Mass

Mass has always been an important factor with every type of manned or unmanned system. By increasing the perching capability of a UAV through reconfiguration, it must have very minimal if not any impact on other properties which affected the UAVs flight capability. A linear approach to this quantitative criterion was deemed too simple as it would not deter the concepts from having a larger mass. Therefore a nonlinear scoring system was used to exploit the possible models which would improve the perching capability rather than lowering it. This criterion was also given the highest weighting of 15%. As the MK Hexa had a payload capability of 1 kg, this became the limiting factor when assigning a score for each concept. Everything below 1 kg was favoured and is exponentially graded to encourage mass loss in the concept, which a linear approach would not do. Using this model, a system which has a mass of 200 g received a score of five, whereas on a linear scale (blue dotted line) it would receive an eight (see Figure 3.8). This method of scoring also drove creativity and inspiration to reduce mass at all costs.

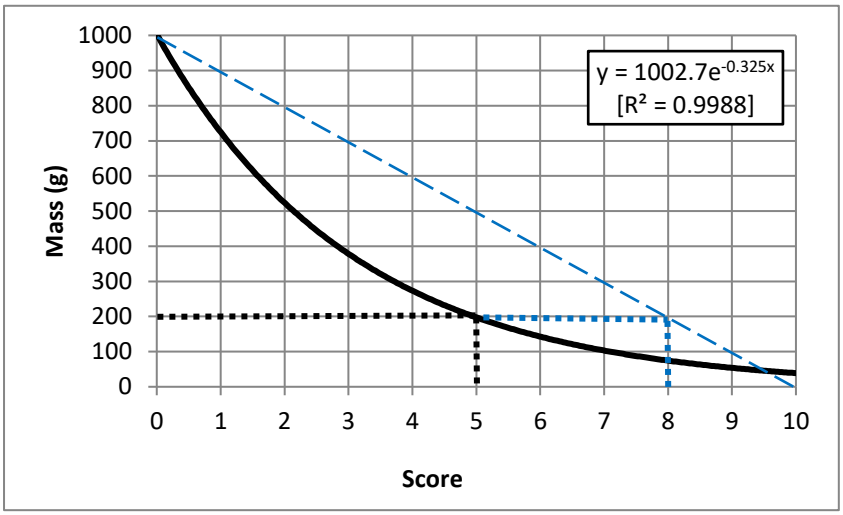

Figure 3.8 - Mass vs. score. Black dotted line indicating 200 g would equate to a score of five. Blue dotted line indicating the score of 8 if the scale was linear.

3.6.3 Emergency Landing

Standard landing gear which are found on small man portable VTOL UAVs are either typical helicopter skis or multi-point contact legs (Figure 3.9). These setups are a passive system which provides a stable method of landing in a controlled manner. They also provide a means of landing in an emergency situation e.g. loss of power at a reasonably low altitude, which cannot be achieved with a landing gear which needs to be activated in order to land i.e. retractable system. This criterion emphasised the need that a landing gear must be ready for any type of landing scenarios which the pilot or autopilot cannot foresee therefore given a weighting of 11%. The scoring used a linear scale which

Figure 3.9 - Landing gear types. (Left) multi point, (Right) skids.

split the score into sets 1 and 2 scoring 10 and 0 respectively, which determined whether the concept can or cannot land in such situations.

3.6.4 Idle Power

Scoring either a 10 or a 0 for sets 1 or 2, this criterion had a simple grading which determined if the system required a constant supply of power to sustain the hold onto the perch site. Considered to be equally important as 'emergency landing' and therefore given the same weighting of 11%.

3.6.5 Environmental Conditions

Being able to sustain a hold during any weather condition was another requirement if this perching system is to be used in the real world. This criterion split into three sets which graded the concepts 10, 5 or 0 depending on how well it can hold on during high wind gusts. Set 1 scoring was given to concepts which were not affected by any weather conditions where set 3 would was for concepts affected by the slightest breeze. A weighting of 9% was given to this criterion as a system which cannot hold onto the perch site, would very likely be damaged if blown off by wind gusts therefore falls into the top five for importance. This was the only criterion which was un-controllable and had an infinite number of variables, where other criteria could be manipulated to meet the PDS requirements.

3.6.6 Perchability

Linked with the previous criterion, perchability also looked out for the UAVs survivability. Approaching the perch site from above (set 1) has no obstructions which may get in the way during perching, whereas an approach from below (set 2) has the lighting column itself in the way which can potentially cause problems especially if the weather conditions are windy. A weighting of 7% was applied to this criterion.

3.6.7 Centre of Gravity

VTOL UAVs best operate when the CoG is in the centre of the horizontal plane (set 1). A CoG which is central to all axes ensures that all propulsion systems are working equally and that power is distributed equally. Having a perching system

which disturbs the CoG is very undesirable (set 3) and can lead to unwanted fight regimes. This criterion has three sets, which has a grading of 10, 5 and 0 which applied to sets 1-3 respectively. It was also considered to be as important as perchability, therefore given a weighting of 7%.

3.6.8 Complexity

Having a system which can perform a perching manoeuvre with fewer moving parts is more desirable, as it can have a longer operational life, lower maintenance and cheaper to produce. It also may be considered to be more reliable, as its operation becomes less complex therefore given a weighting of 5%. This criterion with four sets determined how the moving parts are assessed. Scoring 10, 7, 4 and 0 the concepts with no moving parts were given the highest score of 10 and the most complex moving part concepts were given a zero.

3.6.9 Engaging/Disengaging Time

The criteria for time taken to achieve the hold and release actions were given the same weighting of 5% as they were equally as important to each other. They both have an exponential scoring system, which as mentioned before, encouraged concepts to complete the task quicker than 6 s see (Figure 3.10). Engaging and disengaging both use quantitative scoring and also share the same scoring graph. The longer it takes for the UAV to achieve the hold, the more likely it is to get blown off course, therefore similarly to mass it is heavily punished the longer it take to execute the perch.

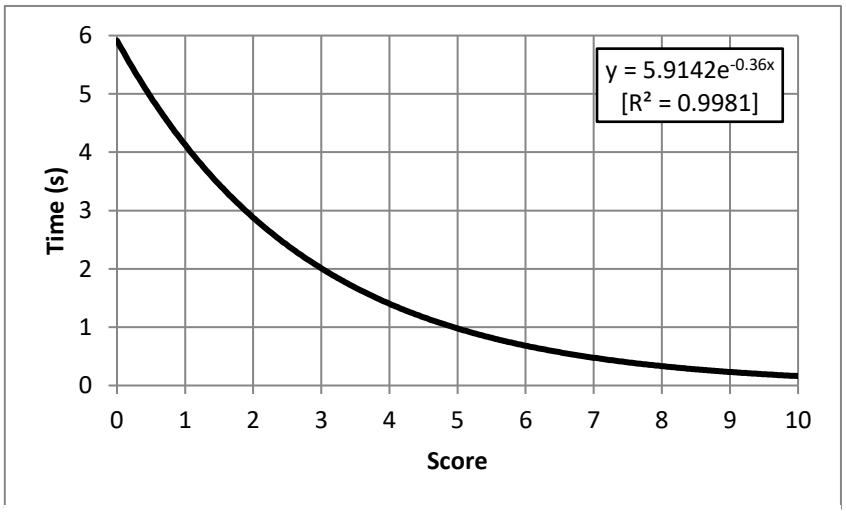

Figure 3.10 - Engaging/disengaging time vs. score.

3.6.10 Volume

This criterion was also given a weighting of 5%, but used a linear scale for the quantitative scoring (Figure 6). The size of the original landing skis fits within the central part of the UAV and in no way was in the prop wash. The aim here was to fit within the central UAV control board and keep clear of the prop wash. For the MK Hexa, this size is 0.3 m diameter and 0.2 m height making a volume of 0.014 m³. A concept with a volume less than 0.014 m³ received a score of five or more.

Figure 3.11 - Volume vs. score.

3.6.11 Operational Power

As the actual operational time of the actuations should be less than 6 s, the operational power, if any, would have little impact on the overall runtime of the UAV. This is criterion is closely linked with engaging time as the longer it takes to execute the perch the more power it will use in. Therefore this criterion was not considered to be the most important and is reflected in the weighting score of 2%, but still important enough to have an exponential scoring to encourage low power usage see (Figure 3.12).

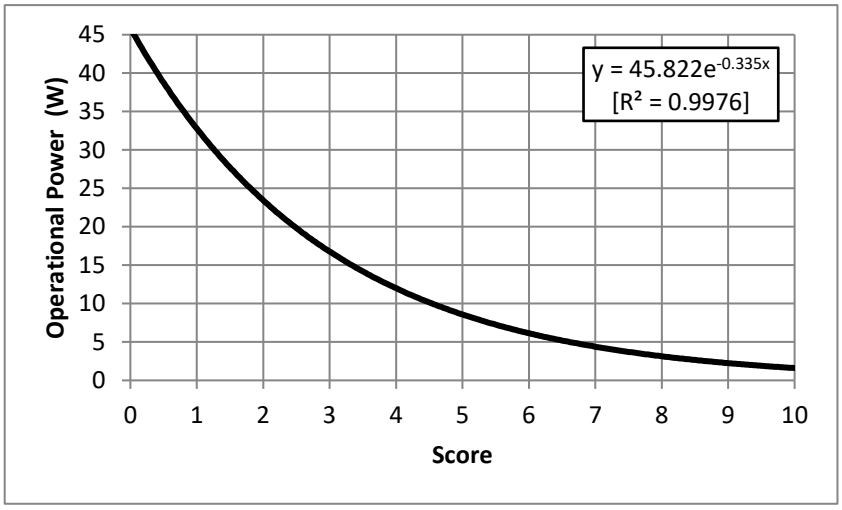

Figure 3.12 - Operational power vs. score.

3.6.12 Multi-Purpose

This category highlighted whether the concept was limited to a certain type of material or terrain. Although the perch site had been determined to be a projection bracket of a lighting column, it is still a desirable aspect to have an option of landing on multiple surface types and materials. With a weighting of 2% it is one of the least important aspects which was split into three sets where set 1 would be capable of perching on more than one type of terrain and various material. Set 2 would be capable of perching on more than one type of terrain or material and finally set 3, where the concept can only perch on one type of terrain or material.

3.6.13 Cost

The least important criterion with a weighting of 1%, had minimal effect as it should not be a major driving point which could suppress the creativity of the concept. A budget of £350 to source the materials and actuators for the gripper and any other fixtures. This figure was set due to other accessories which are available for UAVs such as gimballed cameras, wireless camera systems were also in this price bracket. This made the perching element an attractive addition to any UAV of this size. This final criterion was also given an exponential scoring system which encouraged interesting concepts with minimal complexity (Figure 3.13).

Figure 3.13 - Cost vs. score.

3.7 Final Design

As Concept 3 (The Claw) gained the highest score in the weighted matrix, the modelling was taken to the next stage using a SolidWorks Computer Aided Design (CAD) model. Before a CAD model was created, a more detailed prototype

Figure 3.14 - The Claw design model gripping the projection bracket (a more detailed Lego prototype).

was made in order to understand how the assembly would be done and how it would interact with the projection bracket (see Figure 3.14).

The Claw, with a score of 789 out of a possible 1000 was chosen to move forward with its development. In order to improve this score, close attention was paid to the criteria in which it could have scored higher. Concepts which had a higher score in those categories were examined for inspiration. The Claw originally had straight legs which wouldn't allow the grasping of larger diameters. The hooking design of the 'Slider' was implemented onto the end of each leg which enables The Claw to grasp larger diameters and also aids in self-aligning of the legs onto the projection bracket.

3.7.1 Initial Model

Using a block diagram of the UAV (see Figure 3.15) the forces acting on the UAV due to wind and gravity could be calculated. The next step was to understand the forces which the perching element had to overcome due to these forces acting on the UAV therefore a free body diagram was created (see Figure 3.16).

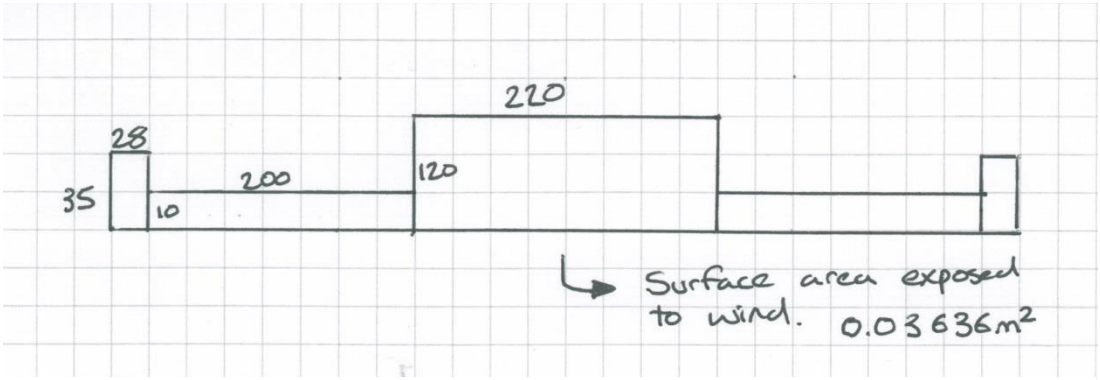

Figure 3.15 - Surface areas of UAV used in blocks to simplify wind force calculations.

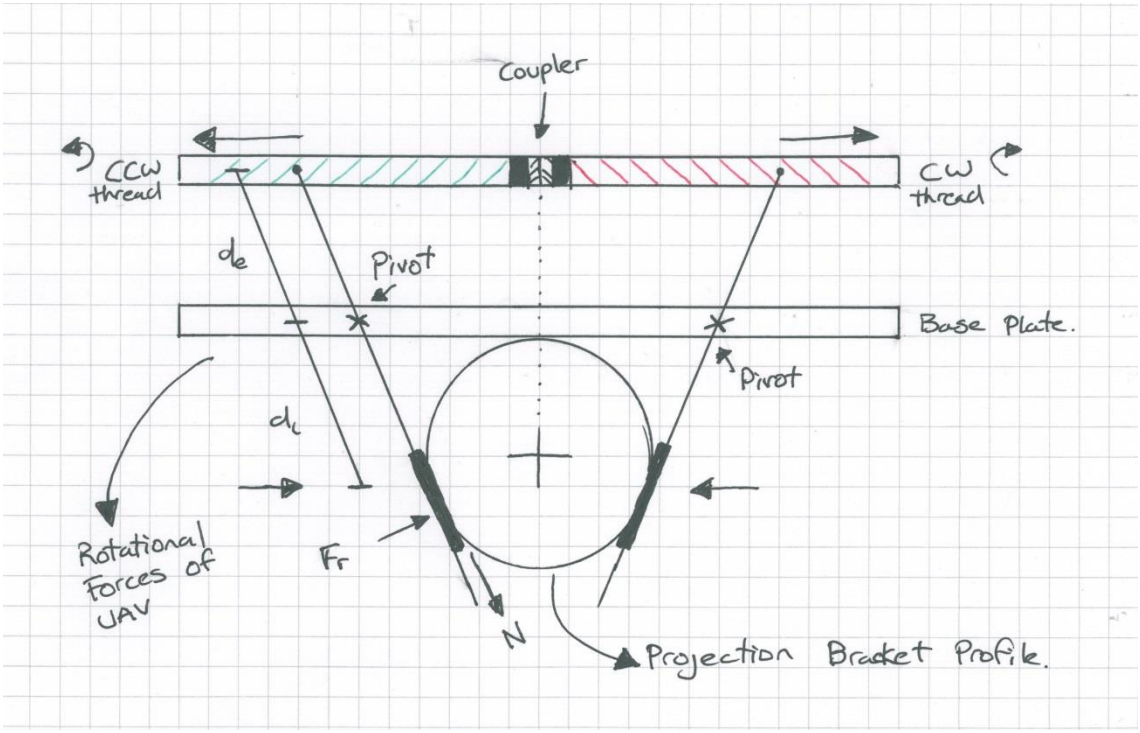

Figure 3.16 - Free body diagram of forces which will be used to calculate various design aspects such as motor selection, lever lengths, pitch angle etc.

A physical model was created based on the original concept sketches. Difficulties with the gear mesh between the motor bevel gear and the non-backdrivable screw thread were encountered. The perpendicular setup of the motor to the non-backdrivable screw thread (see Figure 3.17) had problems. This

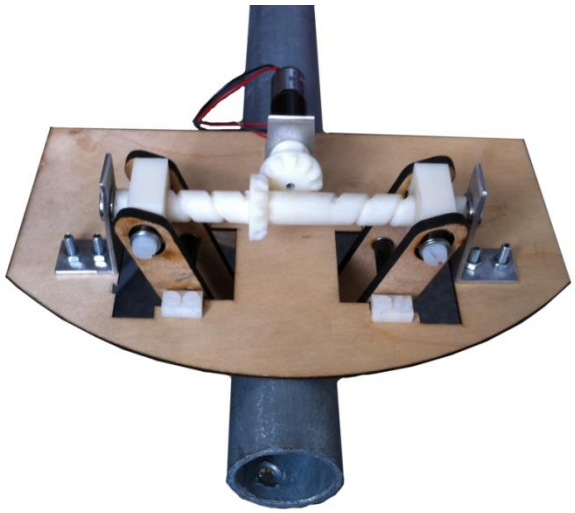

Figure 3.17 - Original design showing bevel gear used for power transfer. (Prototype showing one half of the design only).

configuration allowed the bevel gear to slip and was un-able to provide the required forces to hold the gripper in a hold stance. This was partly to do with the materials used for the prototype along with the lack of support for the motor bracket and the pitch of the non-backdrivable screw thread. According to Controzzi, the use of this type of screw thread was to ensure that once the grip is accomplished, the motor and screw thread will be able to hold the grip without being driven back (non-backdrivable) (Controzzi et al., 2010). To improve the grip and reduce slippage, a different configuration was used.

It's worth noting that at this stage in the design phase the dimensions which were selected was so that the perching element will comply with majority of the projection bracket sizes available. The legs design is optimised for 75% of the common projection brackets available in the UK. From the separation distance of the pivot points of each leg to the height of the non-back drivable screw thread, all were optimised to allow for a low profile mechanical actuation with maximum effectiveness. The shape of the legs were a compromise between opening up wide enough to accommodate a misalignment with the projection bracket during wind guest or descending, along with enough material to provide a stable foot print when it had landed on flat ground.

3.7.2 Motor Selection

With the mass of the UAV determined, the mass of the perching element estimated and using the approximate wind speeds of the UK, the estimated forces the perching element required were calculated. The mass of the UAV and perching element worked out to be approximately 1.5 kg and the wind speed used to work out the disturbance forces was 4.6 m/s as this is the average value for wind in the UK according to Met Office UK, Windfinder and Ordnance Survey (Windfinder.com, 2014, Met Office, 2014, Ordnance Survey, 2014).

To determine the motors which will be used to drive the gripping mechanism, the forces acting on the UAV were calculated. Factors which affected the UAVs ability to sustain the hold were wind speeds, size of projected area which the wind blows against, gravity, drag coefficients, mass, density of air, resistive forces between the interacting surfaces and leverage gains. Due to the non-uniform problem produced by this kind of system, some parameters were estimated. In most cases the numbers used were the worst case scenarios. This

way the gripper was prepared for normal operational conditions along with more extreme situations.

First the drag forces acting on the UAV were calculated using eqn (1):

$$F_d = \frac{1}{2}\rho v^2 A C_d \quad (1)$$

Where:

F_d = Force drag = Force against the projected surface of the UAV (N)

ρ = Density of air (kg/m³)

A = Projected area of object which air is blowing against (m²)

v = Wind Speed (m/s)

C_d = Drag coefficient (dimensionless)

Using 4.6 m/s for v, as this is the wind speeds at 10 m above ground level (AGL), the force acting on the UAV created a turning force due to; the wind eqn (2) and due to its mass eqn (3):

$$T = rF_d \quad (2)$$

$$F_d = ma \quad (3)$$

Where:

T = Turning moment (Nm)

r = Radius (m)

F_d = Drag force (N)

m = Mass (kg)

a = Acceleration (m/s²)

The force which the gripper legs must exert onto the projection bracket is 0.92 N to stay on the bracket projection at 4.6 m/s, which answers the research question: What forces are required to sustain a perch under various environmental conditions? 2.32 N is required for wind gusts up to 28 m/s. To

work out the resistive forces between the gripper and the projection bracket eqn (4) is used:

$$f_r = \frac{Fr}{N} \tag{4}$$

Where:

f_r = coefficient of friction (dimensionless)

Fr = Resistive forces (N)

N = Perpendicular force (N)

Using a value of 0.75 (Fenske et al., 2006) for the coefficient of friction between steel and rubber, this is what the gripper finger will be lined with, which is the mid value for static hold. The force required to hold the UAV in place at the given parameters is 0.69 N.

The contact point and the point of actuation has a leverage affect which when using eqn (5), the force is 0.65 N.

$$F_e = F_l \frac{d_l}{d_e} \tag{5}$$

Where:

F_e = Effort force (N)

F_l = Load force (N)

d_l = Distance of load to pivot point (m)

d_e = Distance of effort to pivot point (m)

Now that the force at the non-backdrivable lead thread has been determined, this force has to be converted using eqn (6) to work out the torque of the motor required.

$$F_u = Ftan(\alpha + \rho) \tag{6}$$

Where:

F_u = Torque (Nm)

F = Linear force (N)

α = Angle of thread pitch (deg)

ρ = Coefficient of friction

In this case the coefficient of friction was the 3D printed parts contacting the surface of other 3D printed parts Acrylonitrile Butadiene Styrene (ABS) onto ABS was 0.35. Using eqns (1-6), the required torque of the motor is calculated to be 0.12 Nm. A excel spreadsheet was created to calculate the forces needed to overcome the forces acting on the UAV in various conditions (see Appendix C).

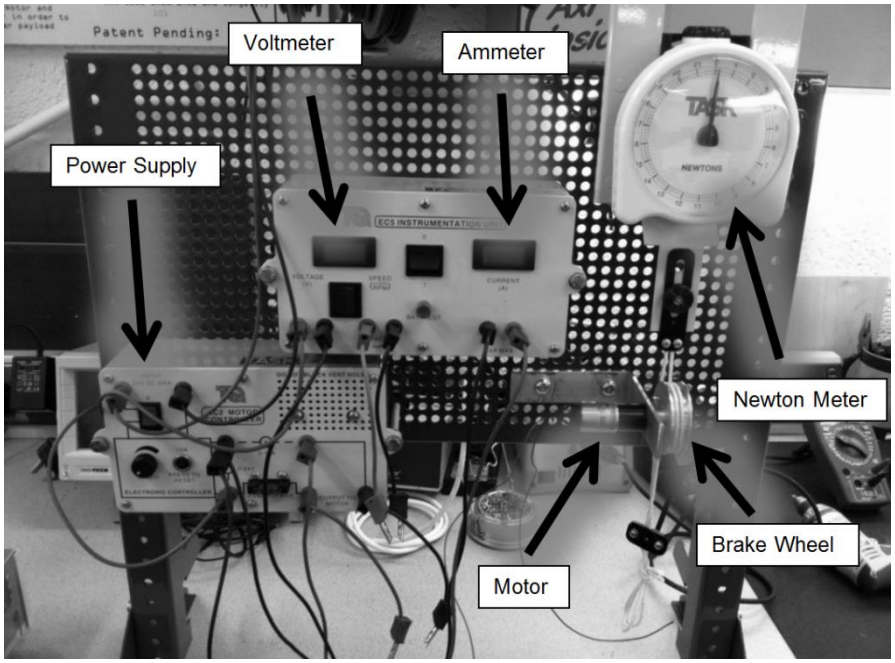

Figure 3.18 - Motor torque testing with a brake wheel setup.

3.7.2.1 Motor Testing

With an approximate idea of how the motors must operate, a Maxon motor was selected. A motor test was conducted using TecQuiment motor torque tester to confirm the specification of the acquired motor (see Figure 3.18) (Tecquipment, 2013). The results in Figure 3.19 proved that the RE-max motor model: 221012 with a 10:1 planetary gearbox would be appropriate for the task. The Maxon motor has torque constant of 0.11 Nm/A and a stall current of 4.25 A which equates to a stall torque of 0.463Nm.

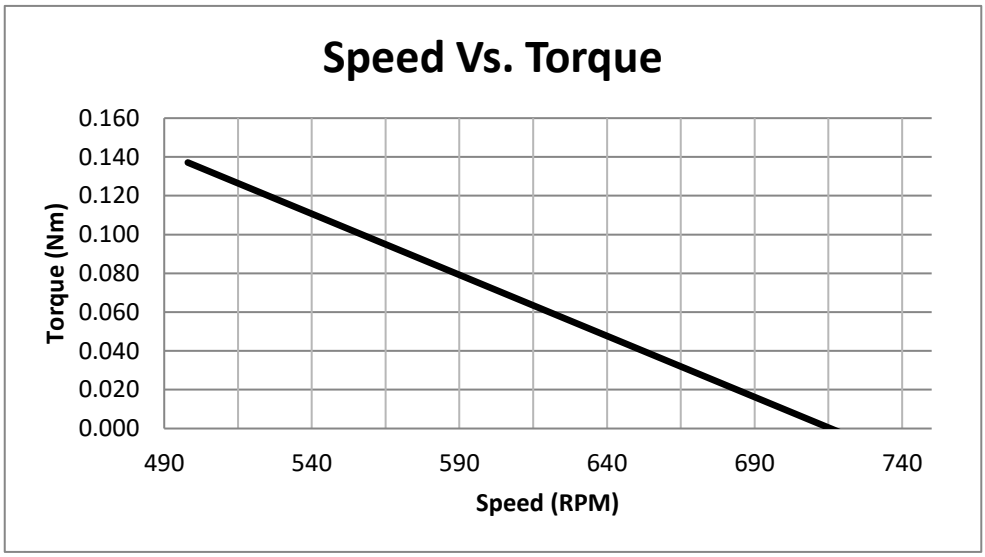

Figure 3.19 - Results of the motor torque tests using the average over 3 sets of results. Maxon RE-max model: 221012.

3.7.3 2nd Attempt

As can be seen in Figure 3.20 the motors were placed in parallel to the non-backdrivable screw thread. The pitch on the screw thread was also decreased from 10 mm to 5 mm to ensure that the non-backdriving screw did not loosen

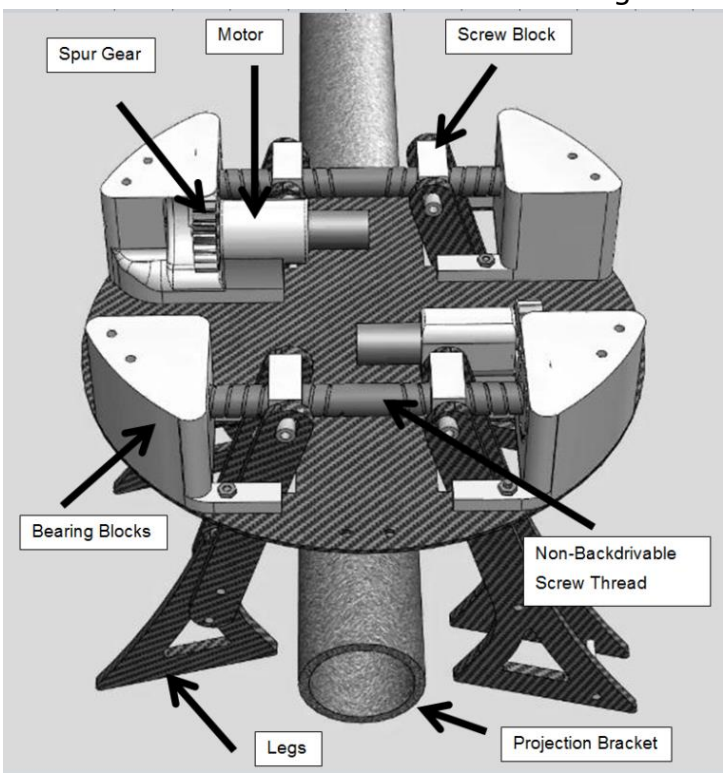

Figure 3.20 - CAD image of mechanism design.

up. As the motor drives the perching element's legs into the projection bracket, the tension between the symmetrically moving screw blocks and the screw thread would ensure the hold to be tight and not loosen when power is cut to the motors. With a more reliable design, calculations were made to work out what properties the motors require in order to hold the UAV in place during 4.6 m/s wind speeds with a leeway for high wind gusts.

3.7.4 Final Gripper

Materials typically used in the construction of UAVs are lightweight yet strong. Carbon Fibre is very popular as it is also used in the automotive motorsport industry as it has outstanding properties under high levels of stress. There are various different composites used to construct the gripper. The base plate and top plates were made out of 1.5 mm thick pre-impregnated carbon fibre sheet which was cut out using a water jet cutting machine. The legs were cut using the same method but out of 4 mm foam cored carbon fibre. The advantages of using foam cored carbon fibre were that whilst maintaining a light weight construction, it was also thick enough to have the appropriate support when gripping. By removing the foam core at the interacting point along the legs, a section of rubber was inserted to aid the hold when the legs close. Rubber was chosen due to its high coefficiency with steel (Fenske et al., 2006, Roth et al., 1942). The non-backdrivable screw thread, driving blocks and bearing blocks were all

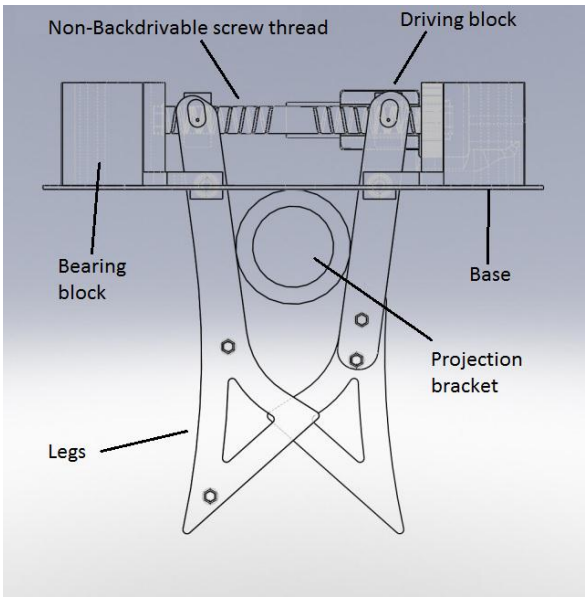

Figure 3.21 - Cross-sectional view of 'The Claw' with main parts being labelled and such labels being used throughout this thesis.

printed out on a 3D rapid prototyping machine using ABS plastic. Figure 3.21 highlights the labels for the parts with Figure 3.22 showing the fully assembled gripper.

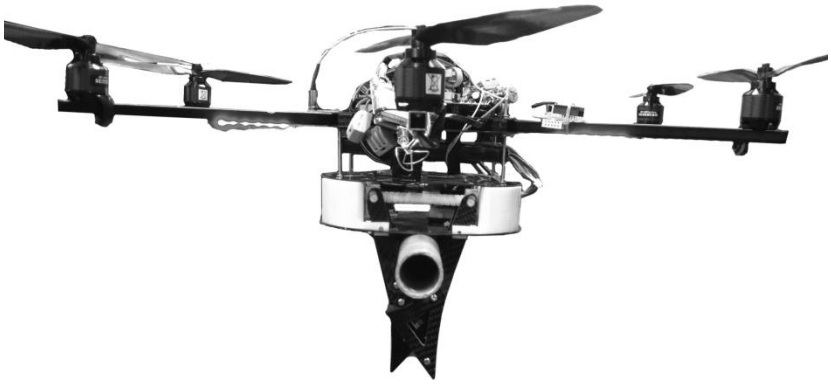

Figure 3.22 - Fully assembled gripping prototype on projection bracket.

The final prototype mass was 420 g with an engaging and disengaging time of 0.5 s, which validated the scoring of the weighted matrix. Due to its independent control of each claw unit, the gripper can also grasp projection brackets with varied taper.

Some of the criteria's such as cost, volume and operational power have increase as these aspects were slightly out, where engaging and disengaging times have decreased. Weighing in at 420g, the perching system equates to about 22 % of the total UAV mass which decreases the 35 minute endurance to 25 minutes. With a surveillance mission usually consisting of hovering wouldn't be much of an issue as it can perch to reduce power consumption therefore increasing mission endurance.

3.8 Summary

The design optimisation process has demonstrated that a reconfigurable perching element can be designed to perch on a range of different sized projection brackets currently found in the urban environment, which truly demonstrates the reconfigurable aspect of this chosen concept (see Figure 3.23). The design optimisation methodology, involving a weighted matrix approach, has led to the creation of a novel gripper, which can perch onto existing street furniture. This method has been validated with a working prototype, which scored highest overall, gaining approximately 2% more than the nearest

alternative. The top of a lighting column which holds the luminaire unit on the end of a projection bracket was found to be an ideal location for surveillance UAVs to be able to perch to conduct extended surveillance and reconnaissance missions (Erbil et al., 2013). The multi-functionality of the design has been proven with its ability to replace the existing landing gear as can be seen in (Figure 3.23) in its landing stance. The mass target has also been met, weighing in at 420 g, which was the predicted mass. By utilising a non-backdrivable screw thread design for the actuation, the scores given to the emergency landing and idle power criteria have been justified. 'The Claw' is always in a ready to land

Figure 3.23 - Gripper attached to UAV platform in a landing position.

stance and only initiates the gripper when required to land on a projection bracket. As it doesn't require any additional power to sustain the grip, it was rewarded the highest score in the idle power criterion. Its low profile and compactness ensures it is not affected by environmental conditions, such as wind. Also this design has little effect on the overall system's CoG. The mechanical design consists of levers, gears and screw thread mechanisms, which keeps the complexity down with minimal moving parts. As the UAV approaches the perch site from above, it also meets this requirement which was set in the PDS. It's fast engaging and disengaging time of half a second is a desirable capability as it ensures a rapid attachment without wasting any unnecessary endurance time. The leg design allows each leg to hyper-contract into the other leg without colliding and preventing a tight grip as can be seen in Figure 3.22. This three finger approach was adopted from nature's bird claw designs.

4. Experimental Hardware

This section breaks down how the test-rig was developed along with details about the platform which is used to test the perching element. The test-rig had several criteria which determined how the final test procedures will take place.

4.1 Test Platform

In order to conduct tests on the perching element, a platform which can carry the load and still remain agile was needed. The chosen platform to be used for testing is going to be the HEXA platform from MikroKopter.

4.1.1 MikroKopter HEXA

The MikroKopter (MK) HEXA platform is a multi-rotor unmanned system which can either be remotely operated or given GPS commands to automatically control it's movement (see Figure 4.1). It can either be used as a recreational remote controlled (RC) model or to carry a payload which can be useful to the operator.

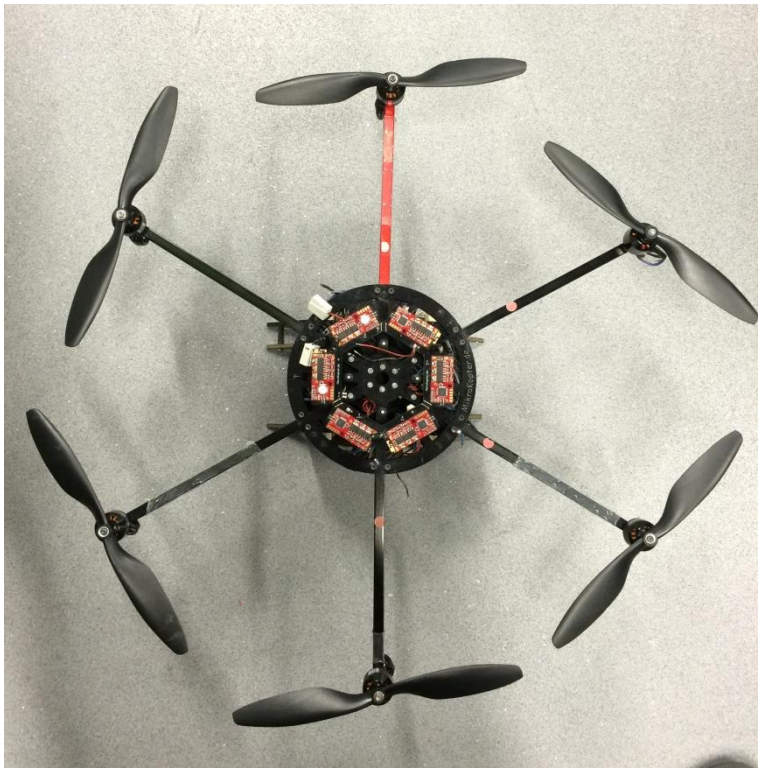

Figure 4.1 - MikroKopter multi-rotor platform from above with the red arm indicating the nominal forward direction.

Common payloads such as stills cameras and video cameras give the UAV the functionality of acquiring images which otherwise would be impossible or too expensive. It weighs just 1.4 kg with the provided battery and measures in at 250 mm high and 808 mm from blade tip to tip. The 1 kg payload of the HEXA makes it very attractive to researchers as it can carry experimental payloads, which was another reason it was chosen for this research.

4.1.2 Anatomy of MK HEXA

The decision to use the multi-rotor with six rotors over the more readily available four rotors (quadrotor) was due to the redundancy which the six rotors have to offer. Due to the nature of this research, the use of a highly efficient and highly resilient system was necessary. Until recently, a quadrotor system was un-flyable if any one of its rotors fails, whereas a UAV with six or more can continue to remain in the air in a controlled manor. The most recent work from the 'Flying Machine Arena' at ETH Zurich is the development of a failsafe algorithm which is able 'catch' a falling UAV from the sky uncontrollably with the loss of one, two and even three propellers (Mueller and Andrea, 2014, Andrea, 2013). Although

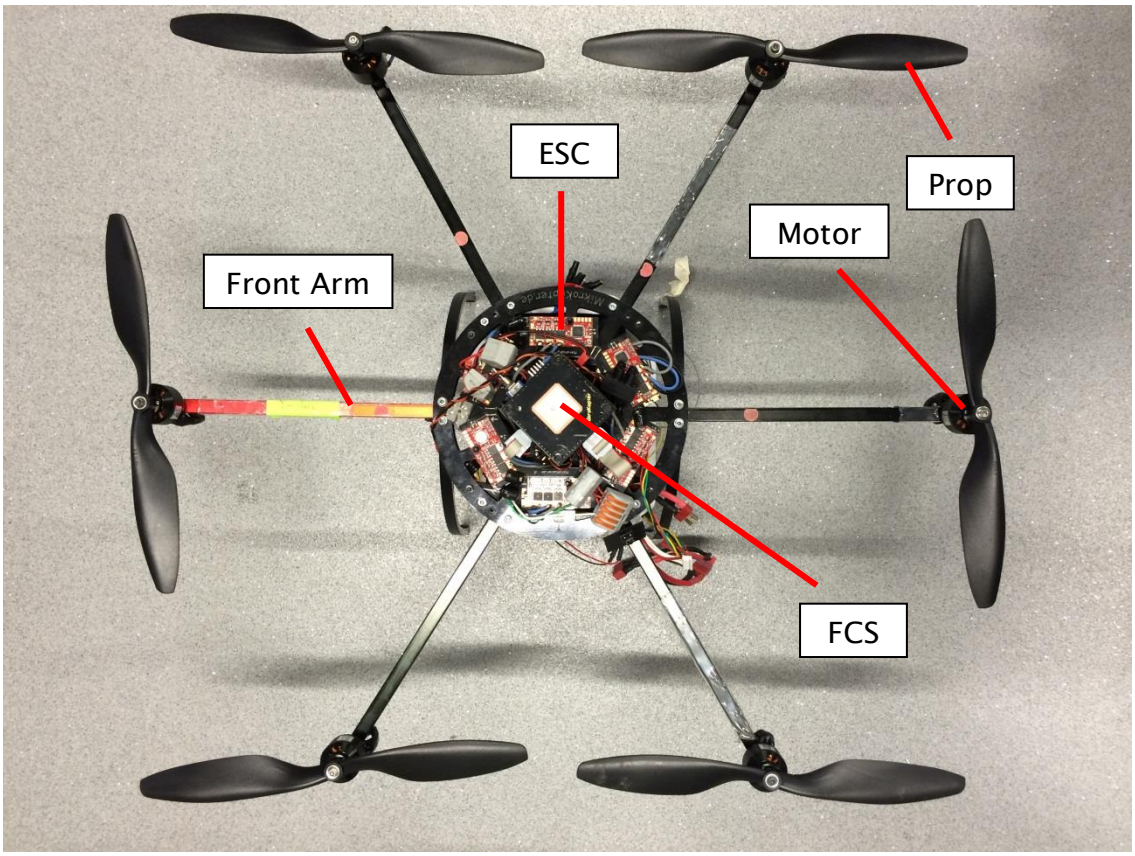

Figure 4.2 - Aerial view of MK HEXA detailing the major components.

the UAV does spin due to the un-balanced torque, it is able to land with less impact. The HEXA's six arms, motors and propeller configuration allows for a more controlled descend. These six arms are all attached to the central part of the chassis which houses the flight control system (FCS) and electronic speed controllers (see Figure 4.2).

The red arm [1] indicates the front of the UAV which is the direction of forward flight. This arm along with [3 + 5] have a 10 inch counter clockwise propeller attached with arms [2, 4 + 6] have clockwise attached. The flight controller in the centre of the chassis has a multitude of sensors to measure the positional movements of the UAV. These sensors are:

- Accelerometers
- Gyros
- Barometric pressure
- GPS
- Compass

Below the chassis is where the battery sits, which isn't visible in Figure 4.2. The battery is able to slide in and out easily allowing the user to swap batteries when needed and is held in place with Velcro straps.

4.1.3 MK HEXA Specifications

The table below details the multicopter's specification.

Table 4.1 - MikroKopter factory specifications.

Flight Time (no payload):	25 minutes
Mass (with battery):	1.480 kg (1.105 kg without)
Payload:	1 kg
Pitch Circle Diameter:	0.555 m from motor centres
Prop Size:	10"x4.5" GWS
Motors:	2832/35 Brushless outrunners
Battery :	Vislero 14.8 V Li-Po @ 3300 mAh

4.1.4 Interfacing with UAV Controls

In order to control the MK HEXA, the FCS must be accessed on board as the processing will be done on the UAV. To find the least intrusive and most reliable control lines, an understanding of the FCS had to be gained. According to the manual, the most effective point to input signals into the FCS was the PPM line from the receiver into the FCS (see Figure 4.3).

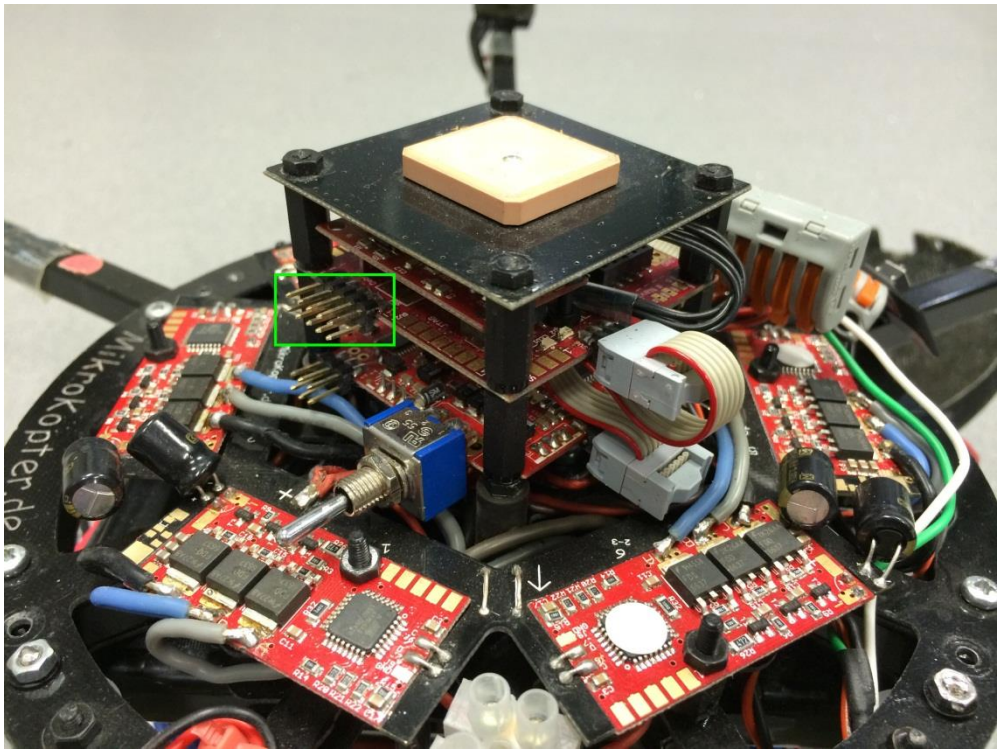

Figure 4.3 - Connection point on UAV which were accessed to gain controls highlighted with by the green box.

4.1.5 Extracting Data from UAV

To extract data such as positional control of the UAV (i.e. accelerometer/ gyro/ altitude data), the best point was from the 10 way port which outputs serial data to either the Navi board or when grounded, the MK USB cable.

4.2 Multi-rotor Theory

As a multi-rotor was being used to facilitate the experiments, understand some of the theory behind the platform was desirable. This ensured that any issues which may arise due to platform instability, could be trouble shot with ease.

4.2.1 Multi-rotor Flight Control

A conventional fixed wing UAV has its rotors in a vertical plane which propels the UAV forward producing lift over the wings. A multi-rotor has multiple rotors typically in the horizontal plane to produce the required lift. The MK HEXA uses six rotors which are placed at the tip of the equally spaced out arms. Each arm is spaced out at 60º from one another and has the brushless out-runner motor with ten inch fixed pitch propeller combination. As mentioned before, the even numbered arms 2, 4 and 6 (see Figure 4.4) have clockwise spinning propellers and the other odd propellers spin counter clockwise. This three and three combination ensures that the rotational torque is in equilibrium and the UAV doesn't spin out of control. To control the yaw of the UAV, the speed of either set of rotors can be increased or decreased to gain the desired rotation. Pitch and roll control is achieved through the increase of speed about the central direction lines. The black dashed lines highlight rotors which change the roll of the UAV and the green dashed lines changes the pitch of the UAV. To achieve the desired flight isn't as simple as sending signals from FCS to the propellers. Other important components such as motors, electronic speed controllers are required.

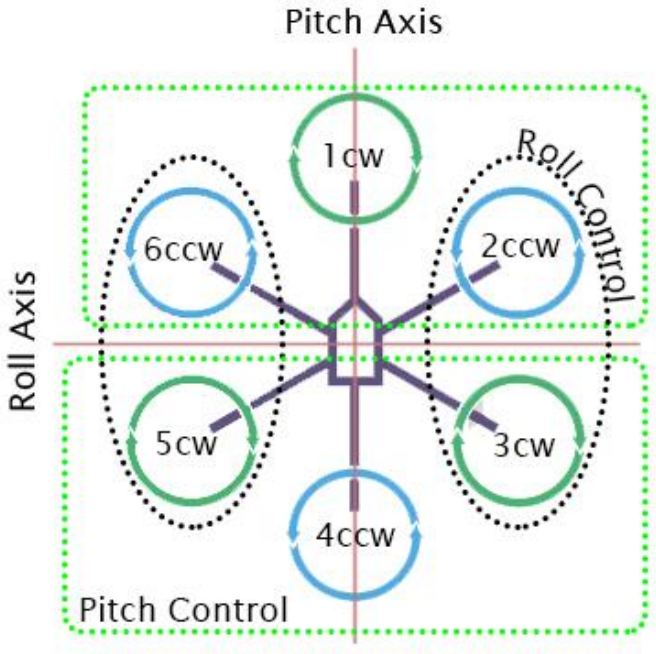

Figure 4.4 - Hex + configuration highlighting the motor numbers, rotational direction of each motor and coloured zones which give the desired motion of roll, pitch and yaw.

4.2.2 Brushless DC Motor Theory

Brushless direct current (BLDC) motors operate slightly different to that of a traditional brushed DC motor. The end result of a spinning shaft and materials used are common features which both brushed and brushless share. The brushed motor has a spinning rotor with two coil wrapped around an iron core and is often called a stator. As the current flows through the coil, it effectively produces an electromagnetic field which either repels or attracts the magnets on the inside of the motor casing, and therefore creating a spinning effect. However, brushless motors operate with similar components, just in a different setup. The stator is stationary and is on the inside of the motor casing and the spinning rotor has the magnet attached. The control of each setup is also different, which is covered in electronic speed controller theory. The main physical differences between brushed and brushless are the number of wires which are used to drive the motor. Brushed has two wires where brushless have three. This is down to how the current flows through the wires. The brushed motor gets its name from the fact that it uses carbon brushes which have to make precision contact with the spinning commutator attached to the stator to drive each coil. This contact often causes a build-up of heat due to the sparking of the brushes against the commutator along with friction. The more efficient brushless motor doesn't have this heat and friction problem. As the name suggest, the brushless motor does not rely on physical contact between the coil and rotor. By passing currents through the three coils, it creates the same rotational forces on the rotor with magnets. Brushless motors can have the magnets on the inside of the coil or outside, which is where the name inrunner and outrunner motors come from. The inrunner motor can achieve greater revolutions per minute (RPM) than the outrunner. But the outrunner has the advantage of being torquier (Pillay and Ramu, 1989) (see Figure 4.5).

The motors on the MK HEXA are outrunners as they have to be able to spin the propeller which sits directly on the rotor, which makes them 'Direct Drive Brushless DC Outrunner'.

The coil spark sequence which is detailed in Figure 4.6 shows the order in which the current is passed down the wire. The control compromises of six stages in which the polarity is switched between the wires. By adjusting the speed at which

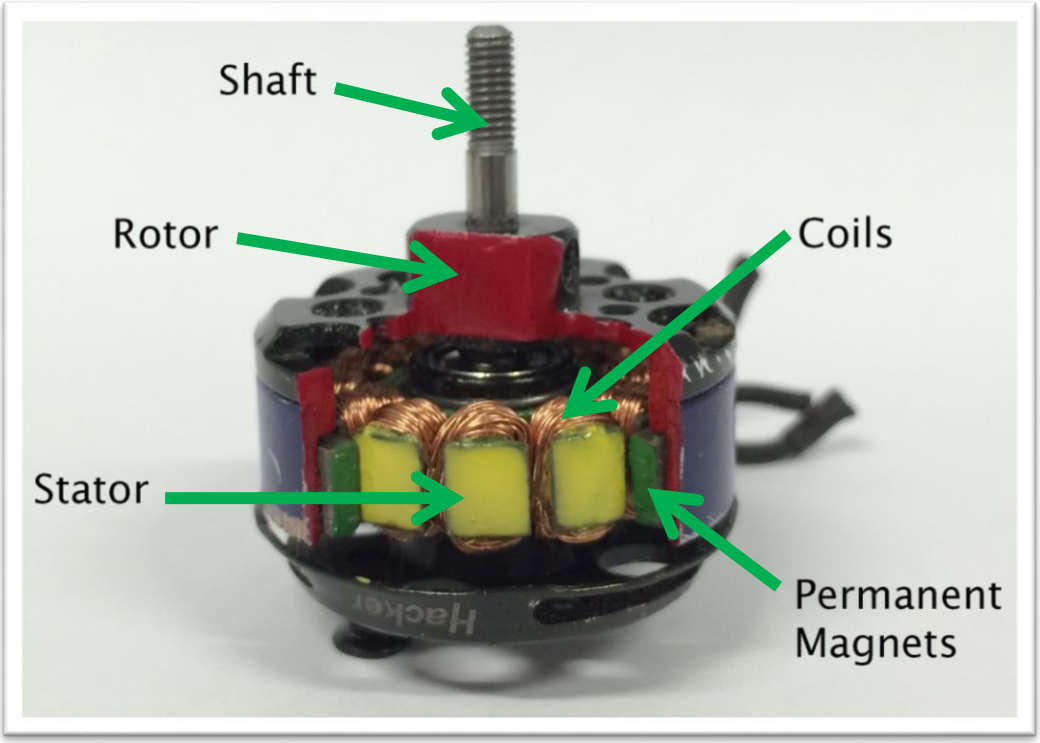

Figure 4.5 - Cross section of DC Brushless Outrunner motor, stator (yellow) with exposed coils (gold) and rotor (red) with magnets (green) attached to the inside of the shell.

they are switched the RPM of the motor increases or decreases. The performance of a brushless motor is determined by factors such as:

- Number of permanent magnets
- The air gap in-between the magnets and stator
- Number of coil windings
- The coverage of the magnets
- Number of stators
- Wire gauge
- The phase winding style
- Core material

The two main factors which ensure a fully functioning motor is the number of stators which must match the phases therefore can only be in multiples of three. The other factor is the number of magnets (also referred to as poles) which must be an even number and cannot be a multiple of three otherwise it would have the rotor and stator in a state of equilibrium and lock (Gencer and Gedikpinar, 2006).

Figure 4.6 - Commutation sequence.

4.2.3 Electronic Speed Controller Theory

Without an Electronic Speed Controller (ESC) the brushless motor would be un-useable unlike a DC motor which could run straight off a battery. Due to its stator and magnet setup, the brushless motor requires an ESC which can output a current to all three wires in a predetermined sequence which can be seen in Figure 4.6. An ESC usually is in the form of a small print circuit board (PCB) with two sets of input wires, one for power one for control, and three output wires. The size of the ESC is determined by its current handling capability (see Figure 4.7). The input voltage power is usually connected to a battery pack, which in this case a Lithium polymer (Li-Po) battery or can be run off a power supply unit

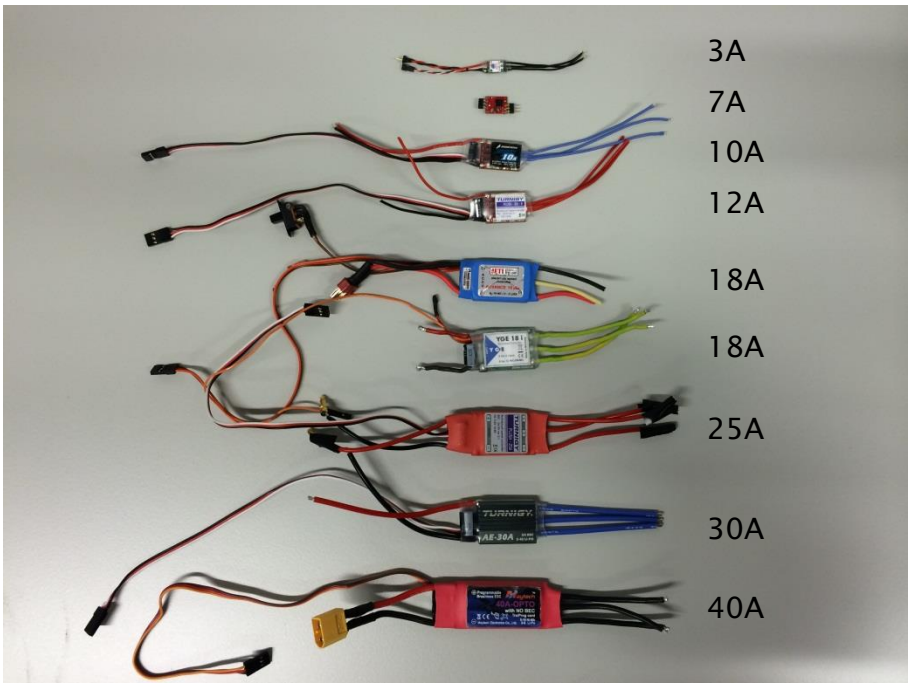

Figure 4.7 - Different size ESC, (top) from 3 A down to (bottom) 40 A.

(PSU). The other input cable is the control from the receiver module which uses Pulse Width Modulation (PWM) to control the speed of the motor. If the settings on the transmitter remain at factory default, the throttle stick on the transmitter should give a linear output to the receiver which in turn will use PWM to control the ESC. The motor speed is controlled by switching the transistors on-board the ESC on and off rapidly to send the current down the wire. The frequency of the on off stage varies between manufactures. Each channel has its own dedicated transistors which controls whether the output is an anode or cathode. The switching speed, also known as duty cycle, determines the responsiveness of the motor control. ESCs tend to have programmable attributes such as the timing of the switching. This function has a critical role when it comes to calibration of ESC to motor. When the motor poles change, so must the timing, which is why it is crucial to match ESCs with the correct motor setup.

4.3 Measurement of Inertia

To understand the forces which the motor and propellers had to overcome to make the UAV move, the mass moment of inertia was calculated using the swinging pendulum effect (see Figure 4.8). Using equation (7), the inertia was calculated to be 0.0399 kgm² for Izz. Where:

g = 9.81 m/s²

m = 1.105 kg

b = 0.2775 m

L = 1.750 m

T = 18.2/10= 1.82 s

$$I = \frac{mgT^2b^2}{4\pi^2L} \tag{7}$$

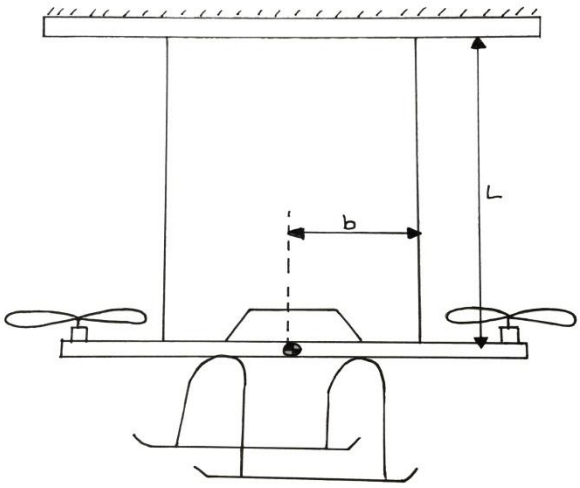

Figure 4.8 - UAV swinging to work out mass moment of inertia using the swinging pendulum method.

For Ixx and Iyy the inertia worked out to be 0.085 kgm². To achieve these results, the UAV was tied up at two points which would create a stable object to begin swinging in the X and Y axis and about Z. The use of the CAD package SolidWorks was also investigated to work out the inertia of the UAV which produced similar results (see Figure 4.9). As can be seen, the CAD model produced an inertial measurement about Izz of 0.045 kgm² where the calculations using the swinging pendulum effect produced 0.0399 kgm².

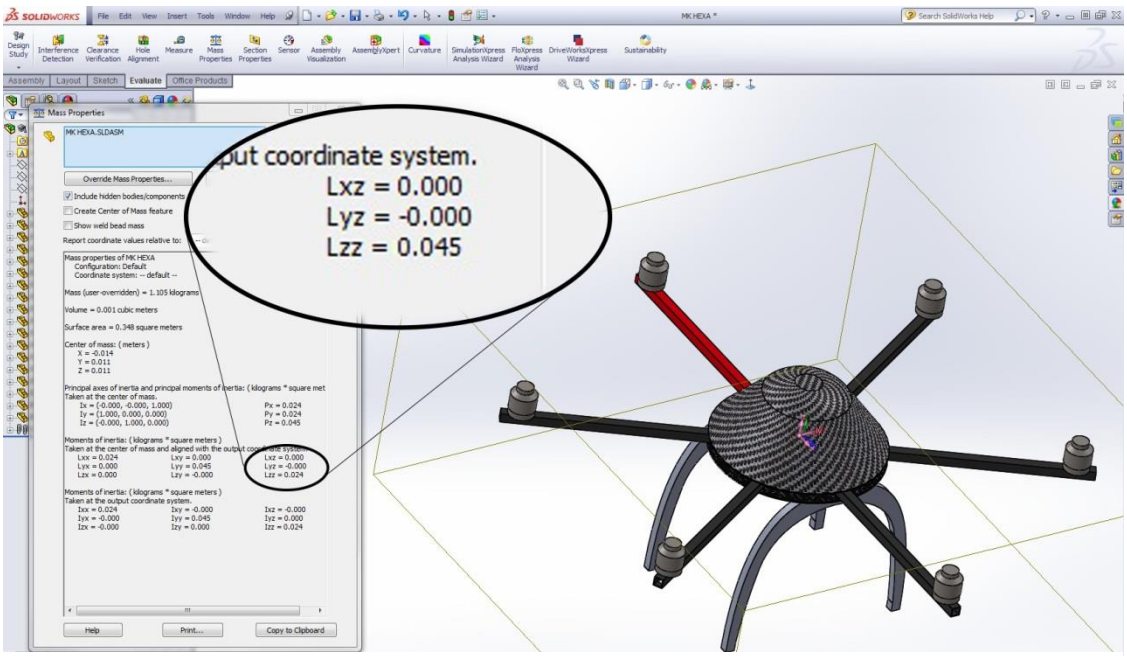

Figure 4.9 - Mass moment of inertia being worked out using a SolidWorks model of MK HEXA with similar results confirming calculations.

4.4 Test-Rig Design

4.4.1 The Need of a Test-Rig

In order to conduct the testing in a safe manner, a gantry style test-rig was required during the development of the search and perch algorithm. Because of the experimental nature of the tests, the rig would allow the UAV to move around freely without hitting the surround people and objects. The implications of having such a rig was the additional constraints put on the UAV by the rig which affected the UAV movements.

4.4.2 Test-Rig Dimensions

The size of the safe fly zone was determined unfortunately by the size of the lab space available. Another issue was the available floor space. Therefore the only option was to have a gantry style rig where it would be attached to the ceiling. Costs were kept low with the use of readily available scaffolding poles which were used to construct the rig. The uniform size of the poles made finding parts for the rig much easier. The final rig which was attached to the ceiling measured 3 m long by 2 m. The distance from the ceiling was determined by the clearance of the lighting rig in the laboratory which happened to be 2.5 m (see Figure 4.10).

The rig allowed for movement in all 6 degrees of motion which is represented by yellow and green runners in Figure 4.10. The blue disc acted as a counterweight, which took the burden of the Z axis off the UAV.

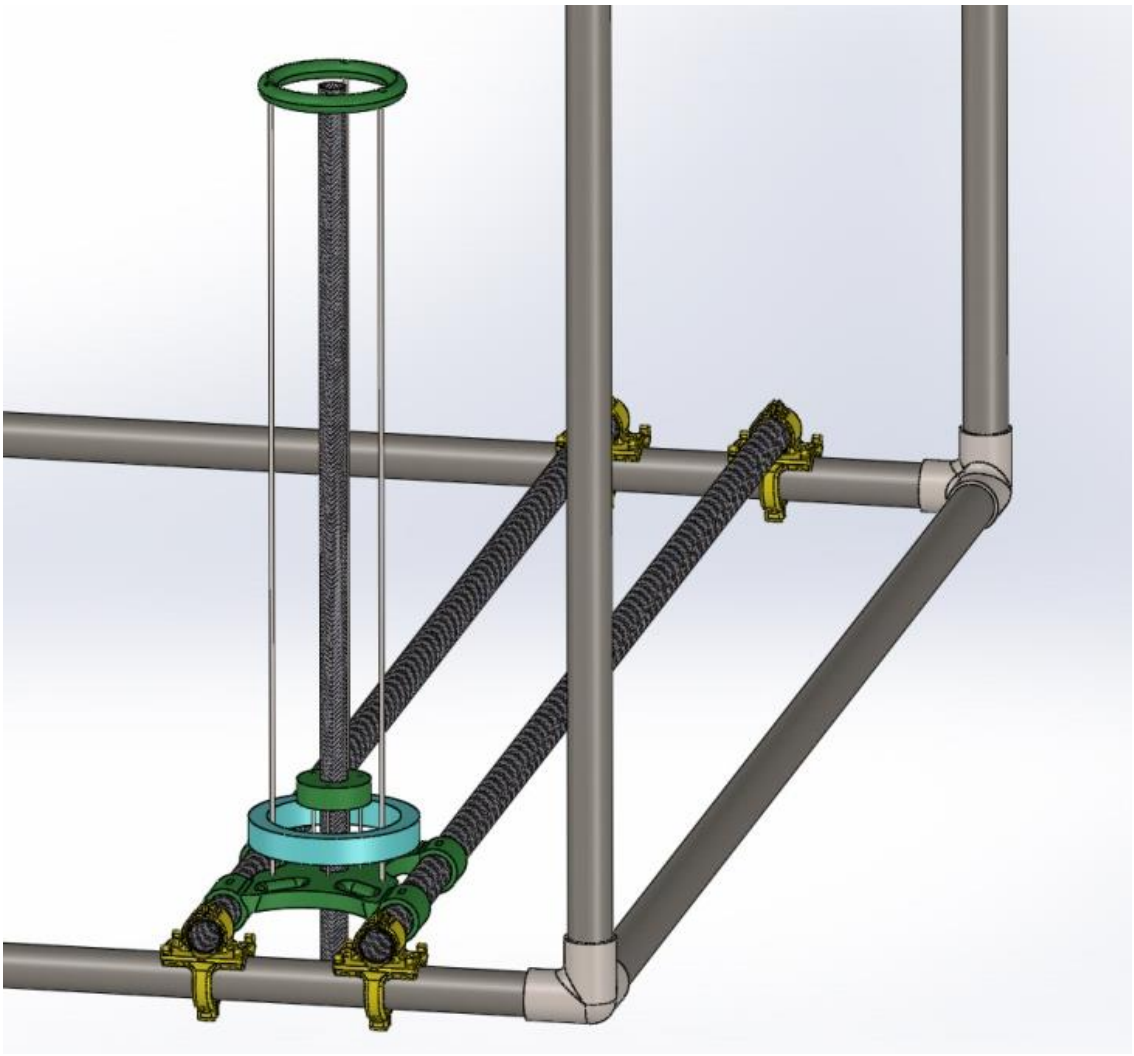

Figure 4.10 - Yellow runners on Y axis, Green runner on X axis, Blue ring is counterweight of Z axis.

4.4.3 Design of the Runners

To ensure that the UAV moved around freely the runners, which guide the support bars along the length of the rig, had to be loosely connected to the X and Y axes poles. Each runner block houses five ball bearings which provided a smooth operation (see Figure 4.11). All three axes had end stops to prevent the UAV from hitting the rig and possibly breaking the 3D printed parts.

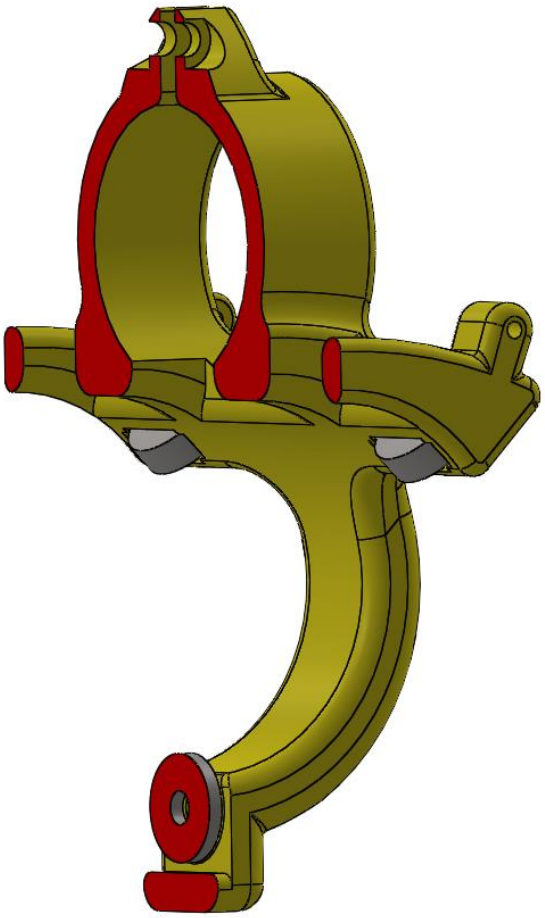

Figure 4.11 - Shows the bearing arrangement of the runners to ensure smooth operation. Red plane represents a mirrored cut away.

4.4.4 Gimbal and XZ Axis

The design of the gimbal and XZ axis runner was a complex procedure as it required great attention to avoid the UAV experiencing difficulties in moving around the rig freely. The X axis runner, which runs along the support bars, held up the mass of the UAV and also the counter weight which offsets the mass of the runner itself, which then ensured that the UAV will only carry its own mass (see Figure 4.12). The Z axis guide tube did limit the free movement of the UAV. Therefore the UAV movements were more geometric rather than being a fluid flow. So this was taken into consideration when trying to program the UAV to move from point A to B. These limitations meant that the UAV moved systematically towards point B. The gimbal mechanism allowed the UAV to move freely about X and Y so that the UAV can push the whole system around the rig. The gimbal also limited the UAV so that the propellers won't make contact with the rig.

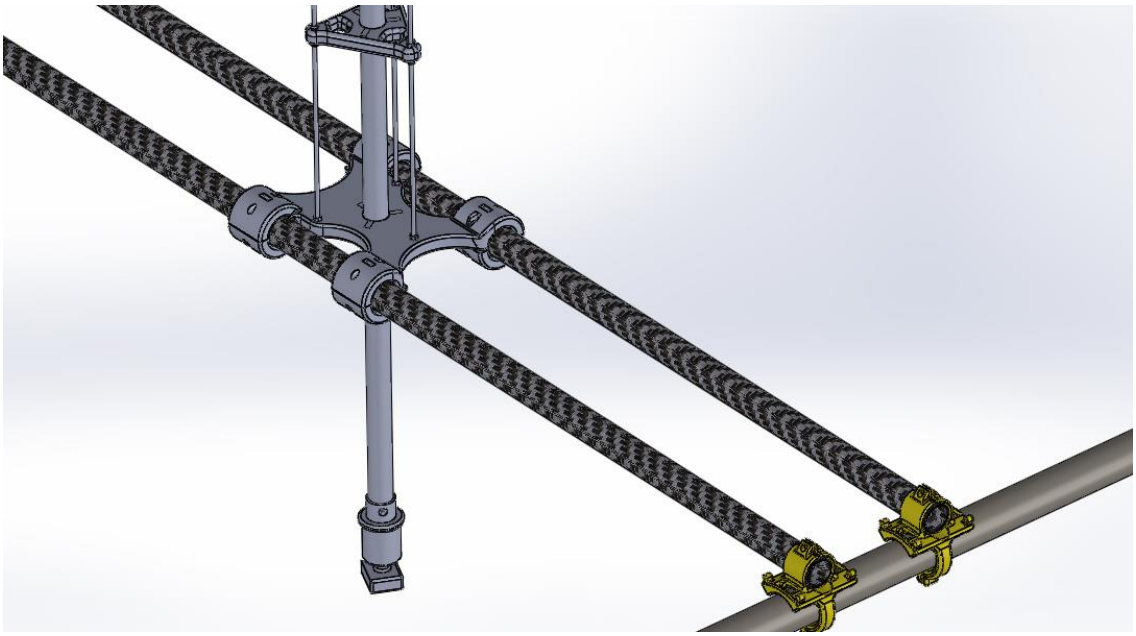

Figure 4.12 - Gimbal and XZ Axis shown on the X axis support bars highlighted in carbon fibre.

4.5 Test-Rig Calibration

To ensure that the rig was installed properly and that the gantry still remained a perfect square rectangle once installed, the rig had the use of lasers and measurement tools to ensure that it was all straight before installation (see Figure 4.13). These rig calibration tools were printed using a 3D printer. Firstly, the rectangular part of the rig was assembled on the floor of the lab and made level using a builders1 meter spirit level (see Figure 4.14). This ensured that when the calibration tool in Figure 4.16 was inserted into the top of the 90º elbow joint of the rig, the laser was pointing straight up into the ceiling (see Figure 4.15). A built in spirit level was also integrated into the calibration tool which allowed fine adjustments to be made until the laser was perpendicular to the floor in the X and Y axis. The laser dot marked the central point for where the ceiling drill calibration tool in Figure 4.17 needed to be placed. This allowed the contractor to simply drill the holes without measuring awkward points on a ceiling. The size calibration tools (corner locators) which can be seen in Figure 4.18 were a guide to help measure the distances between the poles on the ground and laser dots on the ceiling (see Figure 4.19). It ensured that the centre from elbow to elbow was the same distance from dot to dot on the ceiling. This

rigorous process ensured that when the rig was raised into its final position, the rig was straight, level and square.

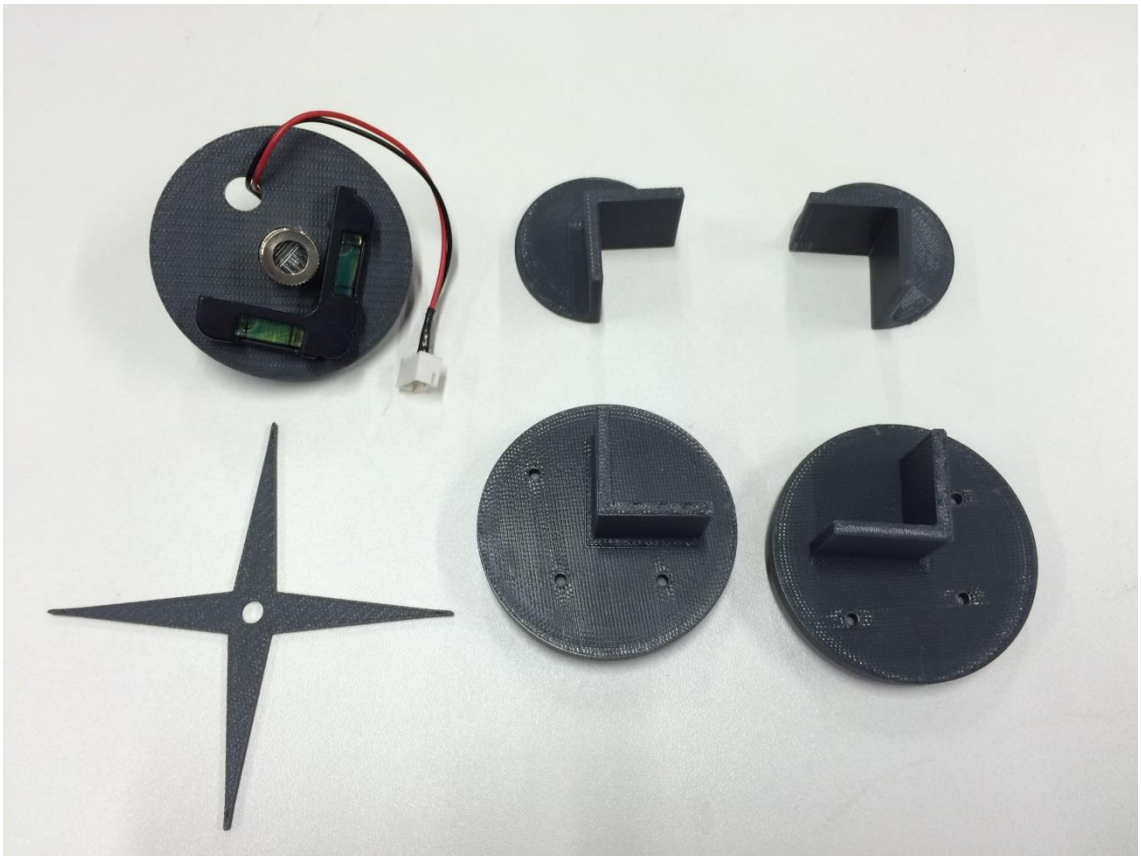

Figure 4.13 - Test-rig calibration tools. From top left clockwise, 1 - Laser corner finder. 2 & 3 - Ceiling corner locators. 4 - Ceiling drill tool 5 & 6 - corner locators.

4.5.1 Test-Rig Measurements

Measurements were taken of the rig whilst it was set up on the lab floor. Attention to detail was essential when cutting the poles down to their correct lengths, as at this stage any errors would have made a significant difference on the efficiency on the runners. Figure 4.20 details the measurements taken using a laser range finder which gave readings accurate to ± 1.5 millimetres (Leica Geosystems, 2016). The two red measurements highlights that the rig was only out by 1 mm (from 2087 mm to 2088 mm) to being a perfect parallel. This 1 mm was an acceptable offset as the runners were designed with an operating tolerance of 3 mm. With a larger taper between the two longer poles, the force required to move the support carbon fibre (CF) poles would be greater.

4.5.2 Forces on Support Poles

Figure 4.21 shows the forces required to move the CF tubes along the Y axis on its runners. To move each individual tube is between 0.1 – 0.14 kg which is the force measured using a strain gauge. This equates to 0.981 – 1.373 N, but when both tubes are pulled together the force required is 2.256 N. This means the UAV will have to overcome these forces in order to move freely which should not be a problem as the MK HEXA has approximately 30 N of thrust to deal with these forces. Once the support poles where installed onto the rig with the XZ runner attached, it provided additional rigidity which reduced the required force to move the support poles along the Y axis down to 1.72 N.

Figure 4.14 - Test-rig set up on floor and levelled out using shims to ensure accurate levelling. Digital level was used to take measurements.

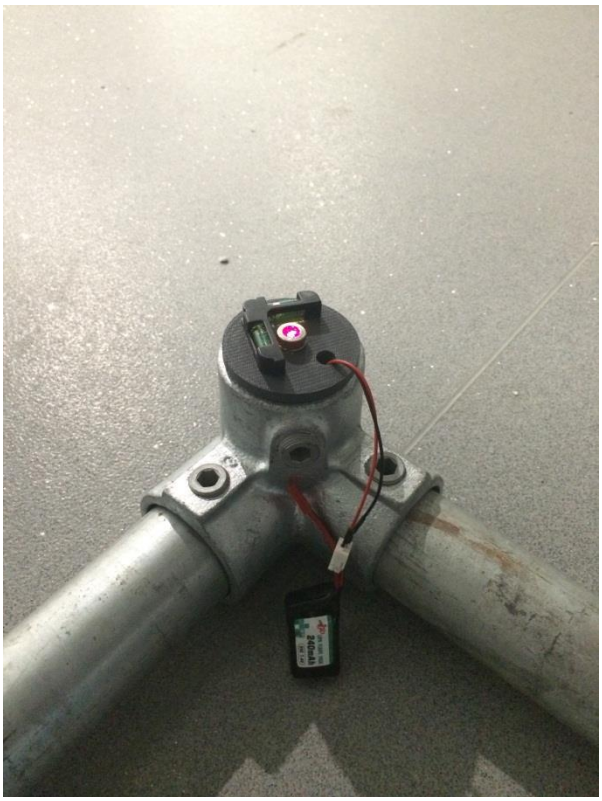

Figure 4.15 - Laser guide lines on the ceiling of laboratory lined up with existing pipe work as an additional guide to ensure rig was installed square.

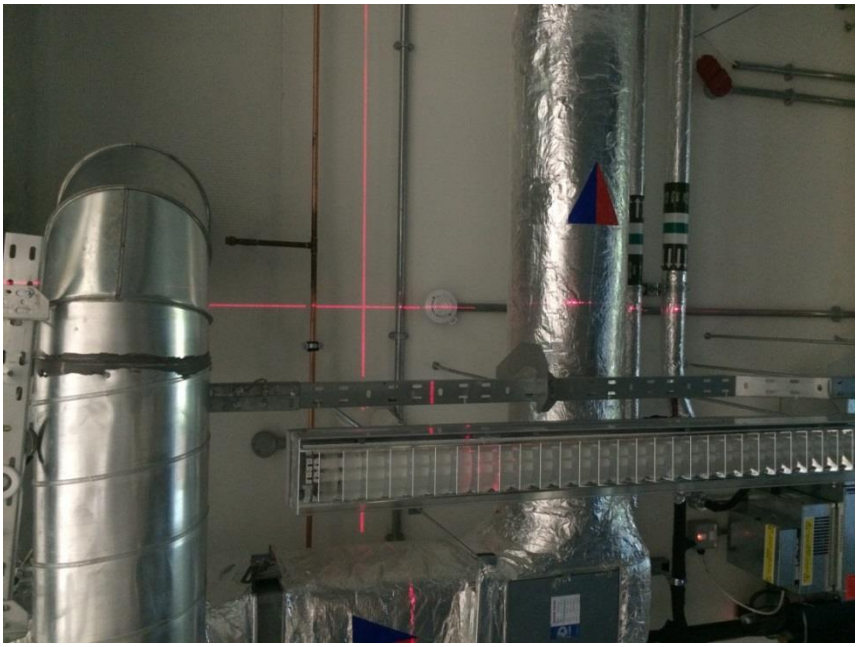

Figure 4.16 - Laser calibration tool inserted into the 90º elbow.

Figure 4.17 - Drill calibration tool which allowed the markings for where the holes needed to be made for the flanged ceiling mount.

Figure 4.18 - Test-rig corner point measuring tool allowed for the laser range measuring device to measure from the centre of the vertical axis of the 3 elbow corner units.

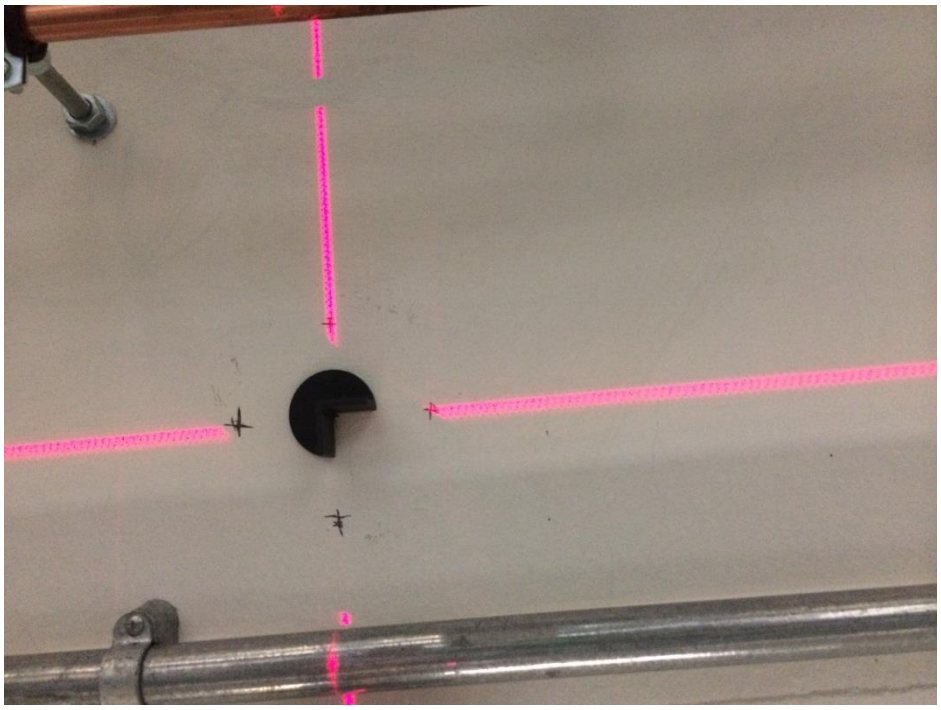

Figure 4.19 - Ceiling drill marking measuring tool which was used to compare the floor measurements to the ceiling which ensured accuracy of the test-rig.

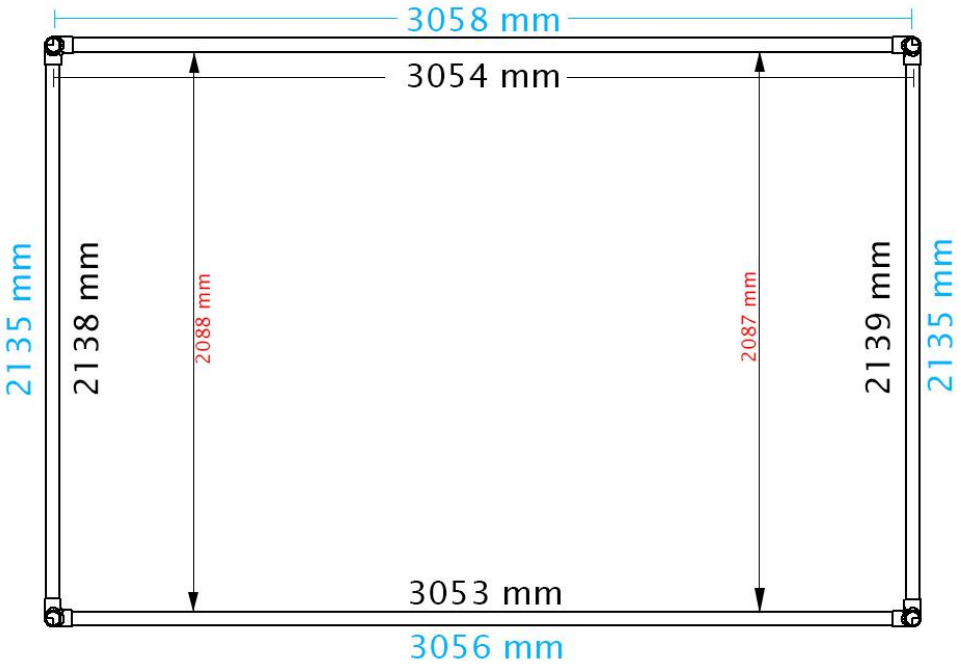

Figure 4.20 - Measurements of the test-rig when set up on the floor (Black) and ceiling measurements (Blue). The Red measurements were taken from the inside face of opposing poles.

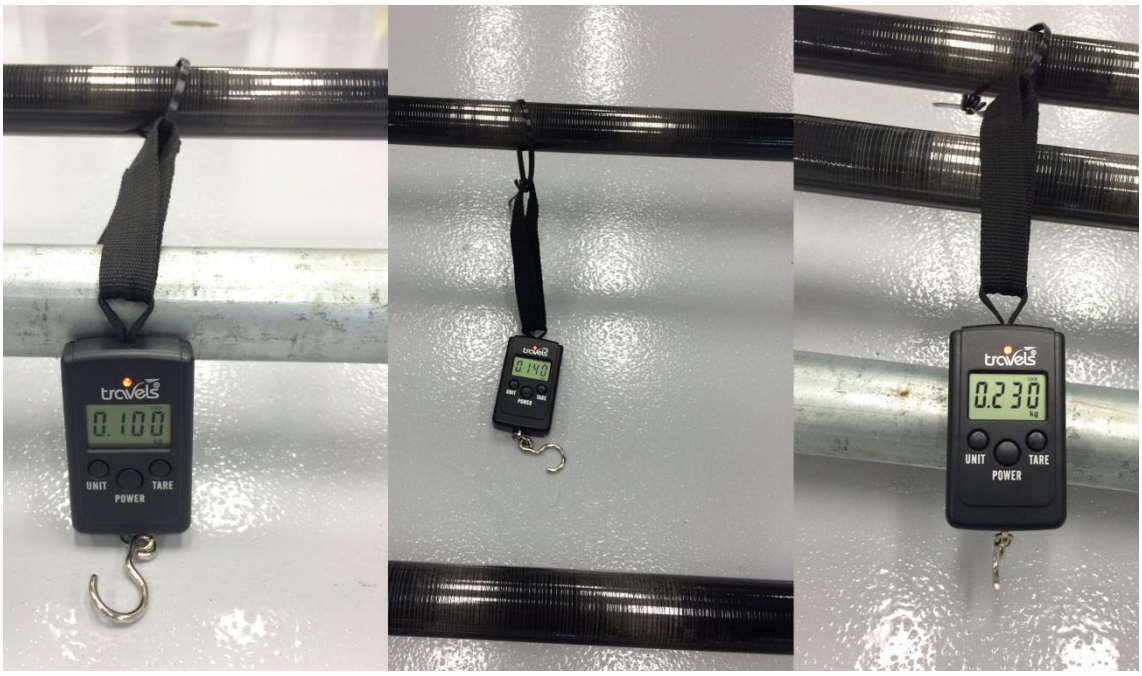

Figure 4.21 - Force required moving the carbon fibre tubes along Y axis (from left to right, first pole, second pole, together).

4.5.3 Forces on XZ Axis

The forces which were acting on the X axis were less to that of the Y axis due to the configuration of the runners. The X axis had greater rigidity as the X axis's bearing housing was 3D printed in one piece where the Y axis was not. The length of the support poles also contributed to the flex in the whole system which demanded larger forces to move on that axis. The force which was required to move the XZ runner along the support poles was 0.54 N.

4.5.4 Forces on Gimbal

The gimbal used is an off the shelf component as this was a more efficient alternative to printing the ball joint. The friction in this part had to be minimal as it had to allow the UAV to roll and pitch with ease. The forces measured for roll and pitch were the same, which is 0.25 Nm of force required to move it. The rotation about Z was measured at 0.17 Nm. But once a coat of lubrication was applied, the forces dropped to 0.19 Nm and 0.145 Nm respectively (See Figure 4.23).

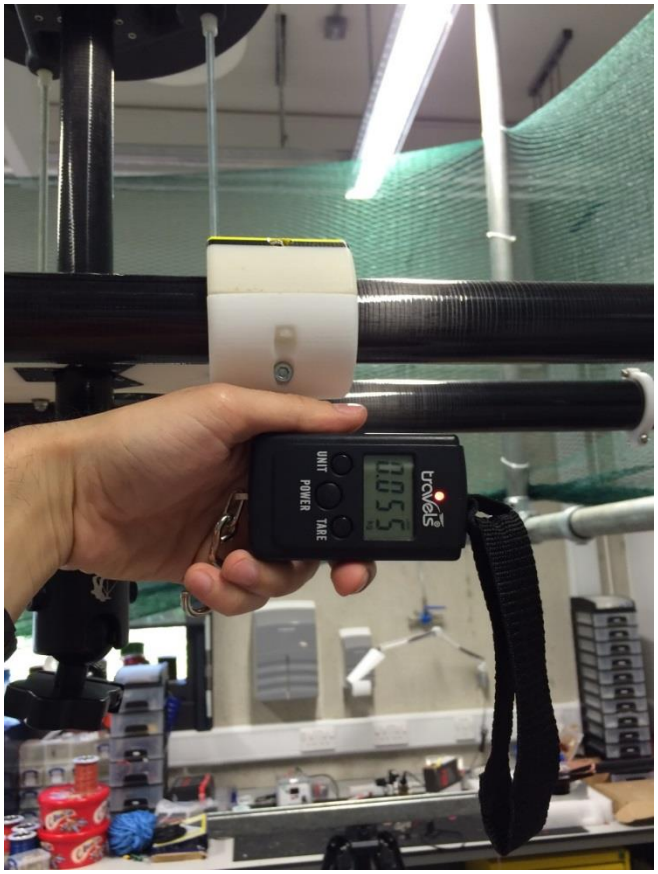

Figure 4.22 - Image of the XZ runner being pulled using a strain gauge.

Figure 4.23 - The gimbal ball joint which shows the ball lubricated and unlubricated.

4.6 Finished Test-Rig

The completed safe flying zone was essential as it provided a safe working and testing environment for all lab users. The health and safety of operators and other lab users was taken into consideration when the rig was being made. The hardware used to mount the vertical poles into the ceiling was over spec'd. The mass of the rig being 60 kg with UAV attached, each of the four corners had four heavy duty raw bolts with each bolt capable of hanging 50 kg. With every neighbouring part being tethered to the next, the possibilities of any injuries due to falling items were made highly unlikely. To finish off the rig, fine green netting was wrapped around the whole frame to provide further safety from the UAV's rotating blades as well as loose items being flung out and therefore completing the safe flying zone (see Figure 4.24).

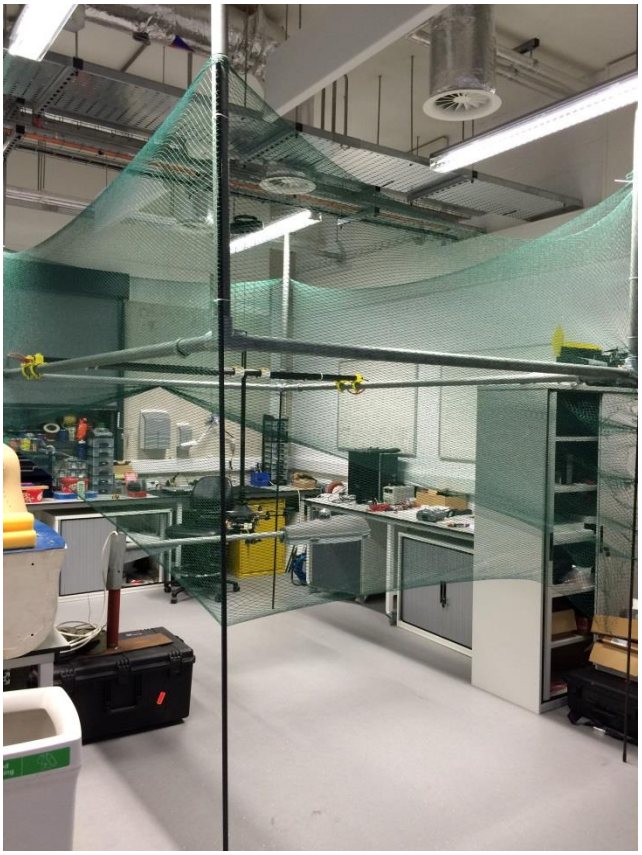

Figure 4.24 - Final finished test-rig with green netting, attached UAV and projection bracket set up.

With the rig completed, the UAV was attached to the rig and the lab space was decluttered to get an initial feel of how the test-rig and UAV behaved in its new operating environment. Each moving part was lubricated including the gripper

itself to ensure everything ran smoothly. Very quickly found that the Y axis runner was snagging onto the netting but was quickly resolved by attaching a guide which allowed the runners to glide past the net. The UAV was able to move around extremely comfortably as it had enough power to overcome the additional forces induced by the support bars. A manual flight was conducted to determine how easy it would be to navigate over to the projection bracket, descend and perch onto it. The careful manoeuvring of the UAV was successful as the operator was able to perch onto the projection bracket and engage the perching element (see Figure 4.25). The operator found the UAV's movements relatively fluid as the UAV was able to move in any direction required without much delay.

With the test-rig up and running, the perch detection algorithm could now be developed in a safe manor.

Figure 4.25 - The UAV was flown manually to quickly determine the movements of the UAV and the free movement of the test-rig.

5. Wind Tunnel Testing

This chapter details how the gripper was validated using experiments to push the capabilities of the gripper and UAV combination. With static and dynamic testing, the results show how close the design specification came to the final prototype.

Understanding the gripper's characteristics helped with ensuring that the gripping undercarriage was not used out of its operational window. By conducting these tests in a controlled environment, which was as close to realistic operational situations and possibly beyond realism at times, enabled the assignment of a flight envelope for the UAV. The dynamic testing (wind tunnel) provided the key data of which the moment the UAV's grip failed on the projection bracket. This dynamic data would be extremely difficult to attain using computer simulations, as the variables involved were far too great.

5.1 Experiment Design

Before designing an experiment, the first order of business was to understand the need for conducting the experiment. This particular experiment was to validate the theoretical failure point of the gripping strength and to determine the operational window of the perching element and UAV combination.

5.1.1 Pre-wind Tunnel Tests

Before using the wind tunnel facilities, static tests were conducted to determine the wind tunnel testing parameters and procedures. Variables and constants needed to be outlined before entering the wind tunnel as mistakes could not have been made. The daily costs of using the wind tunnel were £1500 which meant testing had to be concluded within one day of experimentation (9am to 5pm).

5.1.2 Wind Tunnel Specifications

The wind tunnel used was the University of Southampton's 7 x 5 feet closed circuit wind tunnel. Capable of measuring wind speeds from 4 – 45 m/s (Mach 0.12) to an accuracy of 0.1 m/s. With a height of 1.5 m and width of 2.1 m

(working cross section of 3.15 m²), it was deemed to be suitable for the testing of the gripper a projection bracket (Southampton, 2015).

5.1.3 Static Test

The gripper was designed to sustain a grip in typical wind conditions of the UK's mean wind speed of 4.6 m/s. A force of 2.32 N was what the UAV experiences due to gravity and the side wind gust of 28 m/s therefore a mass of 236 g was added onto the tip of one of the rotor arms to simulate these forces in a static horizontal position. Then the UAV was rotated about the projection bracket at 10º increments until the UAV was at its extreme position of 180º. The gripper was able to sustain the grip throughout all tests with the mass attached. Additionally the excel spreadsheet in Appendix C was used to check the forces which the gripper would slip.

5.1.4 Timing

The timing of the experiments was critical as it directly affected the number of tests which could be conducted. Many factors dictated how much time could be spent per test run. These factors which the available eight hours were split into are:

- Set up time – this was the time it took to move all the equipment into the wind tunnel and install. Total time: 30 minutes.
- Ramp up time – this was the time it would take the wind tunnel to reach 45 m/s from stationary. At this point the wind tunnel technician was consulted to gain more information about how the wind tunnel operates in order to estimate the testing sequence (Marshall, 2015). The quickest time to reach maximum speed of 45 m/s was approximately 20 to 25 seconds. However, the rate at which the air speed increases was programmable and a recommended time of two minutes to reach the top speed of 45 m/s was suggested as this was an optimal time to allow the pitot sensor to refresh. The 2 minutes were split into 2 stages: 0 to 10 m/s was programmed to take 15 seconds and then to reach the maximum 45 m/s took an additional 105 seconds. Total Time: 2 Minutes.
- Number of tests – with 7 projection angle positions and 9 UAV angle positions the number of tests which had to be conducted was 63. (see

Figure 5.1). An allocated 2 minutes per run time resulted in a total time: 126 minutes.

- Angle of UAV change – between each test, the UAV angle needed to be adjusted. Using a stop watch, the time it took to adjust the UAV's angle between one angle and the next was measured. 1 minute of adjustment time was allocated between tests. Total time: 8 x 7 = 56 minutes.
- Angle of projection bracket change – between each sets of tests, the projection bracket angle needed to be adjusted. An additional 2 minutes were allocated for this. Total time: 2 x 6 = 12 minutes.
- Lunch break – food also had to be considered. Total time: 60 minutes.
- Break down – packing the equipment away and leaving the wind tunnel. Total time: 15 minutes.

The total estimated time was 299 which worked out to be just under 5 hours. This meant an extra 3 hours could be used as contingency.

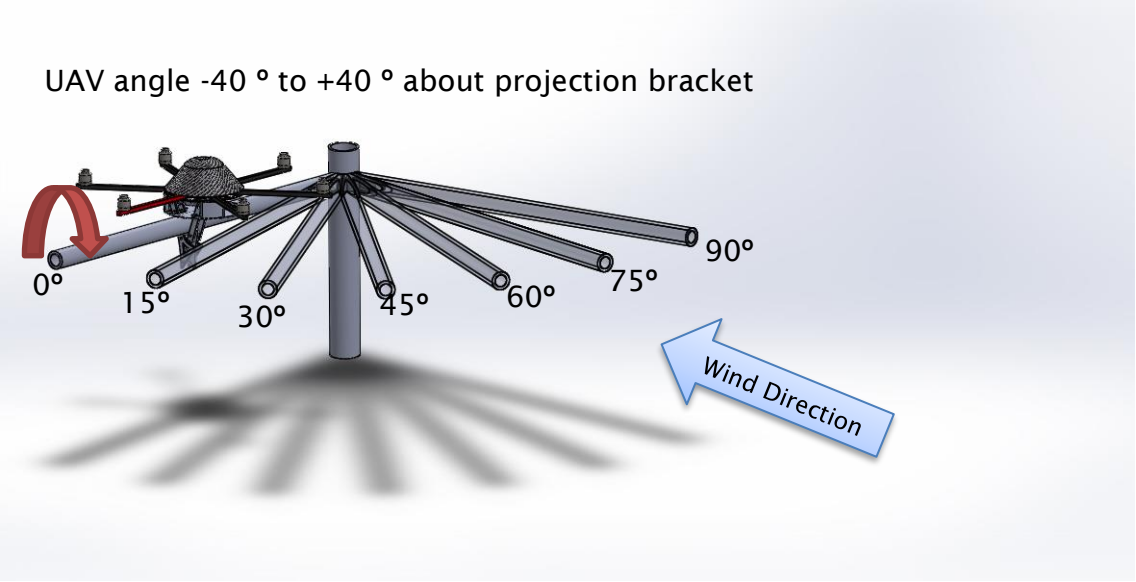

Figure 5.1 - The projection bracket separated by 15° increments between each set of test, UAV angle was variable between -40° to +40° Note: wind direction was perpendicular to the projection angle of 0°.

5.1.5 Gripping Strength

With the stall current of the drive motors being 0.463 Nm, the gripping strength was set at a moderate 0.4 Nm to ensure that the motors were not over worked. This torque was applied to the non-backdrivable screw thread during the setup

of each test using a digital torque screwdriver. Once the desired torque was reached, the screwdriver alerted the operator with the use of visual, audible and haptic feedback.

5.1.6 Constants and Variables

The data gathered from the pre-wind tunnel data allowed for the formulation of the constants and variables of the gripper testing. These were the list of the constants and variables:

Constants

- Gripping strength: 0.4 Nm was applied to the non-backdrivable screw thread.
- Wind speed: rate at which the wind speed was ramped up at. 0 to 10 m/s took 15 seconds and then to reach the maximum 45 m/s took an additional 105 seconds.

Variables

- UAV Angle: this was the angle at which the UAV sits on the projection bracket which was between + 40º to -40º with 0º being the nominal horizontal position of the UAV.
- Wind Angle: this was the angle at which the projection bracket sat in the wind tunnel in relation to the wind direction. From 0º (perpendicular to the wind) to 90º (head on into the wind) at 15º increments.
- UAV grip slippage point: this was the moment the UAV grip slipped due to the forces acting on the UAV. At the time of slippage, the UAV would twist about the projection bracket in a sudden motion.
- Wind Tunnel Temperature: This was recorded at the beginning of each test. This fluctuated between 9.9 ºC and 12.4 ºC.
- Gripping range of gripper Minimum-Maximum profile: 30mm – 105 mm.

These parameters were used throughout the wind tunnel testing phase which made the acquisition of the data collection a simpler task. Not every single data point could be acquired which meant adopting a sampling method which made the recorded data usable (Creswell, 2003).

5.2 Gripper Modifications

During the static testing of the gripper, the ABS non-backdrivable screw thread failed on one side due to being excessively used whilst testing the gripper. These rapid prototyped parts served their purpose to prove the proof of concept. They required an upgrade to be able to withstand multiple opening and closures during autonomous perching. To ensure that breakage wasn't due to excessive force, using the torque screw driver, the working side's torque was verified at 0.4 Nm.

5.2.1 Applied Force

The output from the motors during testing was too much for the existing 3D printed ABS parts. The torque from the motors caused the non-backdrivable screw threads to split and break at the weakest point which were the end stops (see Figure 5.2) and parts of the carbon fibre claw.

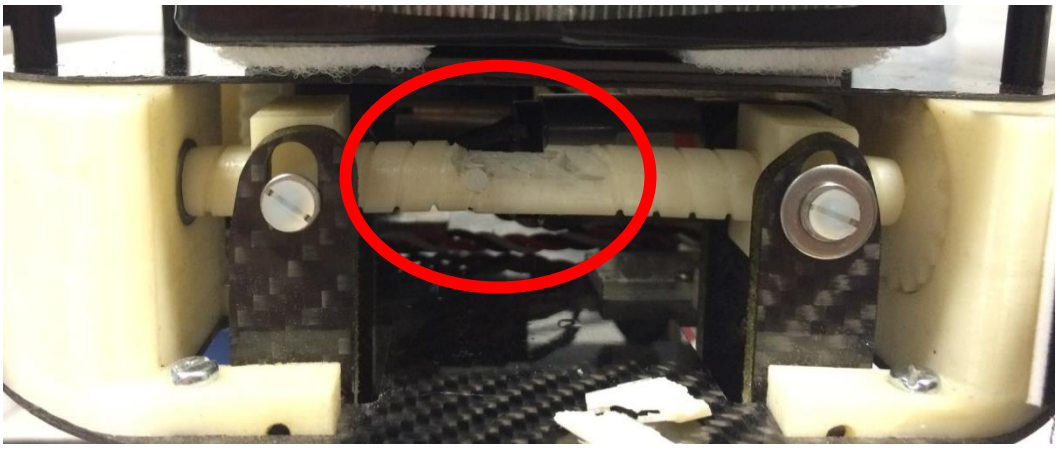

Figure 5.2 - The broken non-backdrivable screw thread broken at the weakest point indicated by red circle.

To stop the non-backdrivable screw blocks from clashing into each other, a dowel was inserted into the shaft to act as an end stop. This end stop was set at the correct position to also ensure that the legs open into its normal landing stance but also inherently caused the shaft to become weak.

These broken parts had to be remade to ensure that this type of breakage will not occur again. So the parts were slightly redesigned to be made out of Aluminium (see Figure 5.3). The only major difference which was made to the original design was the change in diameter from 10 mm to 8mm in order to save mass.

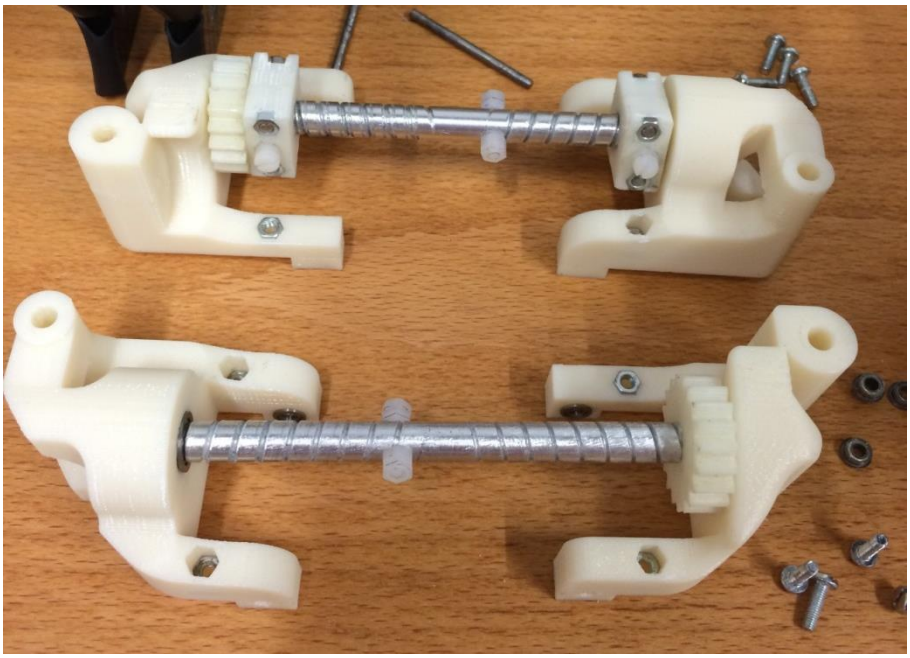

Figure 5.3 - The pair of remade aluminium non-backdrivable screw threads in their new bearing blocks. The use of an end stop was still employed.

Because the non-backdrivable screw thread was remade, the screw blocks were re-printed to match the new diameter of the screw thread (see Figure 5.4). At this point, the bearing blocks were also remade to try and save more mass. A small hole was added as a feature to allow for a torque screw driver to be inserted directly onto the non-backdrivable screw thread shaft which would allow the claw to be manually operated whilst maintaining the correct force. Due to the breakage, the applied force of 0.4 Nm was deemed to be excessive for the 3D printed parts. A lower and safer torque of 0.30 Nm was applied for the wind tunnel testing as it would still provide a sufficient hold whilst preserving the life of the printed parts. Overall, a total of 36g were saved compared to the ABS screw thread version.

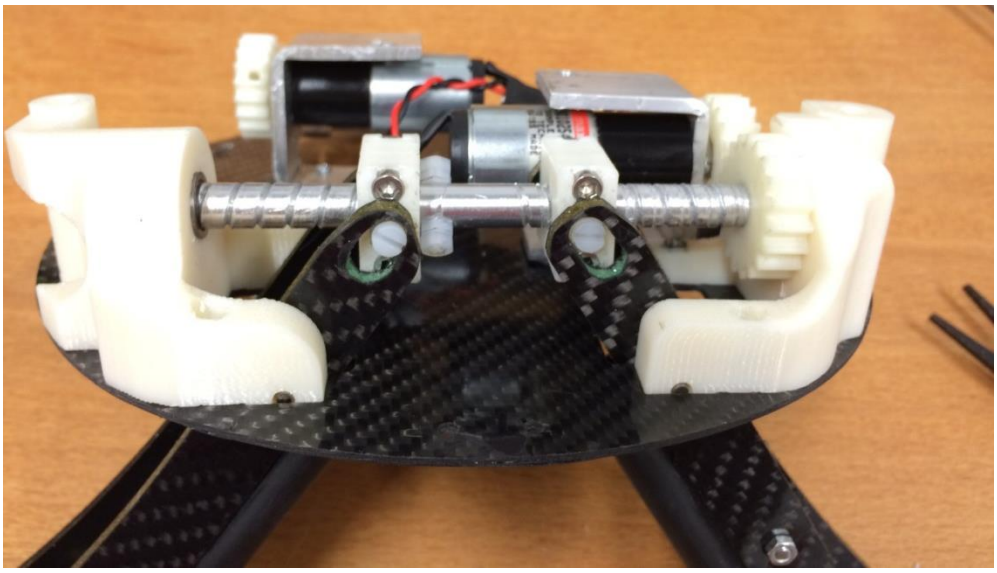

Figure 5.4 - The new screw blocks which are attached to the remade carbon fibre claw leg.

5.3 Testing Procedures

The pre-wind tunnel tests were conducted to ensure that the testing ran smoothly. Unfortunately certain aspects were over looked which resulted in the first two hours upon entering the wind tunnel to be lost.

5.3.1 Initial Setup

Setup involved moving the test equipment into the wind tunnel; the projection bracket, the base, the UAV and weights to weigh the rig down. It was planned that the base would be kept stationary during testing with the use large weights to ensure the projection bracket did not move.

To make sure the setup was acceptable an initial test was conducted to ensure the whole setup was adequate. With the theoretical failure point for the UAV angle 0° and projection angle 0 °, the wind speed was estimated to be 35 m/s. The wind tunnel was set to ramp up to 10 m/s within 15 seconds and then to 45 m/s within 2 minutes of the start time. The whole system was fine until the forces acting on the UAV and rig overcame the force being exerted down onto the rig by the 100 kg mass which was being applied to it (see Figure 5.5).

Figure 5.5 - The setup of the projection bracket and UAV on the floor of the wind tunnel.

Once the gripper reached the point of failure, the UAV rotated around the projection bracket which meant it caught more air due to its increased surface area which caused the projection bracket and base to rotate about the lighting rig's column also lifting the weights. This meant that the use of these weights were not sufficiently safe. The base was then secured using the rails which were built into the walls of the wind tunnel (see Figure 5.6). This meant the base would be very secure whilst still being able to be adjustable in between test stages.

The parallel rails ensured that the base was secure in place and only the UAV would rotate at the point of failure rather than the whole rig. The three securing bolts which adjusted the angle of the projection bracket in relations to the wind direction were tightened before every test to prevent the projection bracket from swinging around and allowing the UAV to become damaged.

With the three securing bolts tightened, the projection bracket sat at an angle of 3.9º from horizontal. As indicated by the lamp post data acquired during initial lamp post research, this was within the projection brackets normal exit angle of between 0º - 15º and was typical for this brand of projection bracket

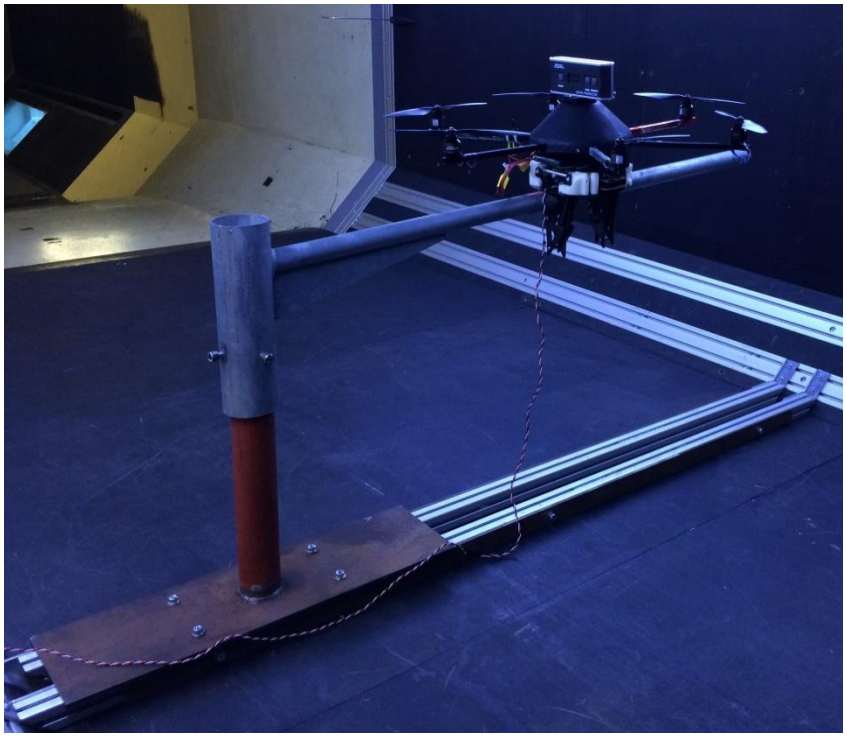

Figure 5.6 - The use of the integrated wall rails to secure the base of the rig onto a fixed body.

5.3.2 UAV Setup

Attaching the UAV onto the rig involved placing the UAV onto the midpoint of the projection bracket and tightening up the non-backdrivable screw threads until the claws had almost firmly held the projection bracket. At this point a digital protractor was attached to the flat on top of the UAV's outer shell; which allowed for attaching onto the gantry test rig. The angle of the UAV was measured and corrected, if needed, to get the UAV into the correct testing angle. The Testing angles were determined to allow for a wide range of data points whilst keeping the test times and sequences to a minimum. This ranged from +40º to -40º with 10º degree increments between each test, which produced nine results for every position of the projection bracket. Once the correct angle was achieved the non-backdrivable screw thread was tighten to 0.30 Nm using a digital torque screwdriver which had a visual, audible and sensory output. Once the gripper was tightened, a confirmation angle measurement was taken to ensure the UAV hadn't moved whilst being tightened. At this point an acceptable alteration in the UAV angle was up to ± 1 ˚.

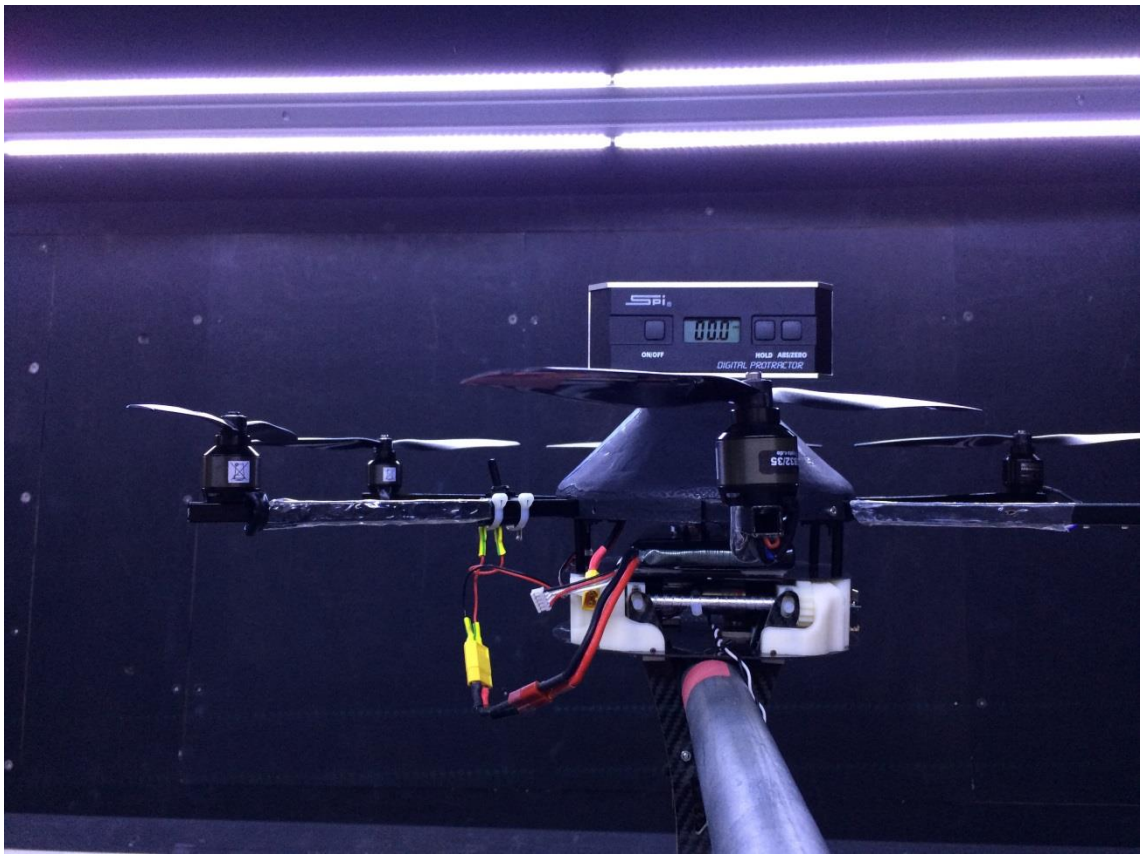

Figure 5.7 - Digital protractor placed on top of the UAV's flat top protective shell indicating the angle at which the UAV sits on the projection bracket.

With the gripper tightened to the correct torque and the UAV securely fixed onto the projection bracket, the test procedure could begin.

5.3.3 Testing Procedure

The wind tunnel operator was then instructed to ramp up the wind speed in two stages, 0 – 10 m/s within 15 seconds then to 45 m/s within 2 minutes. Initial calculations indicated that stage two of the wind speed ramp up was where the gripper would begin to fail hence the rapid ramp up from 0 – 10 m/s. The first set of data was captured with the projection bracket set to 0° which meant the projection bracket was perpendicular to the direction of the wind. Starting at +40°, the UAV was rotated about the perching element +40° into the wind direction which meant the wind would be forcing the UAV onto the projection bracket. The wind tunnel was ramped up and the point of failure was recorded. This point of failure was the moment the forces acting on the UAV overcame the gripping strength and the UAV's grip would slip. For the first test, the grip did

not fail within the operational limits of the wind tunnels maximum speed of 45 m/s. To ensure that the grip did not fail, another measurement was taken upon entering the wind tunnel by placing the digital protractor on top of the UAV. Measurements showed that the UAV's grip did not fail and the next test should be conducted. The next angle was set to +30º at which point the first result was captured with the gripper failing at 36.8 m/s (see Table 5.1). The moment the gripper started to fail, the wind tunnel operator was given the command to cut power to the wind tunnel. The program used to operate the wind tunnel also logged the highest wind tunnel speed before the power was cut.

Table 5.1 - Failed wind speeds of first and second attempts (DNF – Did Not Fail).

Projection Bracket Angle (Deg)	UAV Angle (deg)	Failed Wind Speed (m/s) First Attempt	Failed Wind Speed (m/s) Second Attempt
0	40	DNF	DNF
	30	36.8	35.9
	20	32.2	32
	10	33.9	33.3
	0	38	36.5
	-10	29.4	31.1
	-20	19.7	19.4
	-30	17.7	18.1
	-40	14.7	14.4

After the wind speed in the wind tunnel dropped to 0m/s, the wind tunnel was safe to enter and adjust the angle of the UAV by 10º to the next measurement angle until -40º was reached.

While the projection angle was set at 0º, it was decided that a repeat of the test was required for projection bracket angle of 0º to ensure that the results were reliable. Ideally a repetition of every test would be desirable which would rule out any anomalies in the results, but due to the high costs of hiring the wind tunnel, there was only time for one set of results. However the repetition of this single projection angle was sufficient as the second set of results did not vary

by more than ± 2 m/s. This slight variation was acceptable and therefore the testing continued by changing the angle of the projection bracket.

5.3.4 Projection Bracket Angle

Once the wind speed dropped to a safe 0 m/s, the wind tunnel was entered and adjustments to the projection bracket could be made. This involved loosening the projection bracket from the clamped column and swinging it towards the wind direction by 15° using a compass (see Figure 5.8). Once the projection bracket was in its new position, the bracket was tightened to the column and the UAV was set to +40° again to begin the next phase of testing. This cycle was continued until all variations were tested.

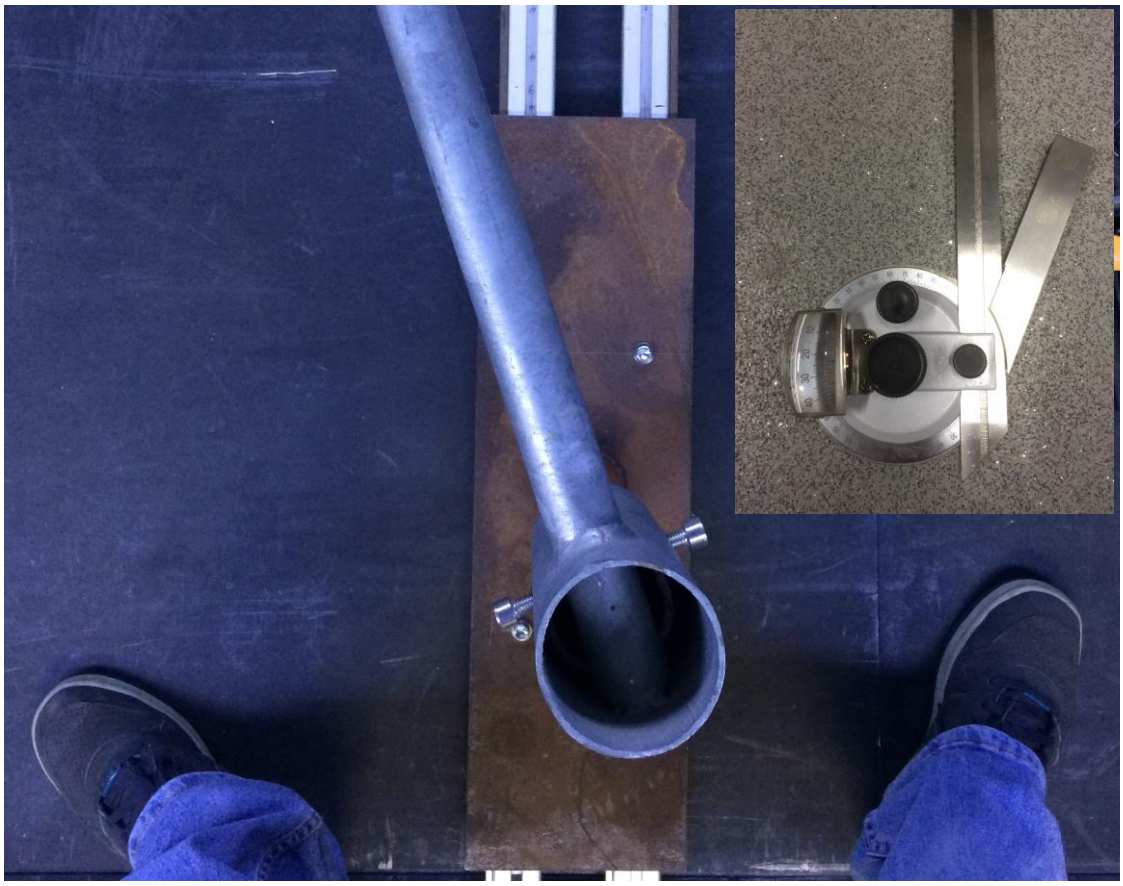

Figure 5.8 - New position of the projection bracket at 15° increment to the starting positon measured using protractor as can be seen in top right hand corner of image.

5.4 Wind Tunnel Results

To gain further understanding of the perching system, the dynamic wind tunnel results were investigated and analysed to formulate a conclusion. The results were organised onto a spreadsheet ready to be processed (see Appendix D). To better visualise the outcome, the data points were plotted onto a line chart for each set of results (i.e. projection bracket at 15º). Six charts were produced (see Figure 5.9), however this would have produced 7 charts but the projection angle of 90º did not produce any usable data as the gripper did not fail. The moment of failure in this case was defined by the forces which the UAV and perching element combination experienced was greater than the grasping strength applied.

As can be seen from the results, only three angles of the projection bracket were able to produce a full set of results using the 7'x5' wind tunnel at the University

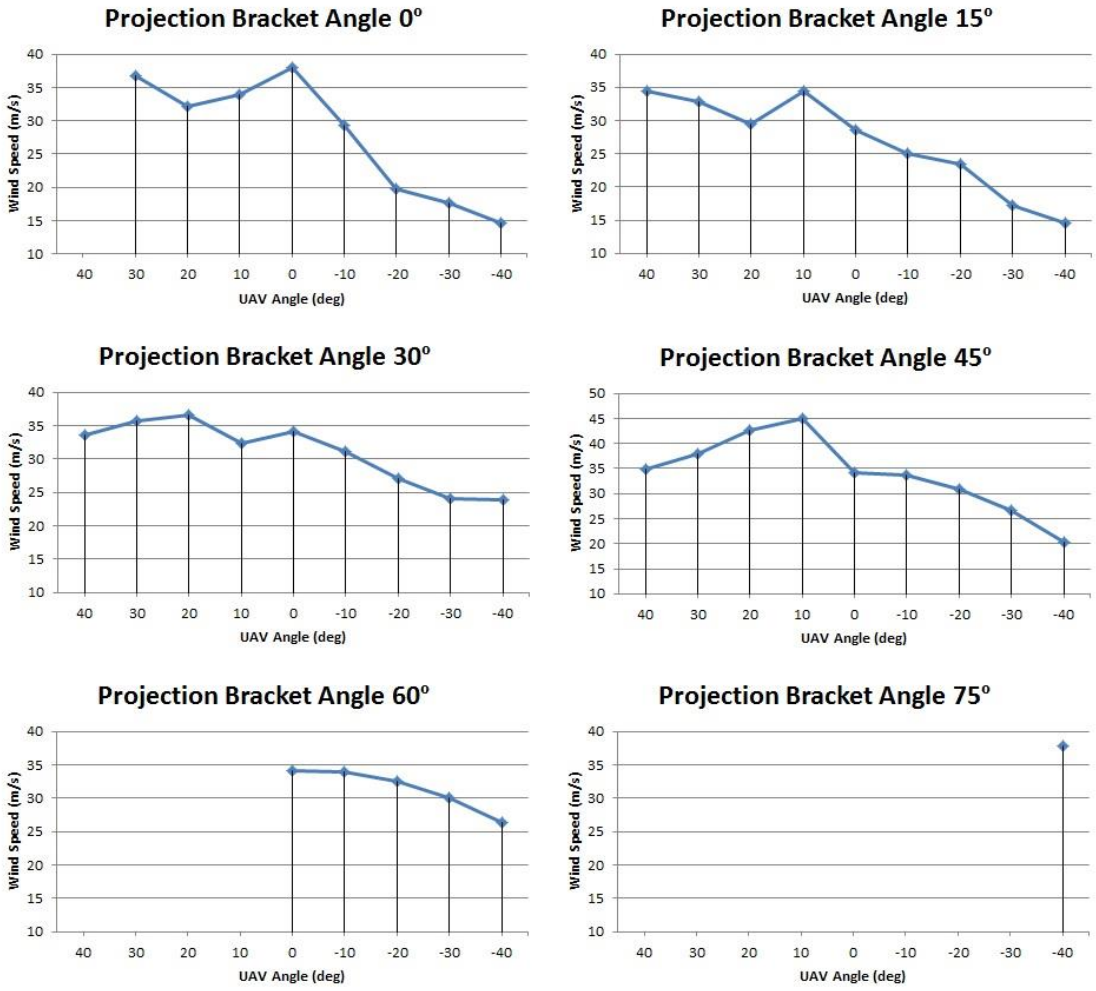

Figure 5.9 - Results of the perching element slippage wind speeds.

of Southampton (angles 15, 30 and 45). This was due to the fact that as the vectored force applied on to the UAV became more parallel with the projection brackets angle, the likely hood of the UAV's grip failing became unlikely. The last two tests, projection bracket angle of 60º and 75º, only producing five and one data point respectively. These incomplete results made the comparison of the data difficult. To extract more data from the current set of results, all the data points were merged and a linear trend line was applied to each set of results (see Figure 5.10).

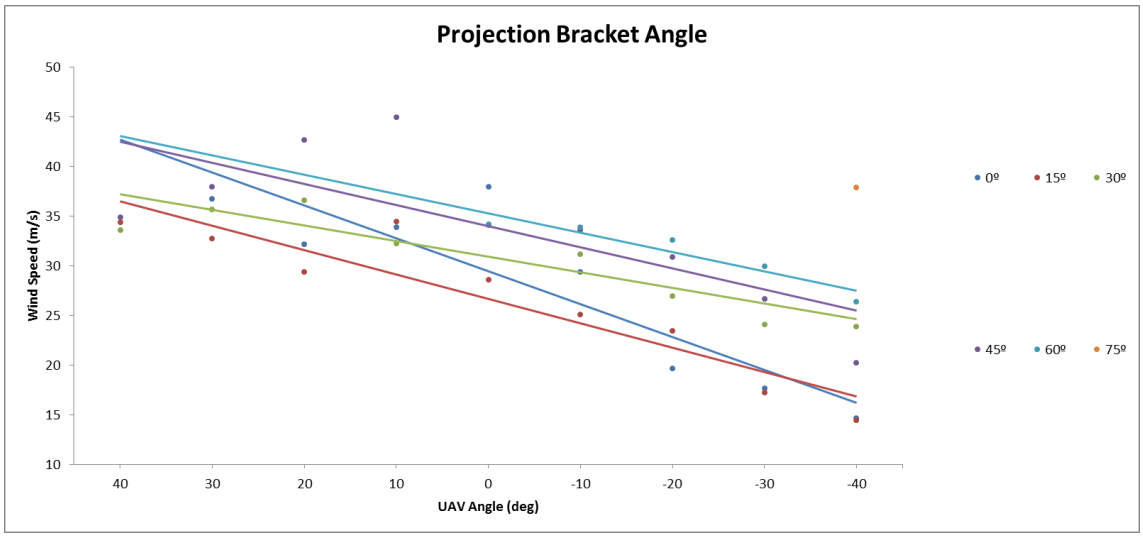

Figure 5.10 - Merged results from the entire range of test with a polynomial trend line applied to each set of data points.

As the projection angle of 75º only produced a single data point, a trend line could not be applied to this range therefore estimated failure points could not be worked out.

The interesting pattern which has emerged from analysing the data shows that for projection angles 0º, 15º, 30º and 45º, there is a correlation in peak gripping strength when the angle of the UAV was between 0º and 20º into the direction of the wind which is the extra down force. This consistency of the UAVs ability to maintain a grip at this range shows potential for an optimal flight envelope range. This was due to the wind milling effect of the props forcing the UAV onto the projection bracket. Whereas the negative UAV angles show that the reversed wind milling effect has an adverse outcome on the gripping capability. A potential capability for the UAV could be the detection of wind direction coupled with the ability to adaptively brake the motor and prop combination when the

wind is approaching from a negative angle, could prove to increase the gripping capability of the perching element.

Initially, the only data points which were going to be extracted was the UAV's points of failure. But after initial testing, it was observed that the propellers would begin to spin consistently at the same wind speed as the wind tunnel was ramped up. Therefore, data points for the wind speed of the propellers entering into a wind milling effect were also taken as they could be used at a later stage (see Figure 5.11).

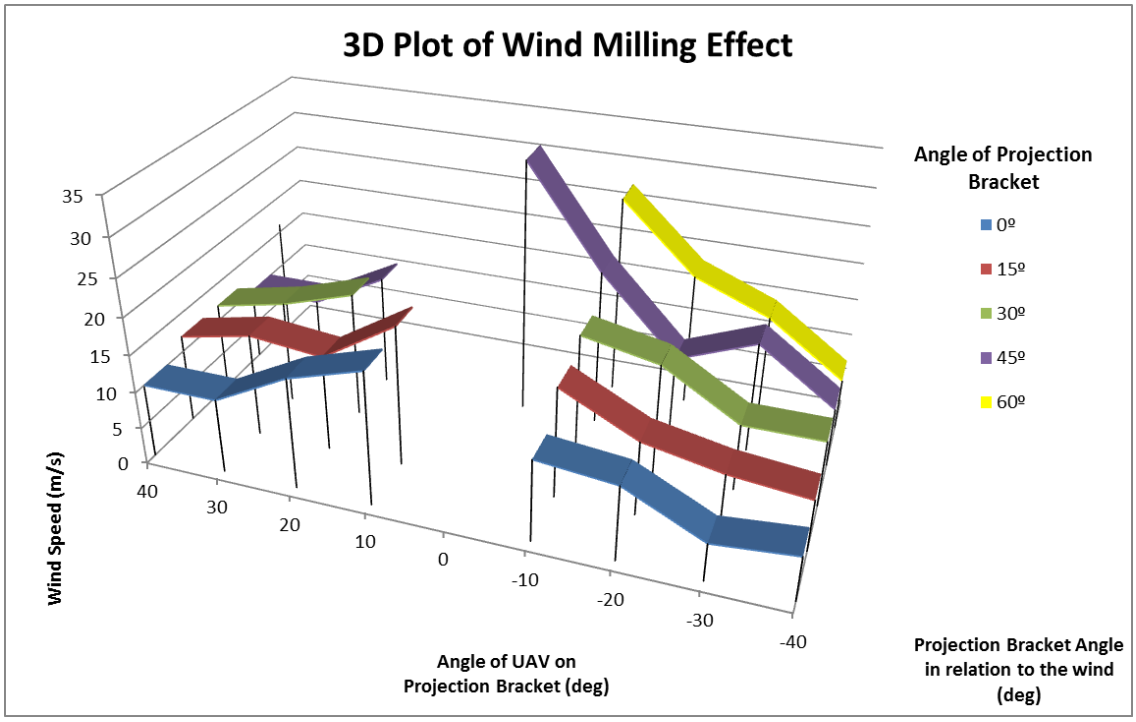

Figure 5.11 - Data points for wind milling effect on the UAV rotors.

The wind milling effect wind speed was taken the moment the propellers on the UAV began to spin. The reasoning for also acquiring these data points was also the reason for conducting the wind tunnel tests; to gain understanding of the wind milling effect the UAV has on the gripping capability. These results highlighted a dead spot for the wind milling effect which took place with the exception of the projection bracket angle of 45°. At all but one projection angle, every test where the UAV was at the angle of 0°, the propellers did not spin. The lack of spinning was due to the wind exerting the same amount of force on the entire surface of the propeller at the same moment. As the propellers were symmetrical, if the wind speed was ramped up and the tip of the propeller was facing the wind direction, then the propeller would rotate until the forces acting

on the surfaces entered a state of equilibrium. This verified that the wind produced by the wind tunnel was laminar. As there were six propellers, the first set of propellers which the air passed over, did not move. The turbulence created by the passing air over the first set of propellers would cause the remaining ¾ propellers to oscillate rapidly clockwise and counter clockwise as the air speed was ramped up.

By comparing the grip failure points against the wind speed of the wind milling, the difference showed a similar profile for both the data points (see Figure 5.12). The comparison, which had been made for projection bracket angles 0º, 15º, 30º and 45º, showed how the wind milling affected the point at which the gripper would fail. This correlation could perhaps pre-empt the failure point of the perching element if the direction of the wind is known. Coupled with an ability to detect the direction of the wind, the system could calculate the rate of the wind gusts and direction to initiate and emergency release or even dynamically increasing the gripping strength by adjusting the cut off current of the grippers drive motor.

It should also be noted that there could be a possible anomaly in the results for projection bracket angle of 45º. For all of the other projection angles, with the UAV angle set to 0º, it shows that the propellers did not experience a wind milling effect before the point of gripper slippage. However, for UAV angle 0º at projection angle of 45º, the propeller started wind milling at 33 m/s and the UAV started to lose grip at 34.4 m/s. This 1.4 m/s difference could be down to the user's inability to notice the exact moment of the gripper slipping which is an error mode that should be rectified to increase the reliability of the results.

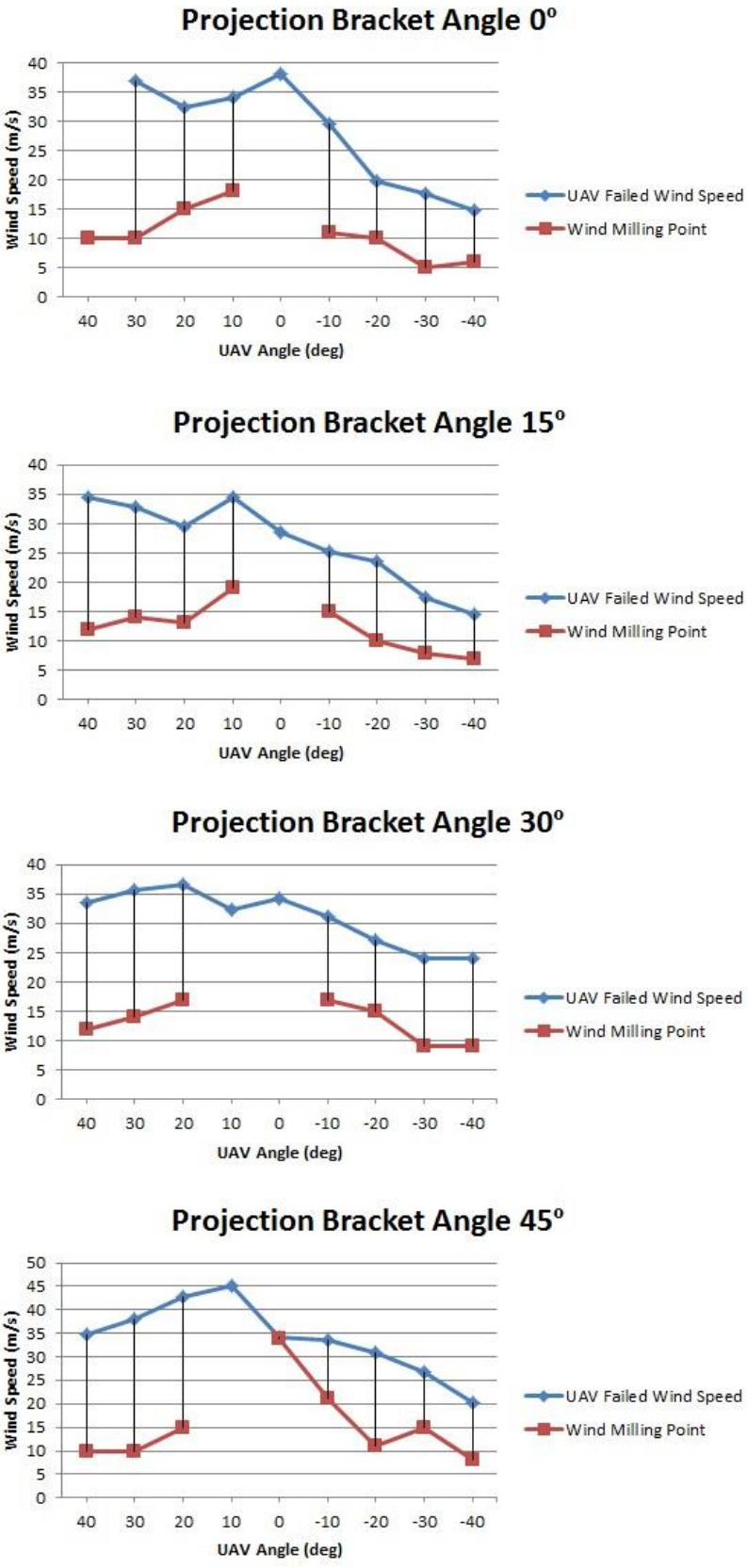

Figure 5.12 - Comparison of the UAV slippage points with the speed of the wind milling effect.

5.5 Preventing Slippages

Being able to detect if the UAV is slipping could be an extremely useful capability which would ensure the safety and security of the UAV. By either accessing the accelerometer data from the flight controller or equipping the gripper system controller with an accelerometer, it can be possible to enable the gripper system to adaptively change its gripping strength. By detecting sudden movements in the UAV, such as slippage, wind guests or even projection bracket breakages, the UAV could pre-empt the failure mode and adjust as necessary. If the UAV was to be blown with such force that it hangs upside down, it could prevent it by increasing gripper power or engaging the motors to counter act the applied forces. The detection of wind speed and direction could also result in improved gripping capabilities. By incorporating a 3 axis solid state anemometer such as the 'Wind Urchin' (see Figure 5.13), the direction of the wind and speed could allow the UAV to estimate the possible failure mode. Slipping towards the light column or lantern unit could obstruct the propellers resulting in the UAV being stuck on top of the projection bracket as it cannot take-off. The mitigating manoeuvre would be to power up and shuffle to the midpoint of the projection bracket by a loosening the grasp without fully opening the claws and to instruct the UAV to move. Locating the midpoint could either be done by fully taking off and finding the central point or by calculating the displacement and move in a

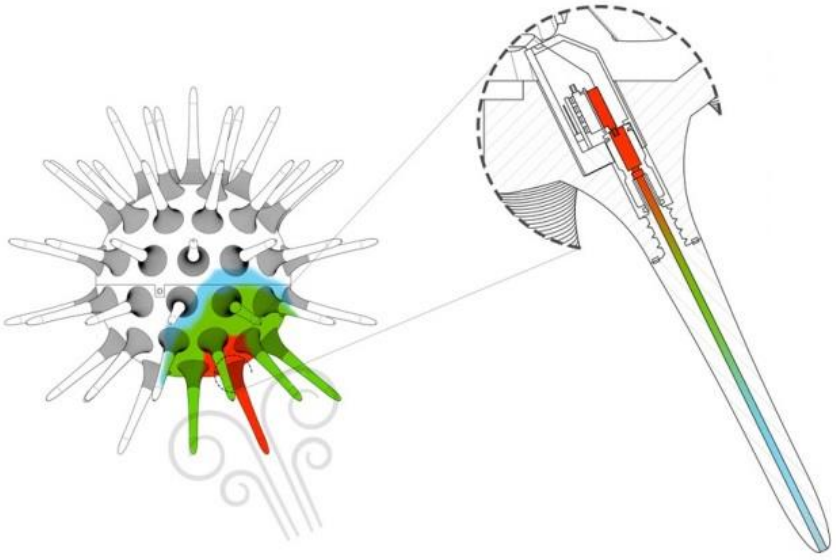

Figure 5.13 - The Wind Urchin – using 64 pitot tubes which can measure wind speed in all directions (developed at Dublin Institute of Technology) (Kearney and Kearney, 2014).

reverse motion. The same 3D anemometer could also be used to check wind conditions before take-off. If the conditions exceed the operating parameters then it would be safer to stay perched/landed. However, if the wind speed is what cause the gripper to slip, then depending on the wind speeds, the UAV may not be able to take off to manoeuvre the alignment as it cannot operate in wind speeds exceeding 20 m/s. In this scenario it would be wiser to increase the grip to eliminate the UAV from slipping at all. The down side to this is the stress exerted onto the gripper components which have failed before and may do so again if pushed to the limits. The benefit of opting for an adaptive gripping system which only adds extra strength when needed, is that it remains power efficient therefore would still score highly on the weighted matrix.

5.6 Wind Tunnel Conclusion

The dynamic testing of the gripper and UAV combination proved to be an essential process which delivered the operational parameters of the combined system. However these results could easily be scaled up or down depending on the type and size of UAV used. The costs involved using the wind tunnel resulted in a single run set of results which was accurate to 1 – 3 m/s. To verify the whole range of data points would have meant a repetition of the experiments which would have led to more reliable set of data. However, the theoretical data which was used to estimate the UAV's failure point at projection angle and UAV angle of 0º was 35 m/s. The failure point of this test in the wind tunnel was 38 m/s. This 3 m/s difference could be compared to the fluctuation of the repetition tests for projection bracket angle 0º, which was conducted at the very beginning of the testing phase. However this 3 m/s difference could also be the result of the wind milling effect which cannot be ignored. The point at which the wind milling occurred is due to many factors, such as health of the bearing in the motors to how well they are lubricated or aligned. Because of these factors, theoretical data could not be relied upon when comparing to dynamic results.

The testing procedure could have been improved by increasing the accuracy of detecting the moment of slippage. The detection of the slippage point could have been conducted in using various complex or simple methods. By incorporating pressure sensors onto the projection bracket to detect the slippage point or recording the UAV on the bracket using high frame rate capture

video with air speed overlaid on the video and then watched back. Either way, more time would have had to be spent in preparation for the tests. Another improvement could have been achieved by spending more time in the wind tunnel but would have involved high cost. Additionally, higher wind speeds would have meant capturing the incomplete data points which were not possible using any of the Southampton University's wind tunnels as the maximum achievable speeds was 45 m/s.

As for the testing equipment used, being able to attach the projection bracket to the built in load cells of the wind tunnel, would have meant capturing the drag of the UAV and gripper. By running the wind tunnel with just the projection bracket the drag value could have been calculated and then subtracted from the overall drag value of the UAV, gripper and projection bracket. This drag value coupled with the previously mentioned mitigable reduction of wind milling propellers, could have led to an interesting experimentation process.

The optimal approach angle is dependent on the direction of the wind speed. Due to the grippers ability to cope at extreme wind speeds, the gripper is almost capable of being able operate outside of the UAV's flight envelope. Because the UAV is capable of flying in wind speeds of up to 20 m/s, as long as the UAV approaches the perch site between +40º to -20º, it should be capable of executing the perch. This over spec'd grip may be deemed as excessive as the UAV will not be able to reach the perch site in those grip failure wind speeds, but perhaps may be used to execute an emergency perch in high wind speeds as an alternative to trying to return back to base or home positon. However, an opportunity to optimise the gripper by using lighter and small parts could decrease the overall mass of the system along with lower power consumption of the gripping system and increased flight time for the UAV. By redesigning the gripper to only grip up to wind speeds of up to 20 m/s to match the UAVs flight envelope, would mean eliminating the extra power to overcome larger wind speeds which could prove dangerous.

A perched bird on a tree branch or wire looks relatively comfortable dealing with wind guest which is what this perching system could provide for VTOL UAVs. By dynamically adjusting its gripping strength, reducing the amount of drag the system experiences or even knowing when to release its grip to get away quickly, it could be that step closer to replicating nature.

6. Search and Perch Algorithm

This chapter details the work which was undertaken to develop the search and perch algorithm which is what controls the UAV into the final perched position. The UAV acquires and analyses the data from its on-board vision sensors and translate the information into a UAV manoeuvre by instructing it to navigate over the perch site and carefully descend onto the lighting projection bracket. The resultant manoeuvre was analysed and critiqued for effectiveness along with the methodology used to achieve the perch. So the overall aim of this algorithm was to remove the burden of the perching controls from the operator by automating the sequence.

To explain the work conducted, this chapter has been spilt into three sections; Detection, Manoeuvre and Perch.

6.1 Detection

Humans make use of their five senses to conduct everyday tasks such as reading, opening doors or cooking. These senses allows for the manipulation of objects and determine the whereabouts of said objects. However, in the world of robotics you have to attach sensors to enable them to read their environments. Every sensor has various specifications which makes them suitable for specific tasks. The different possible sensors which could be used to enable the UAV to detect the perch site was explored. However, before delving into the world of sensors, a small literature review was conducted into how others in the UAV industry go about detecting their surroundings.

6.1.1 Detection Sensors Literature Review

During the research phase, it was noticed that the types of detection could be done in one of two ways or a combination of the two; On-board or Off-board. As the name suggest the on-board is done using sensors on the UAV which allows for a complete standalone system. At this point, the data collected by the sensors is either processed locally on the UAV, which requires a relatively high spec microprocessor (Grabe et al., 2012) or transmit data wirelessly or through wires, where a much more powerful processor could be utilised (Blosch et al., 2010). This is how the combination detection could occur. Such as systems

developed by Institute for Dynamic Systems and Control (ETH Zurich) (Hehn and Andrea, 2015) or at Brigham Young University (Millet, 2010) where they capture on board video and stream the images back to the base station where all the processing is conducted and then commands sent back to the UAV. This option has its advantages and disadvantages. One such advantage would be the reduced mass in the UAV as the processing power is exported to a much higher spec processor for more effective data analysis. The disadvantage would be the limitations on the video transmission range which will affect the UAV operational fence. This option appears to be attractive until the decision on the quality of the video is considered. The higher the quality of the video, the larger and more power hungry the video transmitter needs to be. Of course, going for an off board solution like ETH Zurich have done is the light weight option. They use high speed infra-red cameras to track the UAVs position and relay commands back to the UAV. This system relies on reflective markers (optical-passive) or LED markers (optical-active) to be placed on the UAV and can track the UAV to 0.5mm accuracy in a 4 m^3 volume using 9 mm markers (Vicon, 2016). However impressive this level of accuracy may be, it highly restricts the UAVs operations to an indoor environment. Despite these restriction, ETH Zurich have used the motion algorithms which were developed using the Vicon motion capture system in their machine flying arena, and have created an on-board spatial awareness algorithm (Mueller et al., 2015). This method has relieved the motion capture system but gained another. RF signals are pinged to an internal localisation base stations to achieve triangulation of the UAVs. This method could be further developed to make use of outdoor mobile phone cell towers for the same principle (Yang et al., 2014).

6.1.2 On-Board vs Off-Board Processing

The types of on-board systems are less capable due to their processing speeds but do benefit from a non-constricted flight envelope. The advantages of off-board detection systems are the accuracy of the manoeuvres and speed at which the manoeuvre is executed. They also benefit from being lighter due to having less electronics on-board. Depending on whether it has an active or passive type of positional relaying, the system can be relatively lightweight. For example, if using radio signals to transmit positional information, then the weight of the

transmitter will have to be taken into consideration. But if a passive (reflective markers) system is used, then the mass of the reflectors will be negligible.

In terms of cost, the off-board processing is the more expensive option and is used by top research institutions which have the resources to do so. ETH Zurich is a perfect example of this and have proven that the work conducted in the lab can be taken out into the real world situations if needs be. The algorithms developed for a specific UAV could also be used on various other UAV projects. This ensure that the evolution of the algorithm is passed onto future UAVs and doesn't become specific to a single type of UAV. This cross contamination of developmental work means that new research has an archive of information which can cut future development time.

6.1.3 Suitable Sensors

Nature's flyers such as birds and insects have an array of sensors which they use to control their flying and navigation. For this application, navigation will not be required as the UAV will begin the perching sequence when it is bought into the vicinity of a lighting column. Once the Lighting column is located below the UAV, the use of contactless sensors must be used to navigate the UAV towards the lighting column's projection bracket centre, to initiate the perch. In order to detect the projection bracket the UAV had to be equipped with low cost Commercially off the Shelf (COTS) sensor/s.

6.1.3.1 Vision

Birds use their eyes to judge the distance to the land/perch target which they then process and execute the manoeuvre. Having a vision system would mean that a suitable on-board microprocessor would be required to process the images being captured. The processed images would then determine the next action to be taken by the control system to navigate the UAV over the target in the correct origination). The vision hardware would have to have a good useable resolution to detect details in the lighting column's bracket projection (see Figure 6.1. The field of view would also play crucial role as this would determine the operational height of the perching element. A major drawback to this setup is the processing power required which might affect the image sample rate, which in turn would affect the UAVs response time.

Figure 6.1 - Gimballed camera unit from Bradley Engineering used for visual tracking.

6.1.3.2 Acoustic

The range of ultrasonic sensors which are available to measure distance offers the positional control which the UAV needs in order to execute the perch. Ultrasonic sensors emit an acoustic pulse which then bounces off solid objects and reflects back to the receiver. Using the speed of sound, the time it takes for the pulse to reflect off an object and reach the receiver, the distance of the object can be determined. The important factors which were considered:

- Size of the sensor
- Mass of the sensor
- Frequency of operation
- Output options
- Beam angle

An important factor which affects how efficient the detection process can be is how wide the beam angle is. The angle of the beam would mean how accurately the projection bracket can be detected. The acoustic cone, which is emitted from the sensor, can be adjusted with certain sensors such as the SRF10 from Sharp

(see Figure 6.2). However, to achieve the most effective perch detection, a narrow pencil beam is required which can be accomplished using a MaxSonar-EZ4.

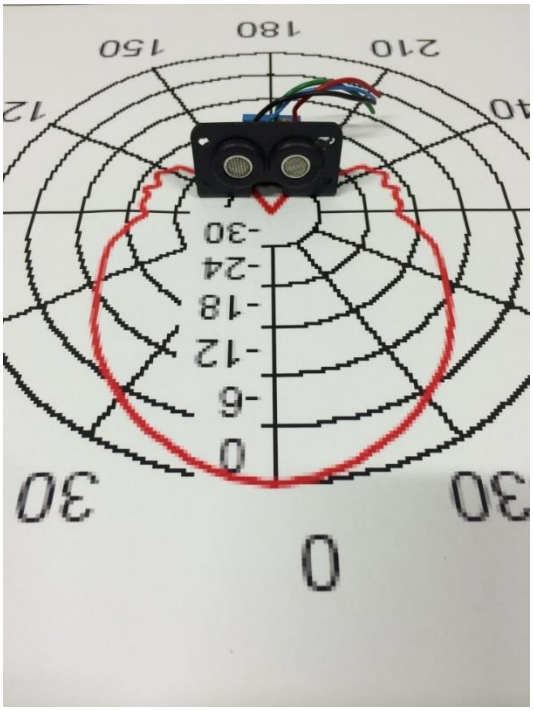

Figure 6.2 - Ultrasonic sensor SRF10 and its acoustic beam.

6.1.3.3 Light

An alternative to ultrasonic sensors would be the use of infra-red (IR) sensors and laser scanners. Working on a similar basis as the ultrasonic sensor, an IR distance sensor emits an IR signal which again reflects off a solid object which is then sent back to the sensor's receiver module to be processed and output a useable signal from the sensor (see Figure 6.3).

A laser scanner uses the same principle but with a photodetector as the receiver and a laser pulse as the emitter. This option has a greater accuracy and resolution but also a larger price tag.

6.1.3.4 Contact

Contact sensors such as micro switches were widely available due to their low price tag. An adaptation of a micro switch to create a sensitive multi directional switch is the whisker switch (see Figure 6.4). The general idea and name taken from natures' cats, a whisker switch could be used in such a manner that is could be utilised to locate the perch site feeling for it. A draw back to this switch is its

primitive search of the perch site which is a likely cause contact between the lamp post and UAV.

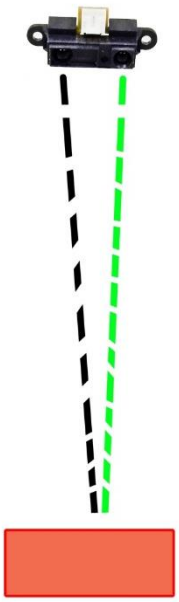

Figure 6.3 - IR sensor operation - Black line representing the transmission and the green for receiving.

Figure 6.4 - Whisker Switch with spring base to ensure contact returns to same position.

6.1.4 Chosen Sensor

All the sensor types showed promise and could possibly be made to work one way or another. However due to the complicated task of detecting something which could be mistaken for a tree or another piece of street furniture, it was opted to go for vision based system as it was the most cost effective solution which could give the most accurate picture of the perch site.

Considering the gentle approach required to execute the perch, a slow approach to the projection bracket from the UAV was acceptable. Therefore an on-board solution was looked at. This gave the system a complete standalone functional perching solution. The next step was to select the specific microprocessor and vision sensor. The specifications which were taken into consideration when selecting were mass, cost, power consumption, processing power and availability. Specifications such as connectivity and the two system's ability to interface with each other were also considered but did not influence the decision as these aspects could be later modified to work with each other.

After searching the market for vision based processors, the popular choice was to select the very cost effective Raspberry Pi 2 along with the PiCamera module. At a combined cost of about £45, it was one of the most cost effective solutions as it also had an extensive online database of support files and examples. Its open source architecture made it easily adaptable to the perching element as the integration and operation was made simple.

At the time of selection, the latest Raspberry Pi release was the second generation model with its quad core processor (see Figure 6.5). It has 1 Gigabyte (GB) of Random Access Memory (RAM) and running Linux operating software which allowed for easy installation of the programming software such as Python (RaspberryPi, 2016b).

The PiCamera measures 25mm x 20mm x 9mm and is has 5 megapixel sensor (2592x1944) which is capable of processing videos up to 1080p at 30 frames per second and weighs only 3 grams.

6.1.5 Computing Software

To develop the algorithm certain applications had to be installed on the Raspberry Pi. First and foremost was Python v3 for Pi. Python is a powerful

programing language which allows the Raspberry Pi to run a variation of code to perform specific task (RaspberryPi, 2016a). Python also works when installed with supporting software. Such software could conduct the specific tasks which the Python code requests. In this instance, Open Computer Vision (OpenCV) v2.7 for Pi was installed alongside Python along with a number of libraries, support packages and drivers. OpenCV accesses many vision based databases which makes the image processing much quicker/effective. Also others in the field have used similar setups to achieve UAV control using vision processing (Lenge et al., 2008).

6.1.6 Early Algorithm Development

The versatility of the Raspberry Pi made it very easy to install into the UAV. The battery on-board the UAV which supplies 14.8 V was stepped down to 5 V for the Pi to operate. With the PiCamera attached, the system drew 1.75 W which was well within the design specification of 45 W. To get started, the Raspberry Pi had to be configured by installing the operating software and the required software which would run the code for the vision processing. Once the Raspberry Pi was setup with the camera functioning, an example program was run to ensure the whole setup worked. Next stage was to develop the flow of the algorithm (see Figure 6.6) which would aid with how the UAV will manoeuvre over the perch site and how the Algorithm will be developed.

The aim of the detect stage was to identify the common features on top of the projection bracket which the camera system could detect and use to navigate around. As mentioned before, the projection bracket consists of the Lantern unit, the neck and the top of the column.

Of these features, the dominant and most consistent was the light sensor which is located on the lantern unit and is found on all UK lighting columns. It is this sensor which switches the power to the lighting column on and off (see Figure 6.7). What made this sensor the subject of interest is its circular shape. As it is a replaceable part, it is found on top of the lantern unit for ease of access and of course the direct view of the sun. This light sensor prompted an investigation into shape detection at an early stage of the detection algorithm.

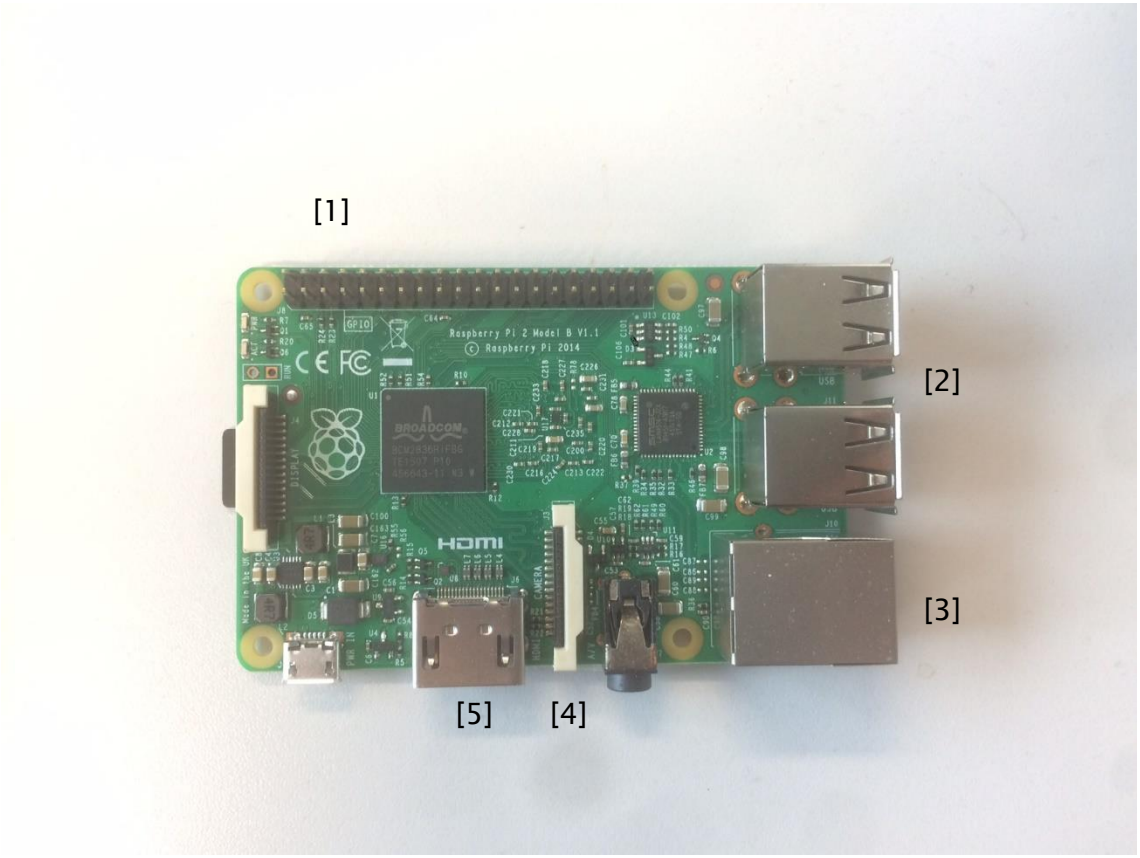

Figure 6.5 - Raspberry Pi 2 Model B. [1] GPIO ports which is also used to supply power to the board. [2] USB ports used for keyboard and mice. [3] Ethernet port used for internet access to download software or to access Pi through Putty terminal. [4] Camera ribbon cable slot [5] HDMI port to connect to monitor.

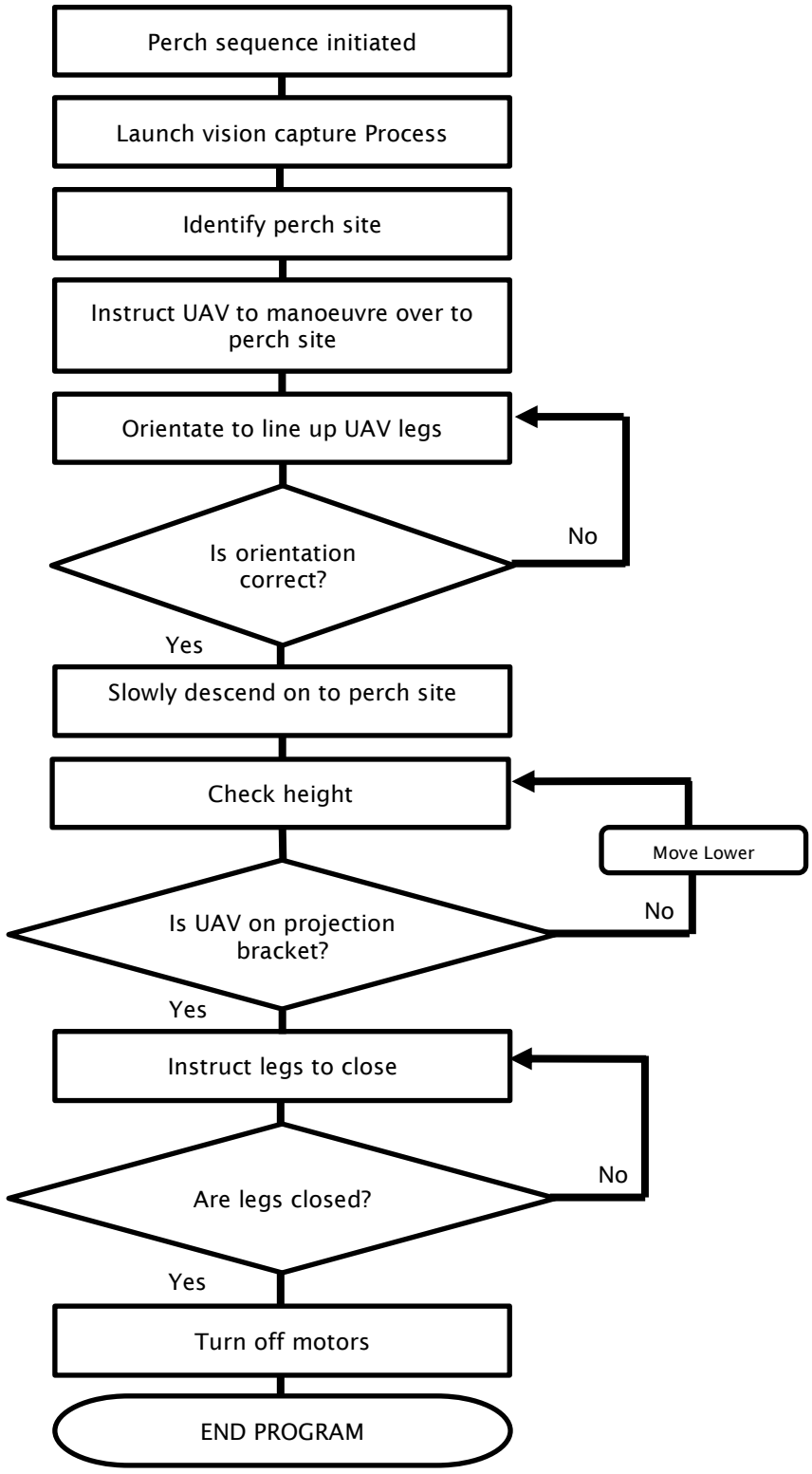

Figure 6.6 - Initial algorithm flow chart.

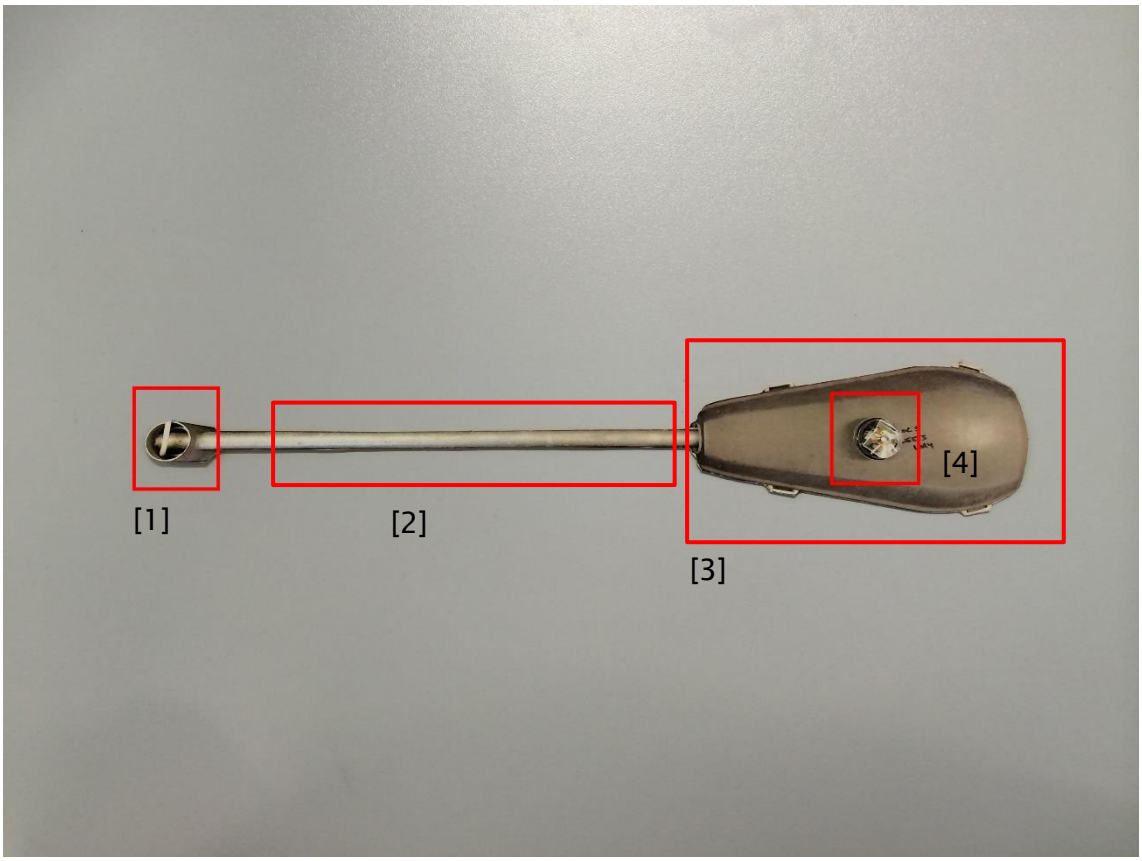

Figure 6.7 - Image of projection bracket from above. [1] Column [2] Neck [3] Lantern Unit [4] Light Sensor.

Before trying to detect the light sensor, a bench test was setup by connecting all the components together to make the early stage development more straightforward. Because the Raspberry Pi can connect to a camera through either the ribbon port on the board or with the use of an USB based camera, the initial part of any code was initiate the camera by calling upon the PiCamera. At this stage the resolution was also set along with the frame rate and the format (Blue Green Red [BGR] in this case). The resolution of 640 x 480 was set as it reduced the processing time and the image which was captured, was still fine enough to use highlight the required features. Then all background clutter was eliminated by using a whiteboard as the detection area and simply drawing the circles on the board and trying out a simple program (see Figure 6.8). The libraries called upon was the Hough Transform Circle function. This function searches for circular shapes within an image or in this case a video. The function has nine parameters which have to be set in order for the detection to be effective. When a using the function in Python, it looks like this:

cv2.HoughCircles(image, method, dp, minDist, circles, param1, param2, minRadius, maxRadius)

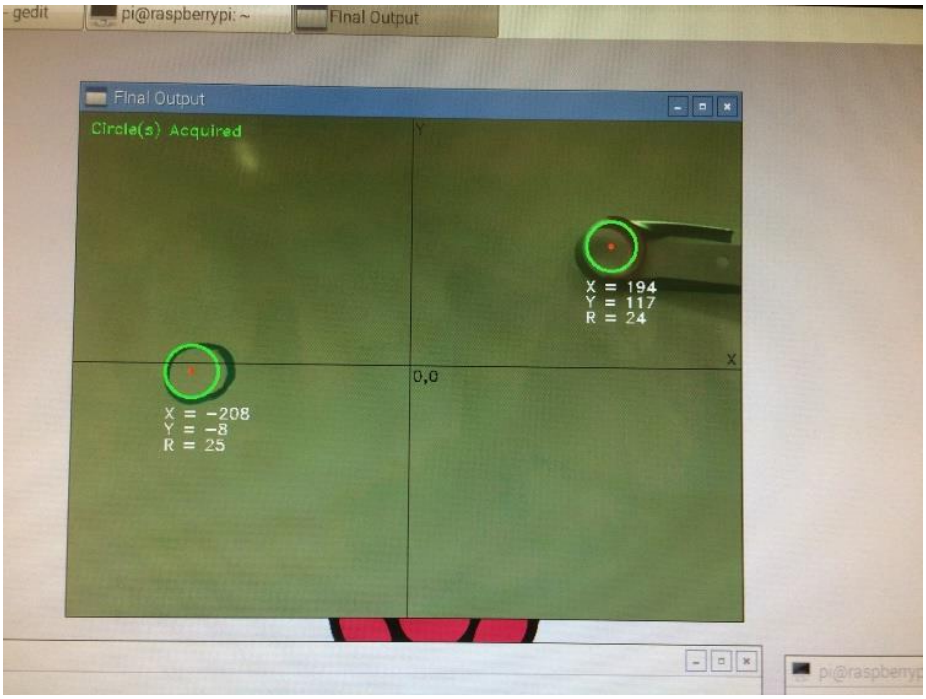

Figure 6.8 - Screenshot of the image from PiCamera detecting two drawn circles.

The nine parameters played an important role in detecting the required circles. Firstly, the function relied on the original colour image being converted into a greyscale image. What this did was it removed the additional work which the processor will had to forego in order to achieve the same end result, as many functions did not rely on the colour information in the image. Once the image had been converted, the next stage was setting the parameters for the function. These were; limiting the size of circles which can be found in an image (*minRadius, maxRadius*) which determines the minimum radius along with the maximum radius of the circles which can be found (measured in pixels). This eliminated some of the unwanted circles which can be found in the background of the image. Another parameter was the distance between each circle (minDist) which again measured in pixels, helped with removing circles which are detected side by side. Some parameters were for telling the function where to look for an image and where to output the circle information. One of the most important parameters were the 'param1' and 'param2'. These two determined how round the circle being detected was. These numbers were examined carefully during

experimentation as the sensor on the lantern unit could appear to look like an oval if approached at various angles.

The parameters which is applied to this function becomes specific to the task at hand. During the bench testing stage, the numbers were adjusted until a lock was achieved on the circles which were drawn on the whiteboard. The way Hough Circle function works was it stores all the relevant information about a circle i.e. X, Y and radius measured in pixels, which were found in an image, onto the memory of the Raspberry Pi. The next stage was to call up the data for each circle on memory and display the information on screen.

Whilst experimenting with the function at this stage, it was discovered that by using the size of the circles, one can determine the distance away from the target perch site. Given that the sensor is locked on and in the centre of the camera, the radius of the circle at a given distance could be calculated using the known radius of the sensor at said distance.

It became very clear at the end of the bench testing that the main structure of the algorithm will rely heavily on being able to consistently detect the light sensor every time (see Appendix F).

6.1.7 Quadrant Division

The Idea to split the search window into an equally spaced quadrant allowed for simple calculations to navigate over the perch site. These simple calculations were also essential to the speed of the processing as the more filters or functions called upon, the harder and slower the vision system would have to work. The theory was, depending on which quadrant the light sensor of the projection bracket was found, it would easily work out the motions required to bring the light sensor into the intersection of the quadrant. The centre of the screen became location 0,0 (X, Y) which was essentially pixel number 320 x 240. In order to display the centre of the detected light sensor, depending on which quadrant the light sensor was found, it would convert the XY position of the sensor into negative numbers if the circle was found in the negative quadrants (see Figure 6.9). Only quadrant 1 would produce positive coordinates.

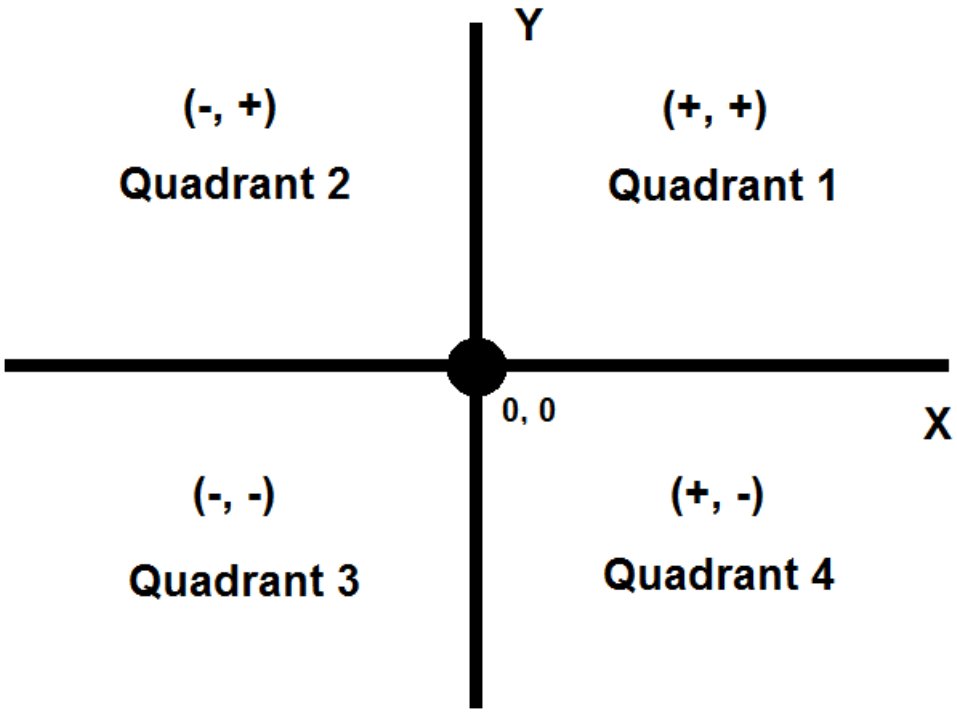

Figure 6.9 - Displaying how the quadrant are split up

By looking at whether the XY coordinates were positive or negative, using logic commands, it was possible to determine which trigonometric function to use. Depending on which quadrant was active, the mathematical function used was:

math.degrees(math.atan(x/y))

A few prerequisite conversions had to be calculated as this function required floating point numbers where other functions required whole integers. This took the X and Y coordinate of the detected light sensor in relation to the 0,0 origin and displayed the angle between the light sensor and the 90˚ line which in this case was on the X axis to the right of the image (see Figure 6.10). The degrees function converted the angle from radians to degrees which is what was sent to the FCS. The angle which was produced from this function had to be offset by 90˚ and then an additional 180˚ added to produce the heading of the UAV in relation to the 0,0. This got complicated as the function used was producing positive numbers in the counter clock wise direction from heading 90˚ and the heading reading had to display in the clock wise direction from heading 0˚.

The next stage was to display the heading direction from the origin 0,0 to the centre of the light sensor. It was this distance which was stored as it would be used at a later stage.

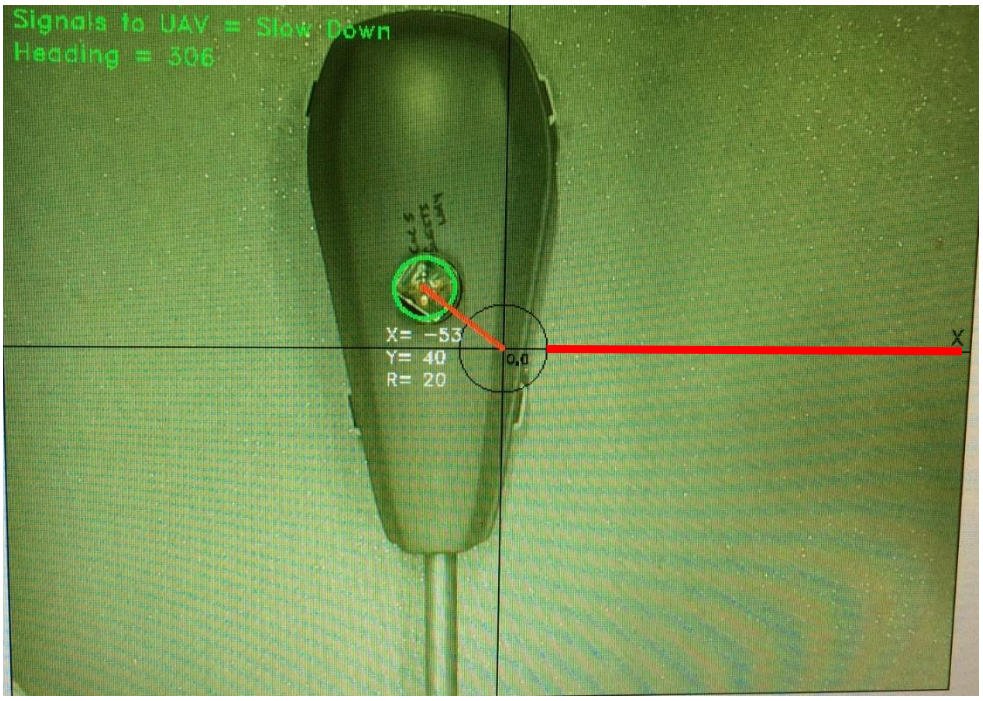

Figure 6.10 - Target acquisition using quadrant setup. Also highlighted with a red line, the 0° start line for the trigonometric function.

6.2 Manoeuvre

With the vision system up and running, the next step was to look into how to command the UAV using the Raspberry Pi.

6.2.1 Initial Commands

As the control of the UAV was being overridden, the first task was to ensure that the UAV would be safe during this initial development stage. To do this, the UAV was fastened to the gantry test-rig as this restricted the movements of the UAV to safe angles. As mentioned before, the intended method of sending commands to the MikroKopter FCS was to use serial commands which the Raspberry Pi could output. There were several ways of achieving control of the MK Hexa. The first was to send direct controls to the FCS or to spoof the GPS signals by taking over the Naviboard which then in turn controls the FCS. As GPS was not available indoors, the spoofing would not be successful as there would be no initial lock. The direct option was executed by enabling the whole perch sequence through a switch on the transmitter. The same switch would also trigger the start of the detection algorithm. The MikroKopter universal asynchronous

receiver/transmitter (UART) protocols had to be understood and made to work with the Raspberry Pi output. A Library on the MikroKopter website was found and used to send direct commands to control Roll, Pitch and Yaw (MikroKopter, 2016). The FCS had to initially be set up to accept the external controls coming from the serial port. It was here a transmitter channel was assigned to controlling the beginning process of the perching. There were many other aspects which could be controlled or overridden using the serial port, however the only control that was required was the ability to make the UAV manoeuvre over the perch site.

At this point, the camera was not placed on the UAV and was somewhat flexible with regards to the final layout. In order to establish a reference point on the image recognition algorithm, it was decided that the camera should be placed at the lowest point of the Z axis. This would ensure that the UAV had a datum point to position it's self centrally in relation with the centre of the PiCamera image. The camera was installed centrally on the lower plate of the perching

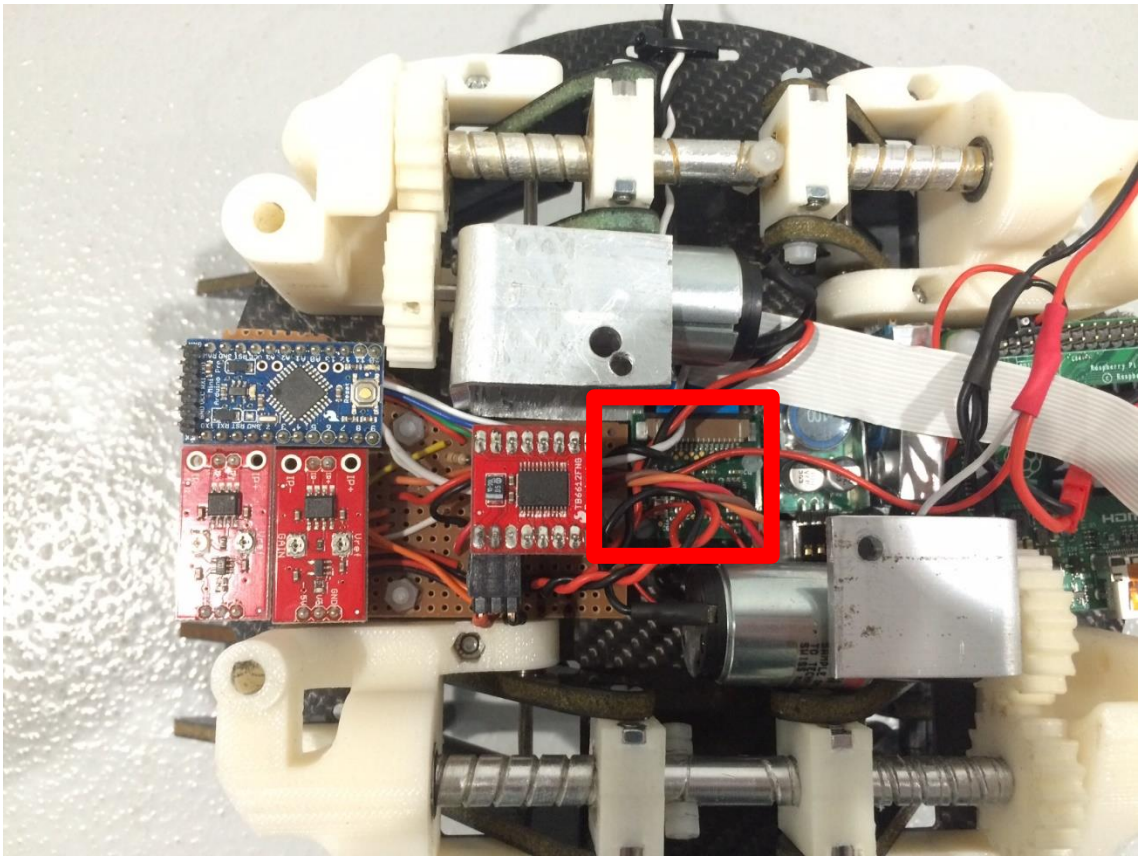

Figure 6.11 - PiCamera placed in between the two drive motors and in the centre position of the lower plate.

element's structure in between the two non-backdrivable screw threads (see Figure 6.11).

At this point, the origination of the camera was vital as this would dictate the final landing position. So the top of the image would indicate arm no.1 on the UAV which is red (see Figure 4.1, page 61). This was perpendicular to the force which the grippers would exert onto the projection bracket. This would also mean that when the UAV is orientating around the light sensor, the projection bracket's neck doubled up as a reference mark for correct alignment.

6.2.2 UAV Movement

The instructions to move the UAV on the test-rig was conducted systematically to ensure all axes of movements were achievable. To begin with, the Y axis was tested by instructing the UAV through the FCS to pitch forward and backwards. The X axis was taken care of by the roll command and the Z and rotations about Z was both throttle and yaw respectively. During all axis movement a minimum throttle command had to be transmitted. This was simulate the UAV in a state of hover. There were parameters to sustain height control, but these were not effective indoors as opposed to outdoors where the turbulence created by the prop-wash did not affect the height readings. As the space in the laboratory was limited, the moving air was easily bouncing off the walls and surrounding furniture (see Figure 6.12). The same test was conducted in a larger indoor space, where there was room for the air to move around freely, and as a result, the altitude hold function worked much more effectively.

To manoeuvre the UAV to the correct perch site, serial commands had to be sent at the correct trigger points to ensure the perch was successful. Once the detect functions of the algorithm were robust enough, the next task was to ensure the motions of the UAV would match the search algorithm.

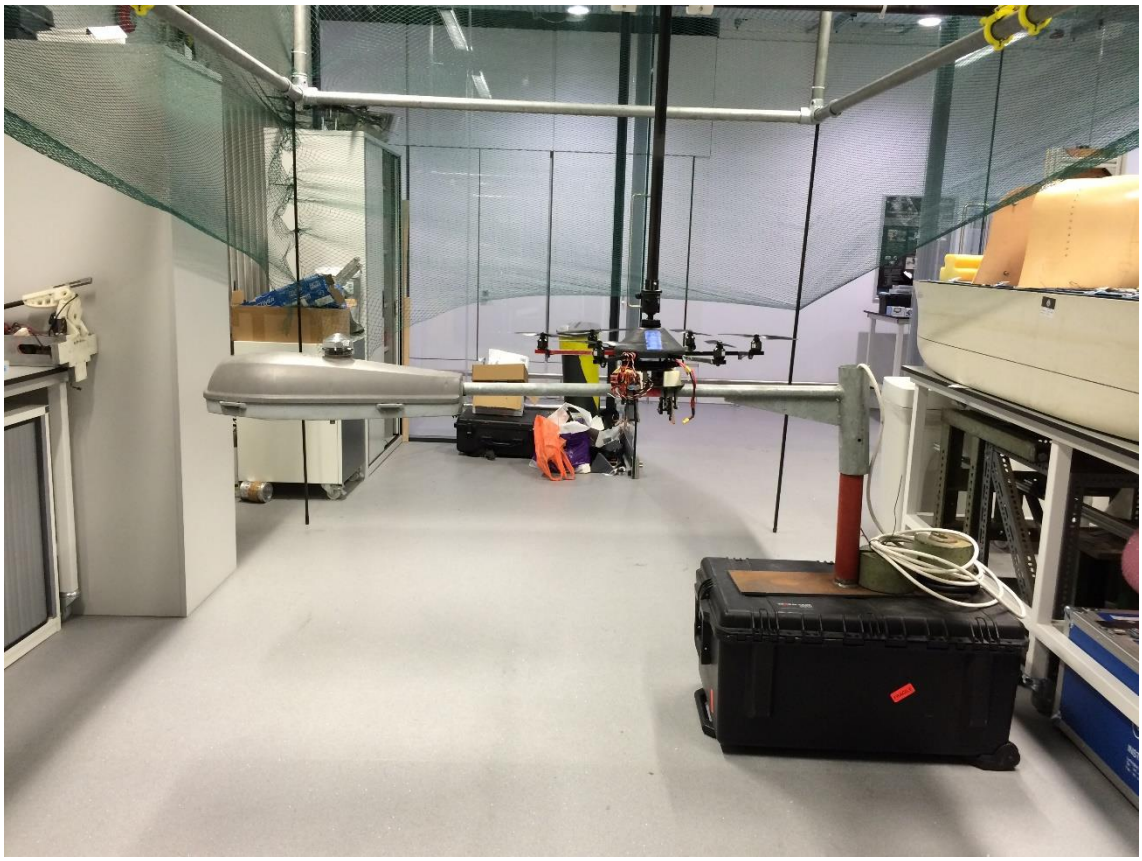

Figure 6.12 - Cluttered environment allowing for prop-wash to cause disturbances.

6.2.3 Speed of Approach

Using the heading number, the UAV could be directed towards the light sensor. As mentioned before, the MK FCS had many other controllable aspects which were not used during initial testing. Now that the heading of the UAV in relation to the origin could be determined, 180˚ was added which gave the correct heading direction of the UAV. This new number was then used to directly to control the direction of the UAV by sending serial commands to the FCS. This information coupled with the distance away from the light sensor (which was stored previously) was used to work out the approach speed of the UAV to the light sensor. As accuracy was key, the approach speed was set to a maximum of 0.25 m/s which limited the angle of attack of the UAV. This ensured that the downwards looking camera's FOV was uninterrupted. Sending this heading number directly to the FCS became very convenient as it removed the need for additional computation i.e. the rate of roll and pitch which is required to achieve the same result.

To ensure a smooth start/stop motion of the UAV, a ramp up and ramp down program was initiated. This not only reduced the amount the UAV would over shoot the target, but it also produced a smooth operation whilst keeping the camera FOV on target. The rate at which the UAV would deaccelerate when approaching the light sensor was programmed such that once the UAV crossed the set radius, it would begin the slow down procedure. The same principle also applied to the halt command which was also set to a given radius. In order for the UAV not to spend too much time trying to lock directly to 0,0 coordinate, the halt radius was set by experimenting with how much the UAV will over shoot. All radius values were measured in pixels. If higher degree of accuracy was required, the resolution could be increased which would result in a lower frame rate as mentioned before.

Figure 6.13 - Camera detection sequence. Top Row, right to left. Light sensor detected and target locked. Manoeuvre sequence can begin. Gets closer in the next frame without deviating from heading too much. Once over light sensor, UAV rotates to ensure projection bracket is lined up with image Y axis.

6.2.4 Projection Bracket Orientation

With the UAV directly over the light sensor, the next step was to orientate the UAV about the Z axis to ensure the perching legs would match up to the projection bracket. To do this, a reference feature had to be outlined. In this case, the neck of the projection bracket was used as a datum. The function used here is called Hough Line Transform which applies filters to detect lines in the image. Once lines are found, they are outputted into their own start and finish X,Y positions. This implemented method allowed for a guaranteed result. Figure 6.13 shows the detection and manoeuvre at various stages. The bottom two images highlights the neck which is used to line up again the Y axis. Once the angle of the neck is 180˚ offset from heading 0˚, the detection phase is complete. During testing, the lines were drawn on the image, but later removed to speed up the processing time.

6.2.5 Line Up

The next stage was to move the UAV further down the projection bracket so that that the legs of the perching element would line up with the perch site with the

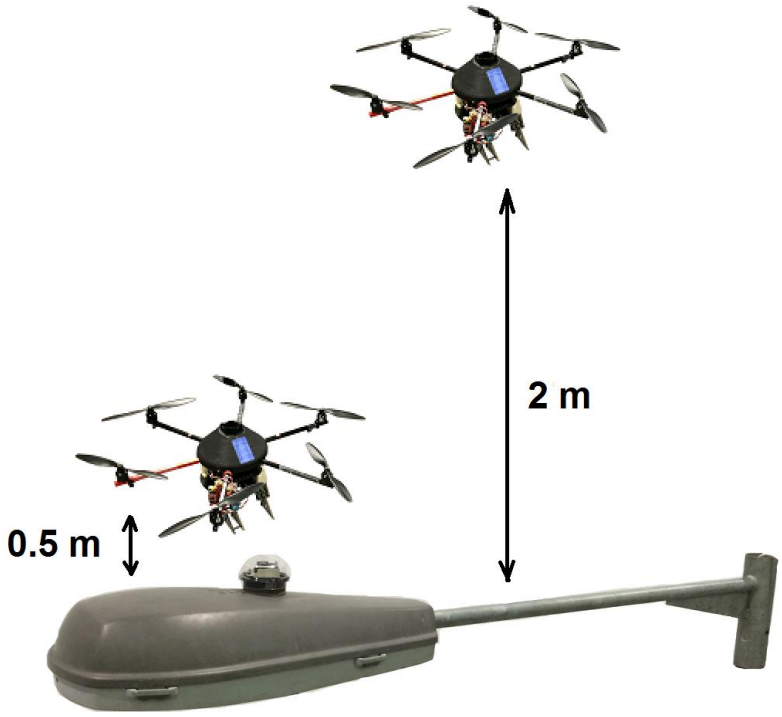

Figure 6.14 - The upper and lower limits of the detection algorithm dictated by the set camera resolution.

rotors of the UAV colliding with the lantern unit. By trying to accommodate to various projections, the ideal perch point was dictated by the how far the UAV was from the projection bracket. The distance was established by using the diameter of the light sensor, a ratio was created which would determine how far down the projection bracket the UAV would have to move (in seconds). Once the UAV had completed its rotations about the Z axis, the size of the light sensor was stored to be used by this part of the algorithm. At this resolution, the detection was set between 0.5 m and 2 m (see Figure 6.14). At 0.5 m the radius of the detected light sensor was 38 pixels and at 2 m the radius was 7.

By using these numbers a scale was created for the UAV to determine how much to move. Depending on the height of the projection bracket, at lower altitudes, the camera would lose its lock on the light sensor. This created too many errors for when the UAV was moving down the projection bracket. By using the heading of the light sensor against the origin, the alignment of the UAV was checked every second. So to fix the drifting problem, once the UAV had rotated about Z, another stage was added which was to increase or decrease the height of the UAV so that the light sensor was always in view of the camera. This meant that there was correct alignment when manoeuvring down the projection bracket. It

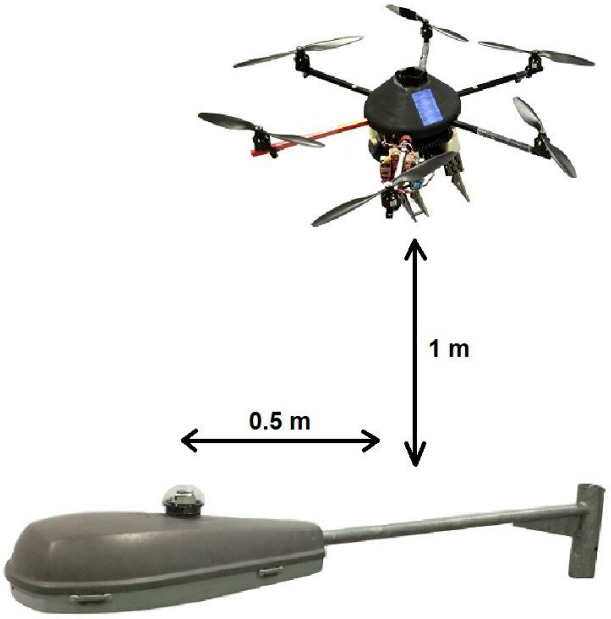

Figure 6.15 - The final descend positon of the UAV once the manoeuvre was complete.

also meant removing the scale look up of the distance away from the lantern unit which therefore increased consistency as the same manoeuvre was carried out each time. This contributed to processing speeds as a whole step was removed and the algorithm optimised. A correction height of 1 m (or 20 pixel radius) was set which meant the light sensor was still in view when the UAV was moving towards the perch site. The UAV was then instructed to move backwards for 2 seconds at 0.25 m/s. This moved the UAV roughly 0.5 m taking into consideration the ramp up and ramp down procedure (see Figure 6.15 and Figure 6.16). This manoeuvre ensure that the UAV's props would avoiding colliding with the lantern unit.

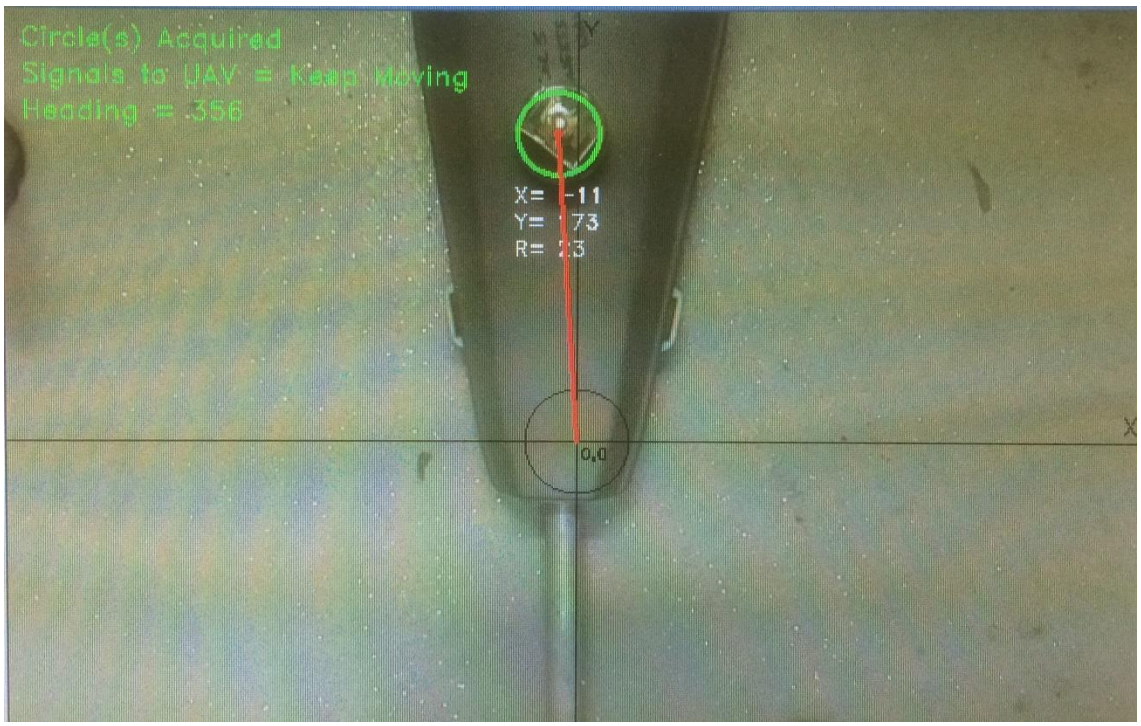

Figure 6.16 - Image from PiCamera from 1 m high and 0.5 m back over perch site.

6.3 Perch

In order for the perching element to be semi-automatic, a few things had to be resolved before moving forwards with the algorithm development. The actuation of the gripper had to be automated and the consistency of the mechanical components had to be improved.

6.3.1 Actuation Control Board

With the gripper assembled, it needed intelligence to control the motors which would engage and disengage the gripping legs. This would come in the form of a microprocessor and in this case, an Arduino Micro (see Appendix E for code). As the non-backdrivable screw threads were driven by independent motors, each motor required a speed controller to control the clockwise and counter clockwise motion. By doing so, the gripping legs which are connected to the screw blocks, would continually move as long as power is provided to it. The idea of being able to grasp multiple types of shapes of different sizes, the Arduino needed an input to instruct the motors when to stop. The most cost effective way of detecting when to stop the motors was to install a current sensor between the speed controller and motor. The current values were then read by the Arduino, and at the appropriate current draw, the instruction to stop the motors would be transmitted.

So the actuation control board was designed to take a PWM signal from the UAV's FCS and could be triggered to open and close at the flick of a switch during development. Figure 6.17 details the component placement on the control board. On the transmitter, a three position toggle switch was assigned for controlling the three states of the gripper, open, neutral and close. The open position was designed to be the extreme position of the non-backdrivable screw thread as it also served a purpose of being the default landing stance. This ensured that the gripper was always ready for landing, which met the emergency land criteria. So when the toggle switch is engaged on the transmitter, the gripper begins to close shut until the legs meets the gripping surface at which point the current draw on the motor increases and triggers the Arduino to send a halt command.

The point at which the halt command was sent had to be determined beforehand. The Arduino program dealt with one variable which was the value given by the current sensor. This was the value which would trigger the halt command. However, as the two motors did not output identical numbers, they were calibrated to give identical if not similar results once the correct torque value was reached. The current sensors had two potentiometers which had to be adjusted to ensure both were operating in a similar range. A calibration program was written to tune these values. The current sensors operate at a voltage of 5V

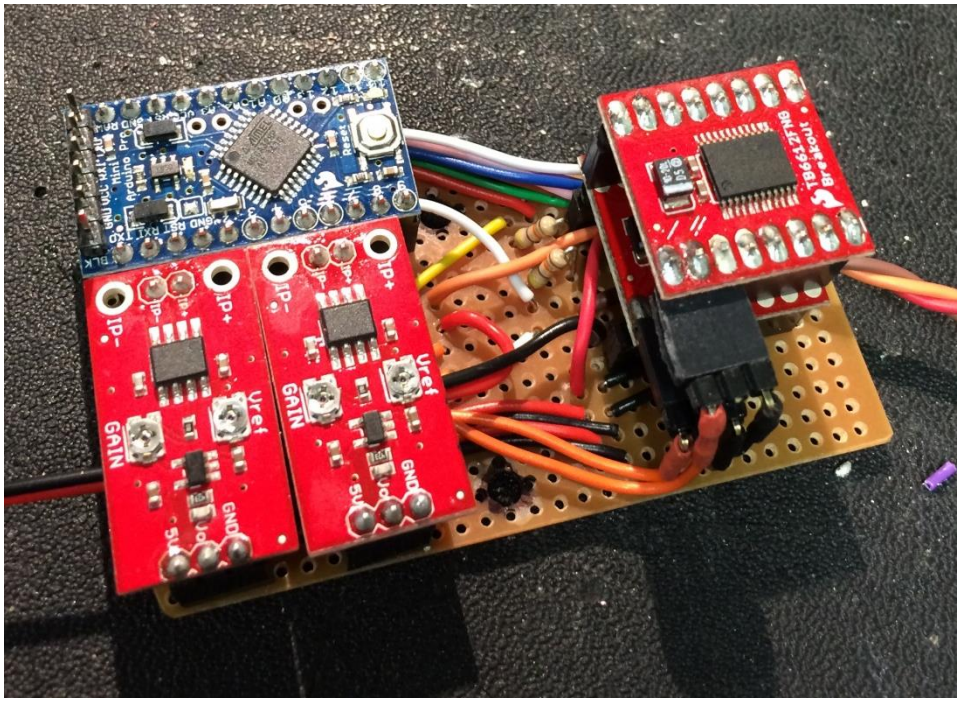

Figure 6.17 - Gripper actuation control board. Blue Arduino Micro (top left corner), two current sensors side by side (bottom left corner) and two speed controllers stacked on top of each other (right side).

and then output an analogue signal which the Arduino's 10 bit analogue-to-digital (ADC) converter translates it to an integer between 0 and 1023. In this case, 0.3 Nm which was the torque value used during wind tunnel testing, translated to a value of 700 at which point the legs should stop moving. To find this number, the perching element was placed on top of the projection bracket and was given an instruction to grip. By starting with a low number, it prevented putting unnecessary stress on the components. When a grip was achieved, the gripper was then released using the torque screwdriver to measure the highest torque value recorded during the release. Once the release torque reached 0.3 Nm, the values were saved and the program was complete. At point it was noted that the initial start-up current had to be ignored as this would trigger the gripper to stop almost instantly. So for every actuation command, the current values were ignored for 100 milliseconds which was enough time for the current value to settle.

With the current sensors calibrated and the appropriate current values set, it was time to place everything on a single board which would fit with the other perching element components. Therefore, the shape of the actuation control board reflects the space which was available on the gripper lower plate. The

board was then plugged into the FCS and was tested to check operations. The PWM signal which the FCS was producing was extremely temperamental which lead to using an alternative PWM signal that came directly from the receiver.

During the final testing phase of the actuation board, the gripper components began to fatigue and fail. This lead to a final overhaul of the mechanical systems.

6.3.2 Final Optimised Gripper

The reliability of the 3D printed ABS parts became a major issue as during the programing phase of the current sensors, the values were inconsistent. This was due to the resistance between the 3D printed ABS parts and the poorly finished handmade screw threads. The two components did not mesh well with each other as the strength and print resolution of the screw blocks resulted in failure. If the non-backdrivable screw thread were not lubricated, the two parts lead to a large current draw which meant the gripper would stop prematurely. Because the current sensors were programmed when screw blocks and non-backdrivable screw threads were dry, once lubricated the non-backdrivable screw threads managed to shred the thread which was printed on the inside of the screw blocks. Another issue was if the current sensors did not stop the speed controllers due to the lubrication, the screw blocks would drive into the gear or central dead stop. The screw blocks became jammed on either side on several occasion. The only way to un-jam it was to manually loosen it by unscrewing the non-backdrivable screw thread.

To rectify this problem, the screw blocks and non-backdrivable screw threads were upgraded to off the shelf components. It did increase in weight, however the mass penalty was justified with an increase in reliability. The upgrade process consisted of sourcing CW and CCW screw threads of similar pitch with matching nuts within a timely manner. Due to lead times, a pitch of 5 mm and a diameter of 8 mm screw threads were not available. The closest item which was available was a 3 mm pitch with a 12 mm diameter (see Figure 6.18). This added unnecessary mass to the perching system and also made it slight slower to actuate. This also meant that the results from the wind tunnel testing were no longer matching to this combination. As the dynamic wind tunnel testing already justified the theoretical data, a repeat in wind tunnel testing was not required. Whilst the non-backdrivable screw threads were being upgraded, it was also an

opportunity to upgrade the leg runners. By adding more support material around the runner slot, it meant the gripper could potentially grip with higher force without damaging the carbon fibre legs (see Figure 6.19).

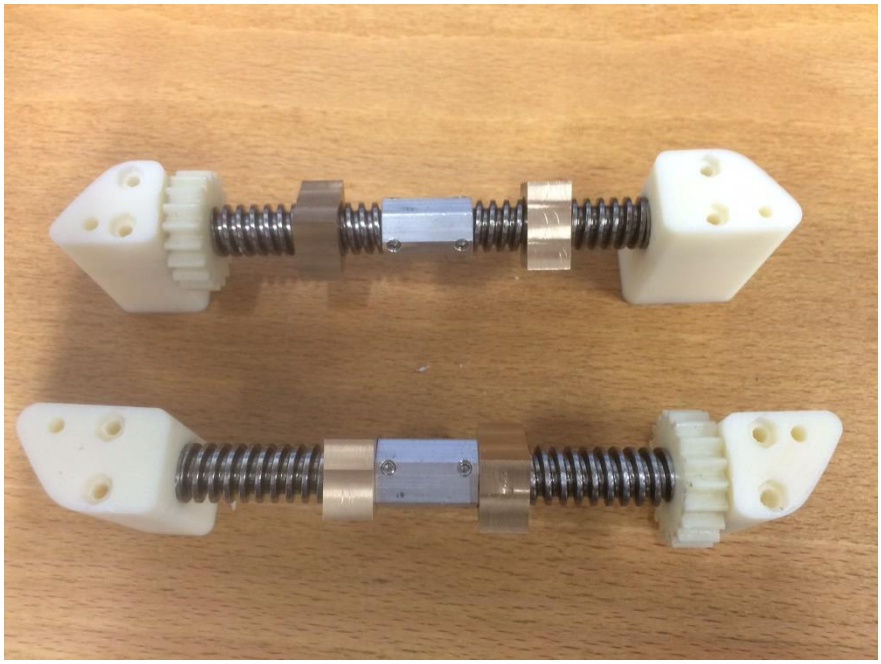

Figure 6.18 - Pair of upgraded non-backdrivable screw threads with brass screw blocks.

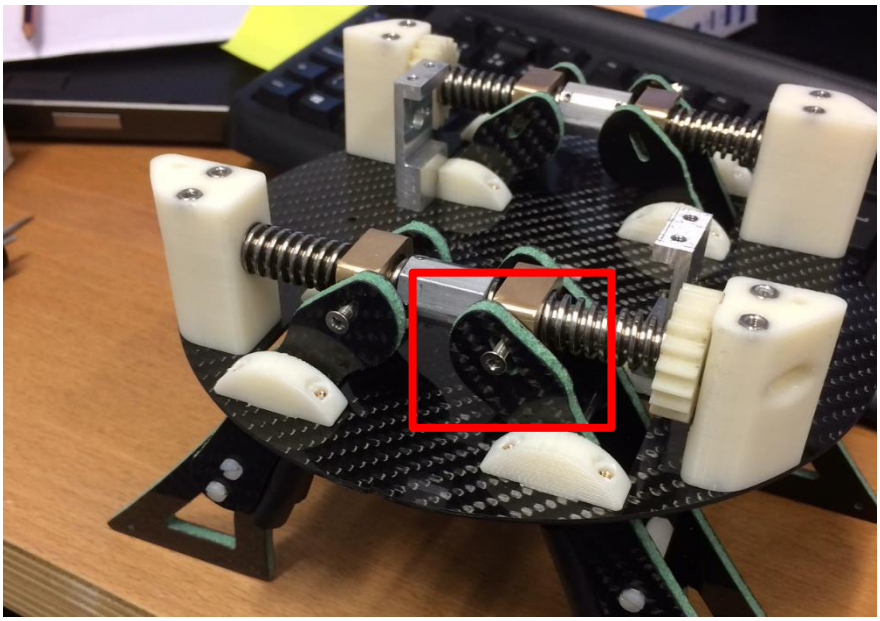

Figure 6.19 - Increase in support material around the runner slot.

The old motor brackets were also an aspect which needed attention. They were large heavy and cumbersome. A 48% mass saving was made by remaking the motor brackets. From 17.01 g each to 8.26 g. However a mass increase of 470% was incurred due to the new non-backdrivable screw threads. Whilst savings were made on some components, others massively offset the savings. Overall, an additional 45 g was added due to the upgrades bring the mass from 403.12 g to 448.07 g. Additional hardware was also added to ensure the motor will not be over worked. By placing a micro switch at both fully open and fully closed positions, the actuations can be stopped at each extremity of the leg travel (see Figure 6.20). These micro switches were wired directly to the Arduino, and when activated, it was programed to halt the motors. The fully open micro switch prevented the screw blocks from jamming into the central coupler and the fully closed switch prevented the screw block from jamming into the gear or bearing blocks. Both micro switch positions could also be adjusted as required.

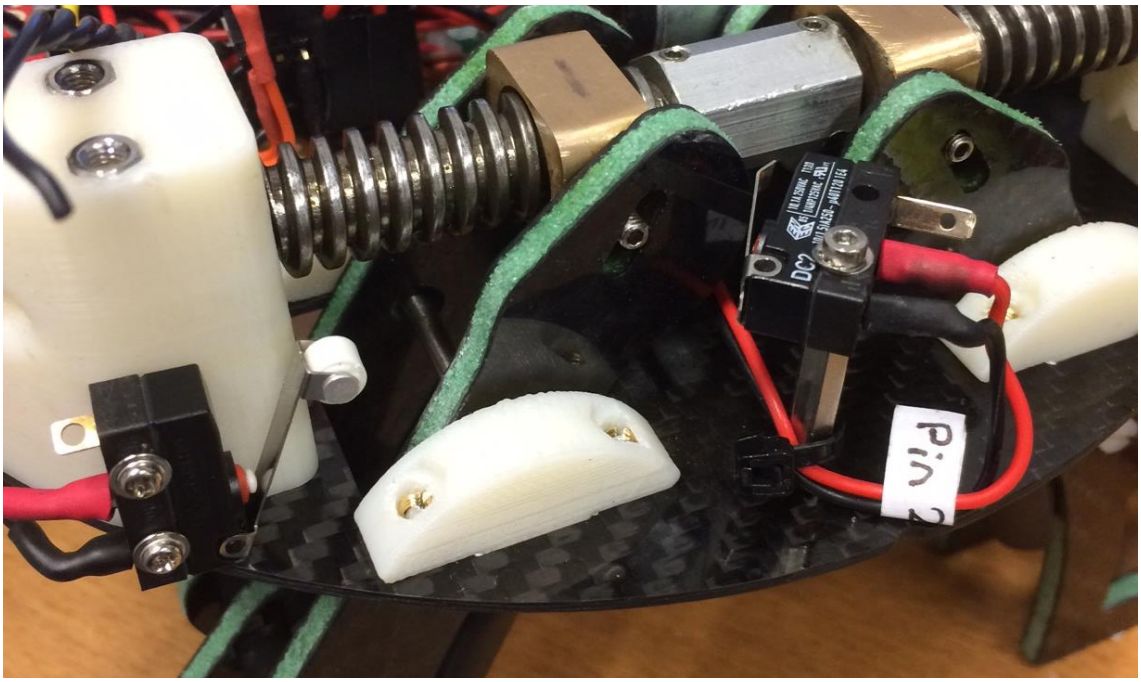

Figure 6.20 - Two micro switches. Left switch - fully closed positon, right switch fully open positon.

The benefits of the latest modifications became very evident once the current sensor values were being reprogrammed. Within minutes the new values were found and worked consistently and smoothly. The longevity of the perching element was also enhanced as the new heavy duty non-backdrivable screw threads increased the overall robustness (see Figure 6.21).

Figure 6.21 - The final UAV with perching element attached and ready to be tested.

The Raspberry Pi did not fit inside the 180 mm diameter of the central hub and had to be mounted with more than half the board sticking out. It did have three points of contact on the lower plate, but nonetheless, the Raspberry Pi Zero was considered as it was substantially smaller. At first glance over the specifications of the Pi Zero, the single core processor was not up to the job of video processing.

6.3.3 Descend

As a height of 1 m was set in the previous part of the algorithm, in laboratory conditions, it ensured the consistency of this part of the manoeuvre. However this would change if any disturbances like wind were to be introduced. The UAV was set to descend at a rate of 0.1 m/s as this was an acceptable balance between speed and accuracy. During the descend phase, the UAV would check it's alignment in regards to the projection bracket. For this stage small minor roll and yaw adjustments were being made to keep the UAV descend path on track (see Figure 6.22).

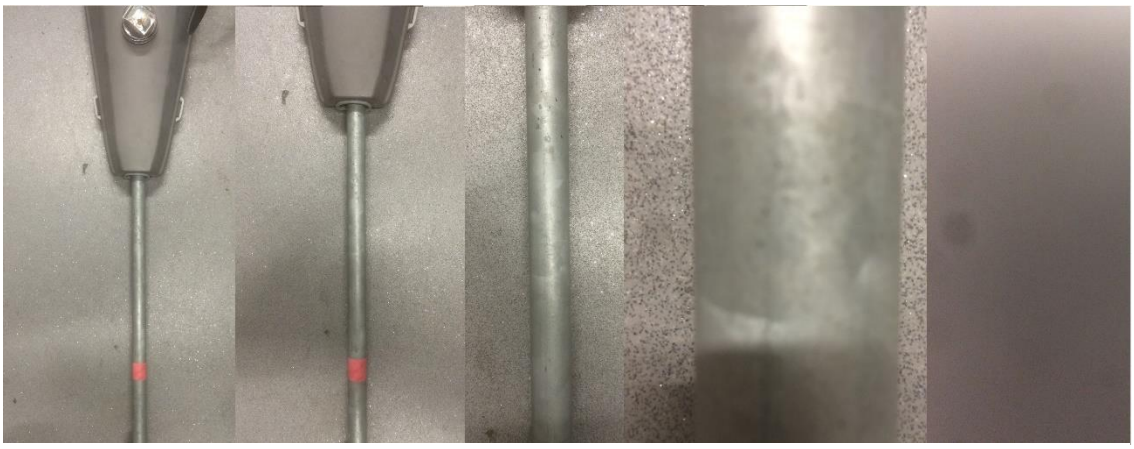

Figure 6.22 - Final approach to the projection bracket neck whilst keeping alignment.

To detect when contact with the projection bracket was made, the FCS's Z axis accelerometer channel was monitored to determine at which moment the UAV made contact. This was also backed up by using the camera. By checking the colour of the image, if the image had a large content of darkness, it was safe to assume that the light entering the camera was being blocked out by the projection bracket, therefore confirming the perch status. At which point the command for the legs to shut were sent.

6.3.4 Grasp

The grasping of the projection bracket was executed as soon as the perch was confirmed. This ensured that the state of the UAV would not change enough to affect the grasp. As the gripper program was already functional and tested to a high level or reliability, the first gripper shut command was successful and the

Figure 6.23 - The final perched position of the UAV with the gripper shut tight.

UAV was in a state of perching. The only thing left to do was to turn of the motors to conserve power which is why this perching system was created in the first place. This was done through the serial lines to the FCS (see Figure 6.23).

6.4 Analysis of Perch

Trying to manually fly a UAV over a perch site, descend and perch showed exactly how difficult a perching manoeuvre was. The perching process had to be automated to relieve the pilot of this burden and to ensure a safe operation of this manoeuvre. Issues with depth perception became very evident during manual flight which also justified the need to an effective solution. The perching system created here enabled this perch sequence to be automated.

6.4.1 The Perching Hardware

Analysing the individual elements helped breakdown the positives and negatives of each aspect. The optimised hardware developed for the specific task of perching on projection brackets is thought to be as close to the initial design specification as possible. Some unwanted hardware changes were made along the way which did contribute to the increase in mass. However the final

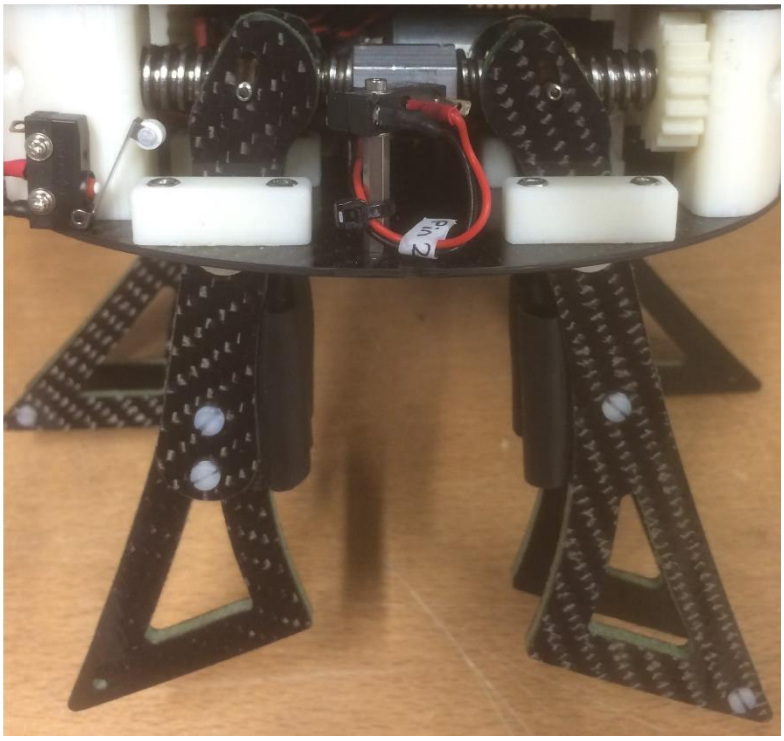

Figure 6.24 - Finalised gripping hardware.

robustness of the system served its purpose well. The concept was created using rapid prototyping, proven during initial testing and then made to be robust enough for multiple perching tests (see Figure 6.24).

The final mass of the additional system which is added to the original mass of the UAV is 760 g. The original system weighed 1480 g with the landing skids at 84.4 g. With the old legs removed and the new perching capable legs attached, the total package weighed 2155.6 g. This was well within the recommended Maximum Take-off Weight (MTOW) of 2480 g.

6.4.2 The Algorithm

The algorithm created here was to serve the purpose of detecting the top of a lighting column's projection bracket with the intention of perching on it. The required skills to compose said algorithm was acquired to specifically complete the task at hand as no other written code could fulfil the required needs. The unique task of trying to perch on top a projection bracket with a multi-rotor had never been attempted until now. The code which was written in Python, used functions within the OpenCV platform which made the vision processing effective and efficient. As the system is capable of detecting the perch site and controlling the UAV, it would appear that the algorithm is suitable. However many improvements can be made. An increase in the image resolution would result in better accuracy which would have to be backed up by a much more powerful microprocessor to run the algorithm. An upgrade in microprocessor would also mean that the video frame rate would increase thus speeding up the perch time. The increase in frame rate would mean that the UAV manoeuvring commands sent via the serial port to the FCS could also be sped up to execute the perch quicker. As this research was dominantly driven by the optimisation of the physical perching element, the algorithm did not have an equal priority in optimisation.

If more time were to be spent developing the search and perch algorithm, it could have been optimised to navigate to the perch site more directly. By detecting the light sensor and descending or climbing to the a pre-set altitude (in this case 1 m above the lantern unit), it could move directly to over the perch site rather than moving over the light sensor first then moving back to the perch position. This could cut the manoeuvre time down significantly. With much

quicker perch mechanism and control algorithm, the optimisation could lead to the UAV swopping onto the projection bracket like a bird would.

6.4.3 The Complete Perching Solution

In the interest of keeping the perching system non reliant on external controls, the option of an on board processor and control system was opted for. This meant that the user only had to initiate the perch and let the perching system take care of the flight control, manoeuvres and the perch itself. With small microprocessors becoming more capable and more affordable, a low cost perching element was produced. The physical hardware worked well with the supporting software which executes the search and perch algorithm. The result is a complete perching UAV which is able to detect, identify and then navigate and perch on a typical street light column's projection bracket (see Figure 6.25).

Figure 6.25 - Final perched position on projection bracket.

6.4.4 Relative Positioning

The requirement for establishing the relative position of the UAV in relation to the projection bracket was to ensure that the UAV could operate independently to any external inputs including GPS. The obvious input from the user eliminates the burden to perch the UAV on top of a projection bracket. Most importantly, the non-reliance on GPS, offers the perching system as a solution to a situation where a UAV has a lack of GPS in the real world. In which case if the UAV loses GPS, it could perch and wait to re-establish GPS communications.

7. Conclusion

This study's objective was to establish whether it was possible to demonstrate a low cost solution to enable UAV perching. This research was driven by the need for UAVs which can hover for extended periods whilst relaying important data. Such scenarios where reconnaissance UAVs need to be positioned with an elevated vantage point over an area of interest. Replacing the existing landing gear of a UAV with a smarter and more capable alternative, resulted in a UAV which can be used in multiple scenarios. The complete standalone perching system developed here demonstrates how useful the ability to perch on top of light column's projections bracket could be. The automatic perch sequence takes distinguishable features of common street furniture and translates them into UAV manoeuvres.

This thesis entails the workings towards achieving a novel approach to perching on projection brackets with the use of a UAV. Unique contributions were made as a result of answering the research questions.

7.1 Answering the Research Questions

What is the most efficient form of perching on existing street furniture?

This question led to the investigation of various types of lighting columns available in the United Kingdom. The outcome shaped the specifications to a perching solution which had to be carefully selected. The selection process consisted of a design generation process, which resulted in 21 different concepts that were then critiqued using a weighted matrix. The top 5 concepts were further analysed and the top scoring concept was turned into a fully functioning prototype. The answer to this question is a perching element which approaches the projection bracket from above to achieve the perch.

How can you recognise the perch site using existing low cost off the shelf sensors?

Whilst exploring the perch site, which in this case was a lighting column's projection bracket, it was identified that a common feature which can be found on most, if not all lantern unit was a light sensor. The light sensor module is what switches the lantern on at dusk and turns it off at dawn. This feature was

the quintessential datum point which was used to navigate about. In order to identify it reliably, a vision system was used. The chosen vision system which needed to be coupled with a processor, needed to be cost effective and readily available. The selected combination was the Raspberry Pi along with the PiCamera. This capable package allowed for the robust detection of the light sensor using OpenCV functions.

How can the UAV know where it is in relation to the perch site without relying on GPS data?

The solution to this question became evident when coding the algorithm. Using the size and position of the detected light sensor, the UAV could determine where it is in relation to the perch site. However this was only a solution to the local positioning of a projection bracket.

7.2 Contributions

This research conducted here resulted in multiple contributions which are all in aid of improving the perching capability of a VTOL UAV through reconfiguration.

1 The design, selection and optimisation of a perching element which can be attached to a UAV.

The essential function of being able to perch is the physical interaction between the UAV and the perch site. The perching element created here demonstrated that it is tolerant enough to allow for slight misalignments which could be caused by external forces or minor over shooting in the perching algorithm. The final gripper like perching system is reconfigurable to various projection profiles and multiple material types.

2 Detailed wind tunnel results of the optimised perching element.

The wind tunnel testing procedure produced interesting data which highlighted patterns which emerged from the results. The analysed data showed how the changes in the UAVs angle on the projection bracket determines how likely the perch is sustainable at various wind speeds. This information can be used to specify the possible operating parameters of the perching element.

3 A set of data points which can predict when the perching element will slip.

This early stage prediction system could prevent the damage of the perched system. By combining the wind tunnel data with a directional airspeed sensor, the UAV could pre-empt the moment the grasp of the perching element would fail. With this failure information, the UAV could either momentarily increase the gripping power or completely release the grip and land on the ground rather than being stranded on the projection bracket due to the wind completely rotating the UAV into an upside down position. However this could be overcome by writing a script which would look out for inverted sensor readings to detect the origination of the UAV before attempting to take off. As the wind tunnel data reinforced the theoretical estimation of failure points, a redesigned perching element could also benefit from the failure prediction method.

4 A method by which the UAV can locate a suitable perch site on a projection bracket of a lighting column.

Created using off the shelf low cost components, the vision based detection system proved to be robust and effective. By instructing the UAV via serial commands, the raspberry pi utilised the search algorithm to manoeuvre the UAV into the ideal perch positon so that the perch part of the algorithm could execute the final command. This recognition package could also be adapted to allow for multiple types of projection brackets which a database could be created. It could also be used by any other VTOL UAV, as long as the vision camera is placed centrally on the UAV. The use of the vision system also resulted in a positioning system where the UAV would know its position in relation to the projection bracket regardless of the GPS data. This meant that if the detection algorithm were to rely on GPS data to perch, and the GPS were to fail, it would result in the possible loss of the UAV. This standalone positioning method ensured a successful perching manoeuvre irrespective of any external input.

7.3 Further Work

This section details what further work could be conducted taking the perching UAV developed in this thesis.

7.3.1 Auto Landing

With multi-rotor UAVs, it is very common to be replacing the batteries to continue with any missions. An auto-land function could be activated by remembering where the last known perchable site is when the UAV needs to land away from the home positon. This could be to either recharge through some means of solar power or inductive charging through the projection bracket's electrical system. But the auto-land function is not limited to just low power mode. It could also be activated if adverse weather conditions are detected or there is a loss of connection to the base station or even GPS to a certain degree. If recharging is not an option, then it could perch safely out of the way of the public where it could either cause damage or be damaged, until the user can safely recover it.

7.3.2 Docking

The idea of having docking stations for fast recharging could be a thing of the future where a UAV is in need of safely charging quickly without the possibility returning back to the home position. Or it could be trickle charging on top of a lighting column awaiting to be deployed for various tasks.

7.3.3 Sagging Perch, Breaking Tree Branch

It was mentioned in the design specification for the UAV to have the ability to have an emergency release protocol. This applied to the physical design of the perching element. However, the software detection was never developed. It could result in a UAV that can actively monitor its positon and detect whether the perched item is still safe enough to be perched on.

7.3.4 Permanent Electro Magnet

During the time of this study, the release of a certain technology could have changed the overall ranking of the weighted matrix. A switchable permanent electro magnet introduces the option to sustain a perch without the need to constantly keep power applied to the magnet. This piece of technology would be have been interesting to investigate further, however it is worth mentioning that it would limit the perch sites to only magnetic surfaces.

7.3.5 Amazon Drone Patent

Finally worth mentioning is the recent patent application by 'Amazon' for a lamp post docking UAV system. With the patent being granted July 12th 2016, it shows that the need for such systems is ever growing (Gentry et al., 2016).

Appendix A

Corus Lampposts

4/5/6 Metre Nominal Height Columns - Post Top/Side Entry

Nominal Height (mm)	Column Reference	Column Type	Shaft Dia. (mm)	Neck Cross Section	Neck Dia. (mm) estimate	Base Dia. (mm)	Planting Depth (mm)
4000	4PT4A	Small Base	76.1	-	-	114.3	800
	4PT5A	Standard Base	76.1		-	139.7	
	4PT6A	Large Base	76.1		-	169.3	
5000	5PT4A	Small Base	76.1	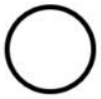	35	114.3	800
	5PT5A	Standard Base	76.1		35	139.7	
	5PT6A	Large Base	76.1		35	168.3	
5000	4PT5A	Standard Base	76.1		50	139.7	800
5000	4PT5A	Standard Base	76.1		50	139.7	800
6000	5S4M	Small Base	76.1	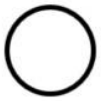	76.1	114.3	800
	5S5M	Standard Base	76.1		76.1	139.7	
	5S6M	Large Base	76.1		76.1	168.3	
6000	6S5M	Standard Base	76.1		76.1	139.7	1000
	6S6M	Large Base	76.1		76.1	168.3	
4700	5PT4L	Small Base	76.1		35	114.3	800
5000	5PTSL	Standard Base	76.1		35	139.7	
5000	5PT6L	Large Base	76.1		35	168.3	

5,6,8,10 and 12 Metre Nominal Height POPLAR/BIRCH - Single Arm & Single Door

Nominal Height (mm)	Column Reference	Column Type	Shaft Dia. (mm)	Projection Cross Section	Neck Dia. (mm) estimate	Base Dia. (mm)	Planting Depth (mm)
5000	5SS (A)	Standard	76.1	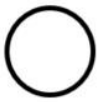	35	139.7	800
6000	6SLT(A)	Light	76.1		35	139.7	1000
	6SO(A)	Quinton	76.1		35	139.7	
	6SS(A)	Standard	76.1		35	139.7	
8000	8SS (A)	Standard	88.9		35	168.3	1200
	8SH (A)	Heavy	114.3		35	168.3	
	8SX (A)	Extra heavy	114.3		35	193.7	
10000	10SQ (A)	Quinton	114.3		35	168.3	1500
	10SH (A)	Heavy	139.7		35	168.3	
	10SX (A)	Extra heavy	139.7		35	193.7	
12000	12SLT (A)	Light	139.7		35	193.7	1700
	12SX (A)	Standard	168.3		35	193.7	
	12SH (A)	Heavy	168.3		35	219.1	
	12SX (A)	Extra heavy	168.3		35	219.1	

6,8,10 and 12 Metre Nominal Height POPLAR/BIRCH - Double Arm & Double Door

Nominal Height (mm)	Column Reference	Column Type	Shaft Dia. (mm)	Projection Cross Section	Neck Dia. (mm) estimate	Base Dia. (mm)	Planting Depth (mm)
6000	6DS (A)	Standard	76.1	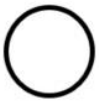	35	168.3	1000
8000	8DS (A)	Standard	88.9		35	168.3	1200
	8DH (A)	Heavy	114.3		35	168.3	
	8DX (A)	Extra heavy	114.3		35	193.7	
10000	10DS (A)	Quinton	114.3		35	168.3	1500
	10DH (A)	Heavy	139.7		35	193.7	
	10DX (A)	Extra heavy	168.3		35	219.1	
12000	12DLT (A)	Light	139.7		35	193.7	1700
	12DS (A)	Standard	168.3		35	193.7	
	12DH (A)	Heavy	168.3		35	219.1	
	12DX (A)	Extra heavy	168.3		35	219.1	

8,10 and 12 Metre Nominal Height ELM - Double Arm - Single Door

Nominal Height (mm)	Column Reference	Column Type	Shaft Dia. (mm)	Projection Cross Section	Neck Dia. (mm) estimate	Base Dia. (mm)	Planting Depth (mm)
8000	8ES (A)	Standard	88.9		35	168.3	1200
	8EH (A)	Heavy	114.3		35	168.3	
	8EX (A)	Extra heavy	114.3		35	193.7	
10000	10ES (A)	Quinton	114.3		35	168.3	1500
	10EH (A)	Heavy	139.7		35	193.7	
	10EX (A)	Extra heavy	168.3		35	219.1	
12000	12ELT (A)	Light	139.7		35	193.7	1700
	12ES (A)	Standard	168.3		35	193.7	
	12EH (A)	Heavy	168.3		35	219.1	
	12EX (A)	Extra heavy	168.3		35	219.1	

Stainton Lampposts

Nominal Height (mm)	Column Reference	Neck Projection (mm)	Neck Deflection Angle (deg)	Neck Cross Section	Neck Dia. (mm)	Shaft Dia. (mm)	Base Dia. (mm)	Planting Depth (mm)
5000	5M Metro Boro	300/500/800	5		76.1	76.1	139.7	800
6000	6M Metro Boro	300/500/800	5		76.1	76.1	139.7	1000
5000	5 SGBS	300/1100/1400	5		33.7	76.1	139.7	800
6000	6 SGBS	300/1100/1400	5		33.7	76.1	139.7	1000
6000	6 SJCS	300/1100/1400	5		42.4	88.9	168.3	1000
8000	8 SJCS	300/1100/1400	5		42.4	88.9	168.3	1200
8000	8 SJES	300/1100/1400	5		42.4 or 60.3	114.3	168.3	1200
8000	8 SKGS	300/1100/1400	5		42.4 or 60.3	139.7	193.7	1500
10000	10 SJES	300/1100/1400	5		42.4 or 60.3	114.3	168.3	1500
10000	10 SKGS	300/1100/1400	5		42.4 or 60.3	139.7	193.7	1500
12000	12 SKGS	300/1100/1400	5		42.4 or 60.3	139.7	193.7	1700
12000	12 SKJA	300/1100/1400	5		42.4 or 60.3	168.3	193.7	1700
15000	15 SKJA	300/1100/1400	5		42.4 or 60.3	168.3	193.7	2000
5000	CC3505	300 - 500	5		33.4	74	150	800
6000	CC3507	300 - 500	5		33.4	74	169	1000
8000	CC3550	500 - 1500	5		60.3	76	249	1200
10000	CC3551	500 - 1500	5		60.3	76	292	1500
8000	CC3509	500 - 1500	5		60.3	76	240	1200
10000	CC3510	500 - 1500	5		60.3	76	270	1500

Appendix B

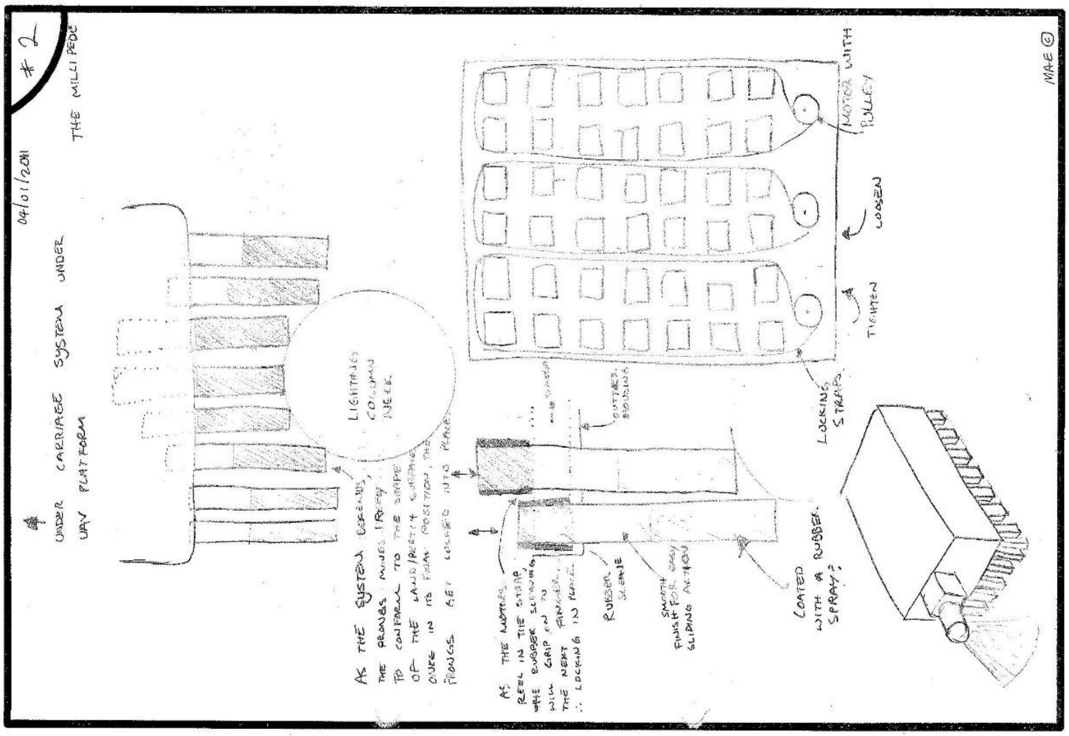
#2
THE MILLIPEDE
04/01/2011
UNDER CARRIAGE SYSTEM UNDER UAV PLATFORM
LIGHTING COLUMN NECK
MOTOR WITH PULLEY
LOOSEN
TIGHTEN
LOCKING STRAPS
COATED WITH A RUBBER SPRAY?
MAE©

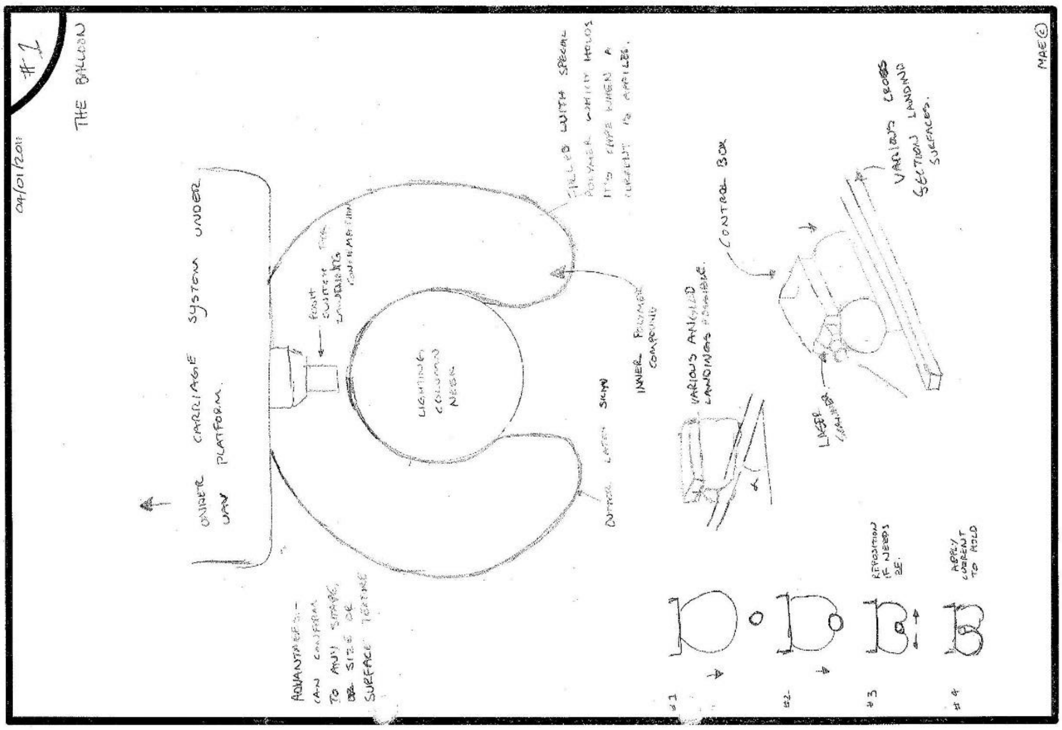
#1
THE BALLOON
04/01/2011
UNDER CARRIAGE SYSTEM UNDER UAV PLATFORM
LIGHTING COLUMN NECK
INNER POLYMER COMPOUND
OUTER LATEX SKIN
CONTROL BOX
MAE©

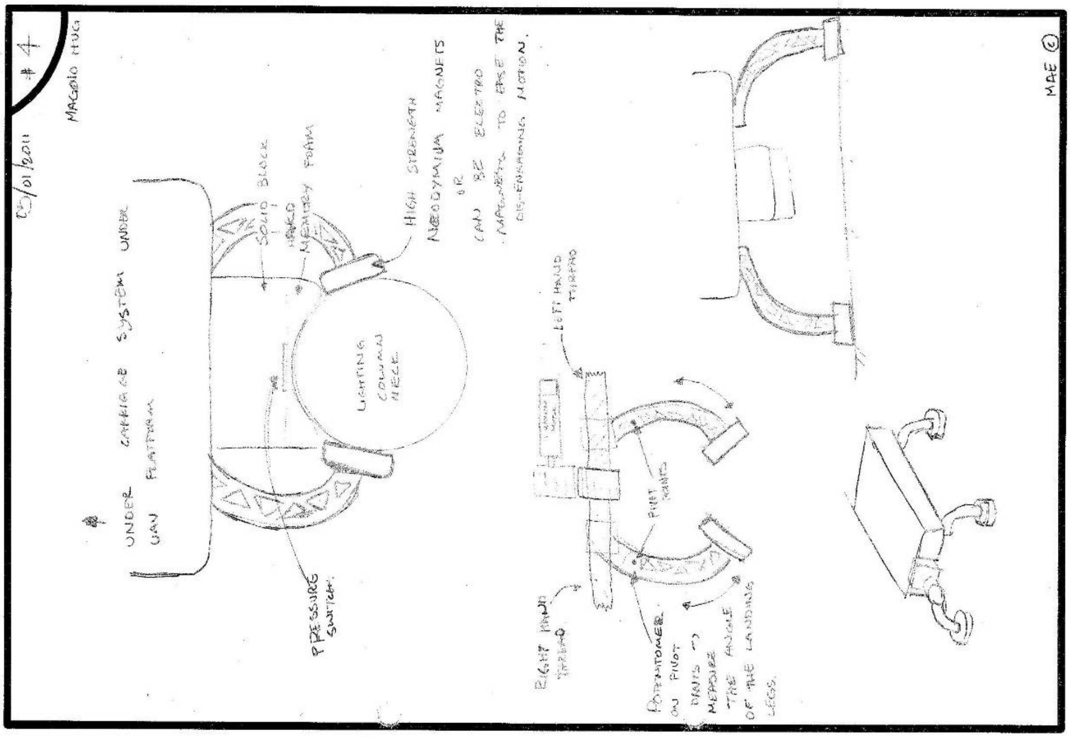
#4
MAGNO HUG
05/01/2011
UNDER CARRIAGE SYSTEM UNDER UAV PLATFORM
LIGHTING COLUMN NECK
PRESSURE SWITCH
HIGH STRENGTH NEODYMIUM MAGNETS
LEFT HAND THREAD
RIGHT HAND THREAD
PIVOT POINTS
MAE ©

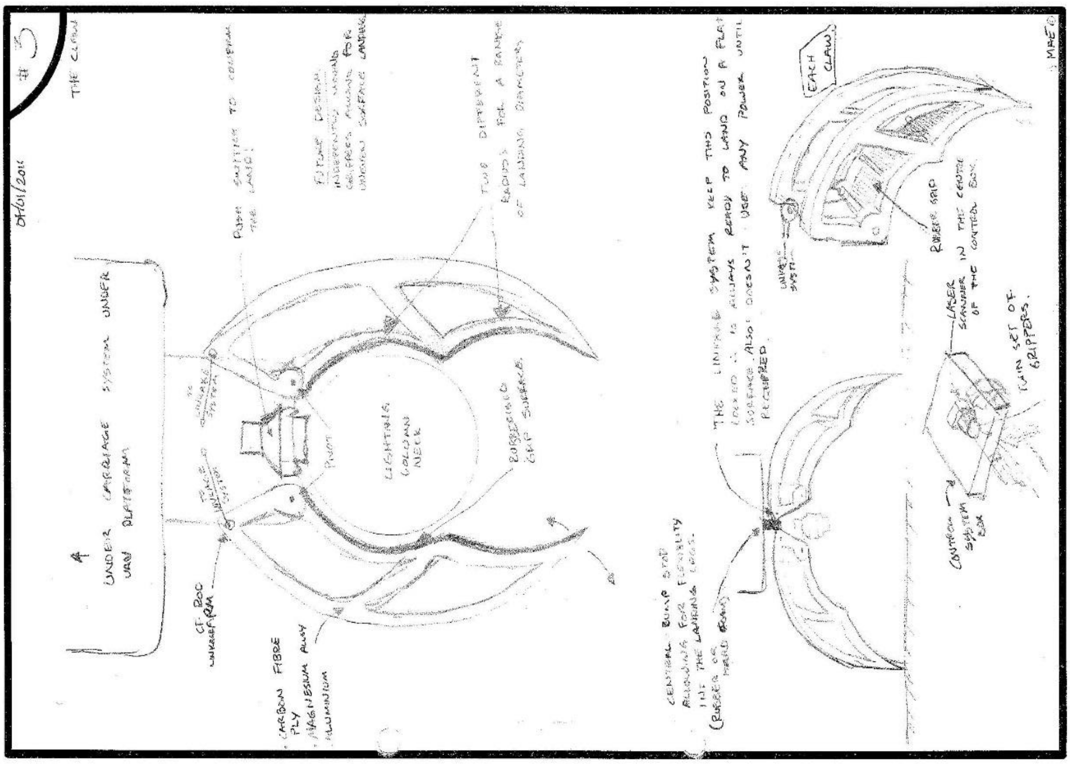
#3
THE CLAW
04/01/2011
UNDER CARRIAGE SYSTEM UNDER UAV PLATFORM
LIGHTING COLUMN NECK
PUSH SWITCH TO CONTROL THE LAND!
TWO DIFFERENT RADIUS FOR A RANGE OF LANDING DIAMETERS
RUBBERISED GRIP SURFACE
CARBON FIBRE PLY
MAGNESIUM ALLOY
ALUMINIUM
CENTRAL BUMP STOP
EACH CLAW
RUBBER GRIP
CONTROL SYSTEM BOX
TWIN SET OF GRIPPERS.
MAE ©

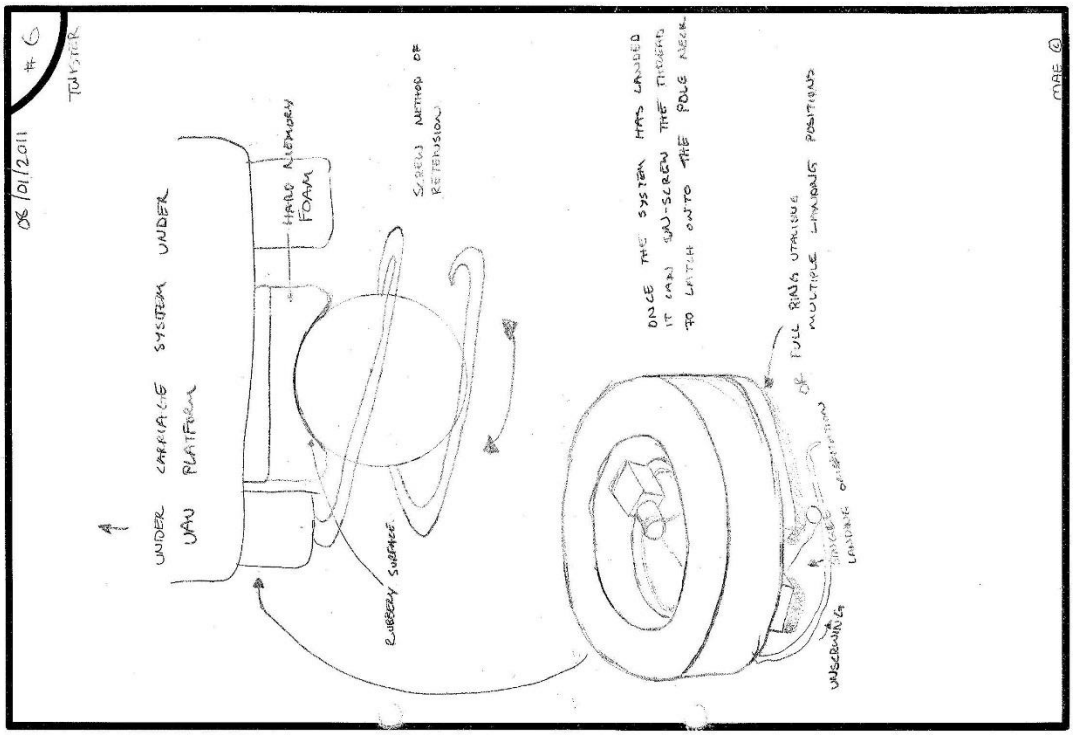
06/01/2011
#6
UNDER CARRIAGE SYSTEM UNDER VAN PLATFORM
HARD ALLEMDEMY FOAM
RUBBERY SURFACE
SCREW METHOD OF RETENSION
ONCE THE SYSTEM HAS LANDED IT CAN GRIP-SCREW THE THREADS TO LATCH ONTO THE POLE AREA.
FULL RING UTILISING MULTIPLE LANDING POSITIONS
MAE ©

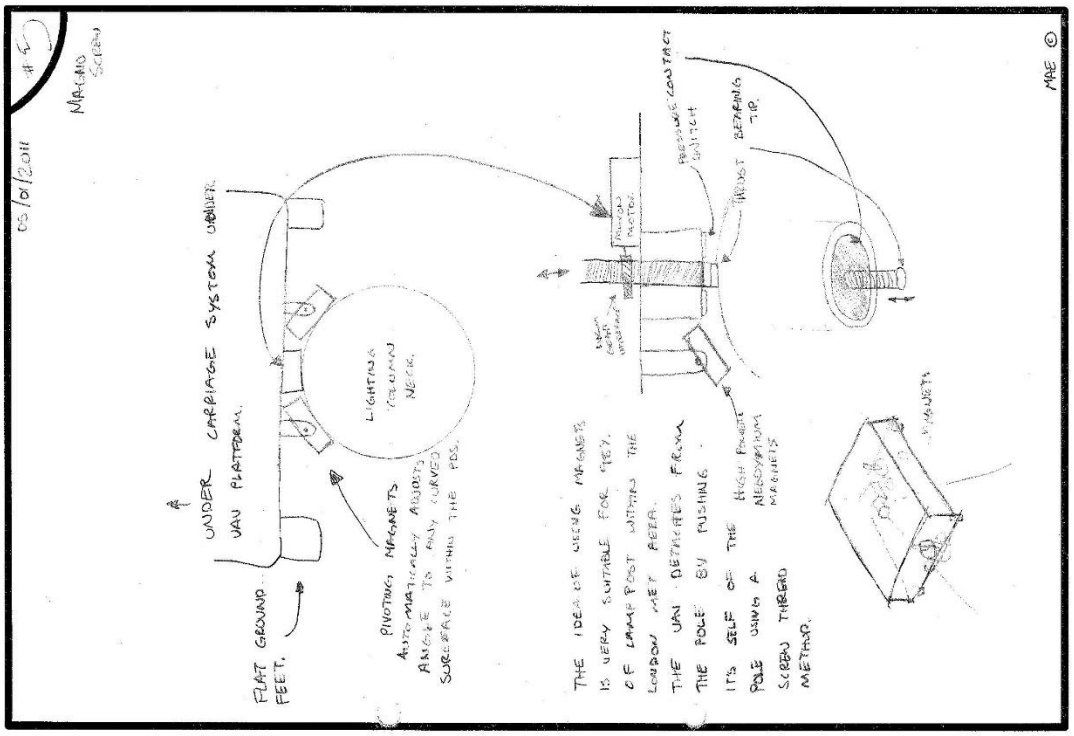
05/01/2011
#5
MAGNO SCREW
UNDER CARRIAGE SYSTEM UNDER VAN PLATFORM.
FLAT GROUND FEET.
PIVOTING ARMS TO AUTOMATICALLY ADJUST ANGLE TO ANY CURVED SURFACE WITHIN THE POLE.
LIGHTING (GROUND NEON)
THE IDEA OF USING MAGNETS IS VERY SUITABLE FOR THEY OF LAMP POST WITHIN THE LONDON AREA.
THE VAN DETACHES FROM THE POLE BY PUSHING IT'S SELF OFF THE POLE USING A SCREW THREAD METHOD.
HIGH POWER NEODYMIUM MAGNETS
PRESSURE CONTACT SWITCH
FRONT BUMPER TIP
MAE ©

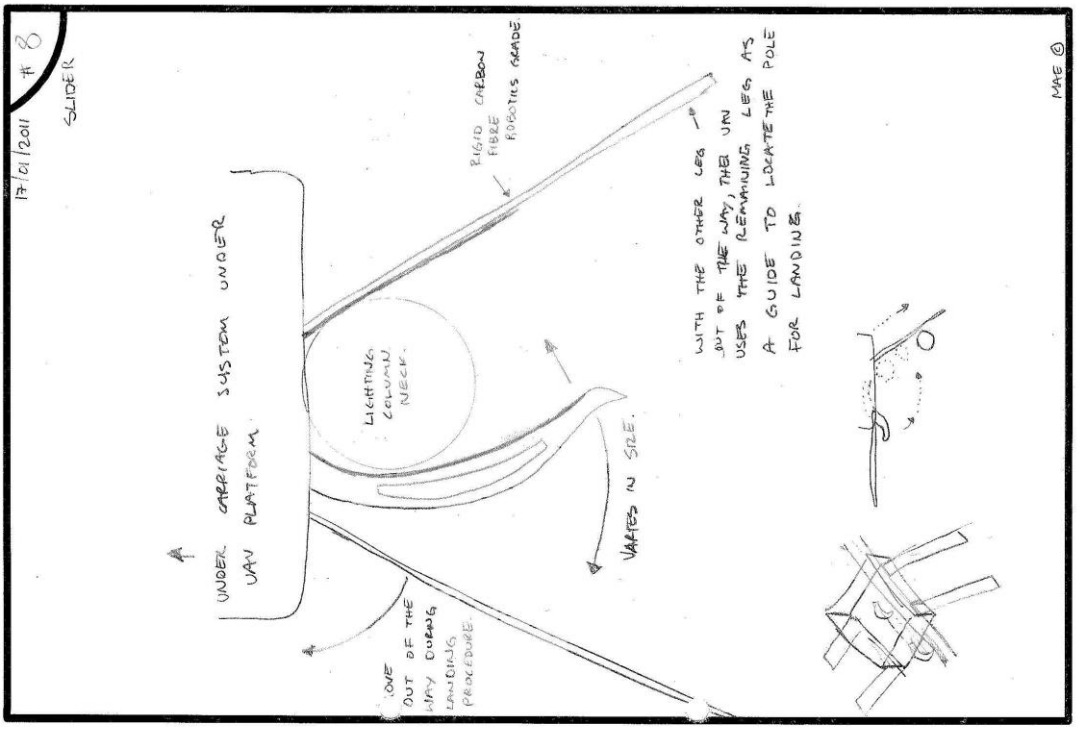
#8
SLIDER
UNDER CARRIAGE SYSTEM UNDER UAV PLATFORM
LIGHTING COLUMN NEEK
RIGID CARBON FIBRE ROBOTICS GRADE
VARIES IN SIZE.
WITH THE OTHER LEG OUT OF THE WAY, THE UAV USES THE REMAINING LEG AS A GUIDE TO LOCATE THE POLE FOR LANDING.
MAE ©

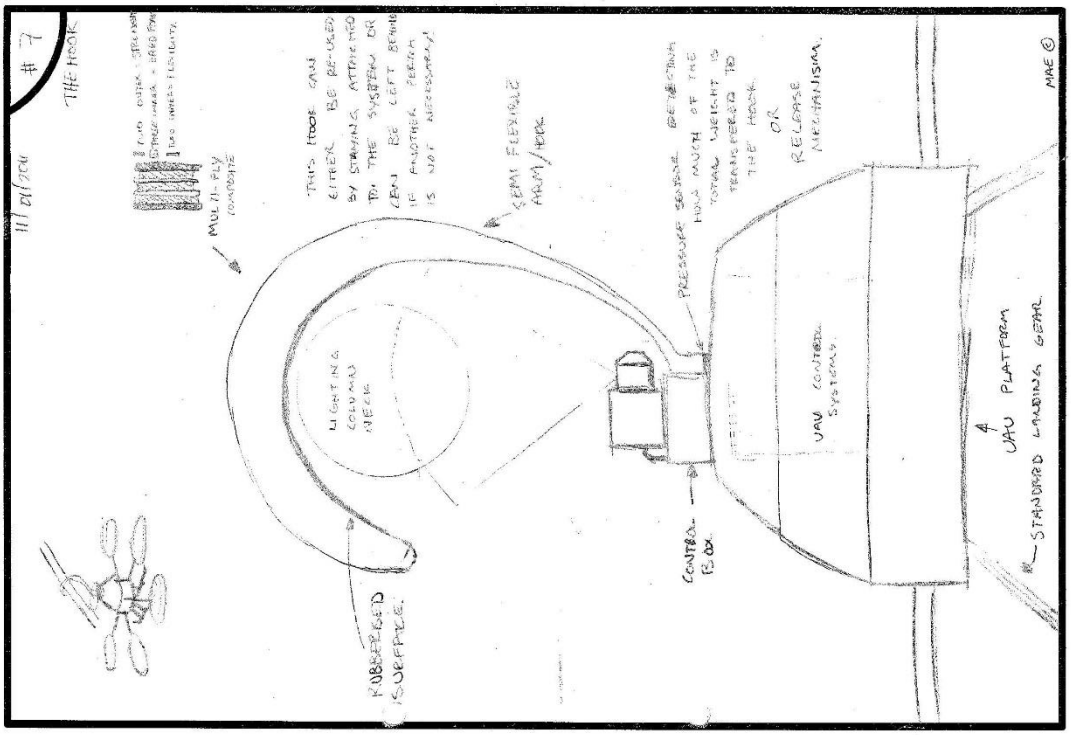
#7
THE HOOK
MULTI-FLY TOMOTOE
LIGHTING COLUMN NECK
SEMI FLEXIBLE ARM/NECK
PRESSURE SENSOR BETWEEN HOOK MOUNT OF THE TOTAL WEIGHT IS TRANSFERED TO THE HOOK
OR
RELEASE MECHANISM.
UAV CONTROL SYSTEMS
UAV PLATFORM
STANDARD LANDING GEAR
MAE ©

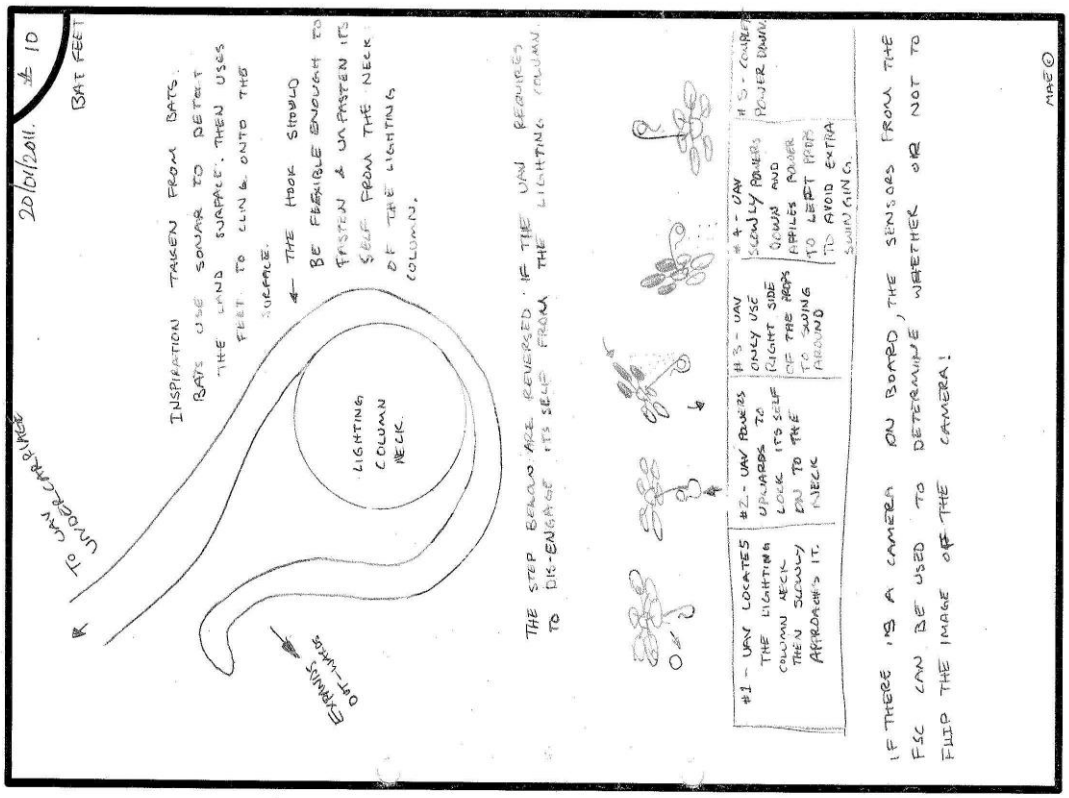
20/04/2011
10
BAT FEET
INSPIRATION TAKEN FROM BATS.
BATS USE SONAR TO DETECT
THE LAND SURFACE. THEN USES
FEET TO CLING ONTO THE
SURFACE.
← THE HOOK SHOULD
BE FLEXIBLE ENOUGH TO
FASTEN & UNFASTEN ITS
SELF FROM THE NECK
OF THE LIGHTING
COLUMN.
LIGHTING COLUMN NECK
THE STEP BELOW ARE REVERSED. IF THE UAV REQUIRED TO DIS-ENGAGE ITS SELF FROM THE LIGHTING COLUMN.
#1 - UAV LOCATES THE LIGHTING COLUMN NECK THEN SLOWLY APPROACHES IT.
#2 - UAV POWERS UP, MAPS TO LOCK ITS SELF ONTO THE NECK
#3 - UAV ONLY USE RIGHT SIDE OF THE PROP TO SWING AROUND
#4 - UAV SLOWLY POWERS DOWN AND APPLIES POWER TO LEFT PROP TO AVOID EXTRA SPINNING.
#5 - COMPLETELY POWER DOWN
IF THERE IS A CAMERA ON BOARD, THE SENSORS FROM THE FSC CAN BE USED TO DETERMINE WHETHER OR NOT TO FLIP THE IMAGE OF THE CAMERA!
MAE ©

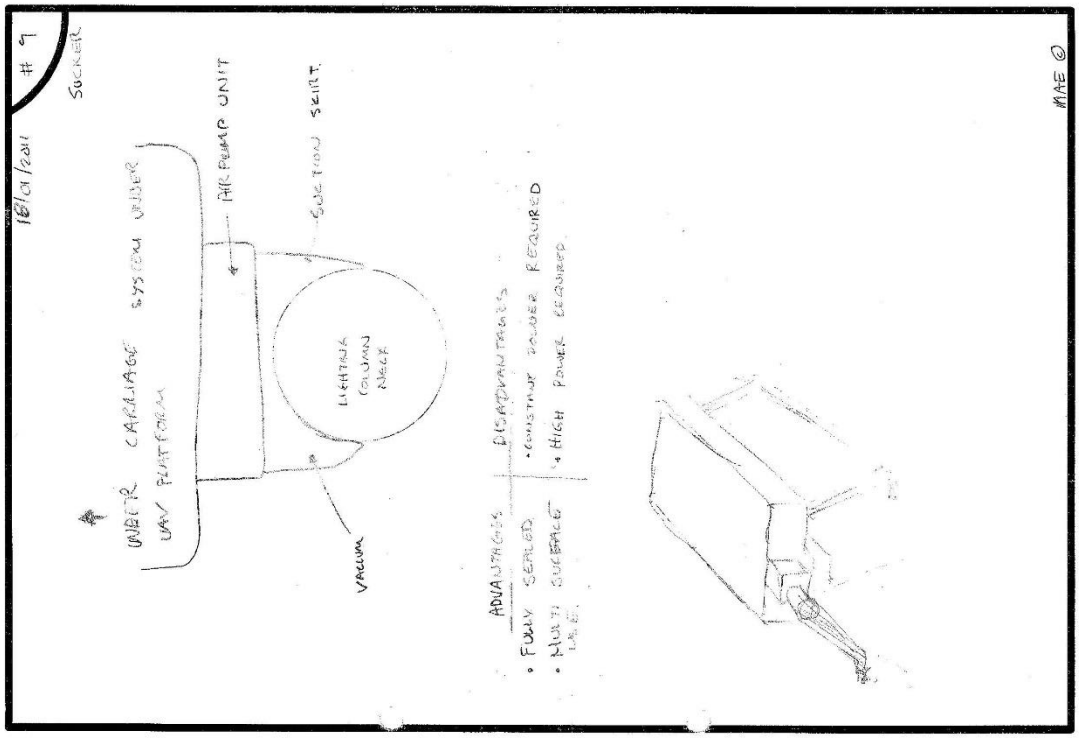
18/04/2011
9
SUCKER
UNDER CARRIAGE SYSTEM UNDER UAV PLATFORM
AIR PUMP UNIT
SUCTION SKIRT
LIGHTING COLUMN NECK
VACUUM
ADVANTAGES
• FULLY SEALED
• MULTI SURFACE
DISADVANTAGES
• CONSTANT POWER REQUIRED
• HIGH POWER REQUIRED
MAE ©

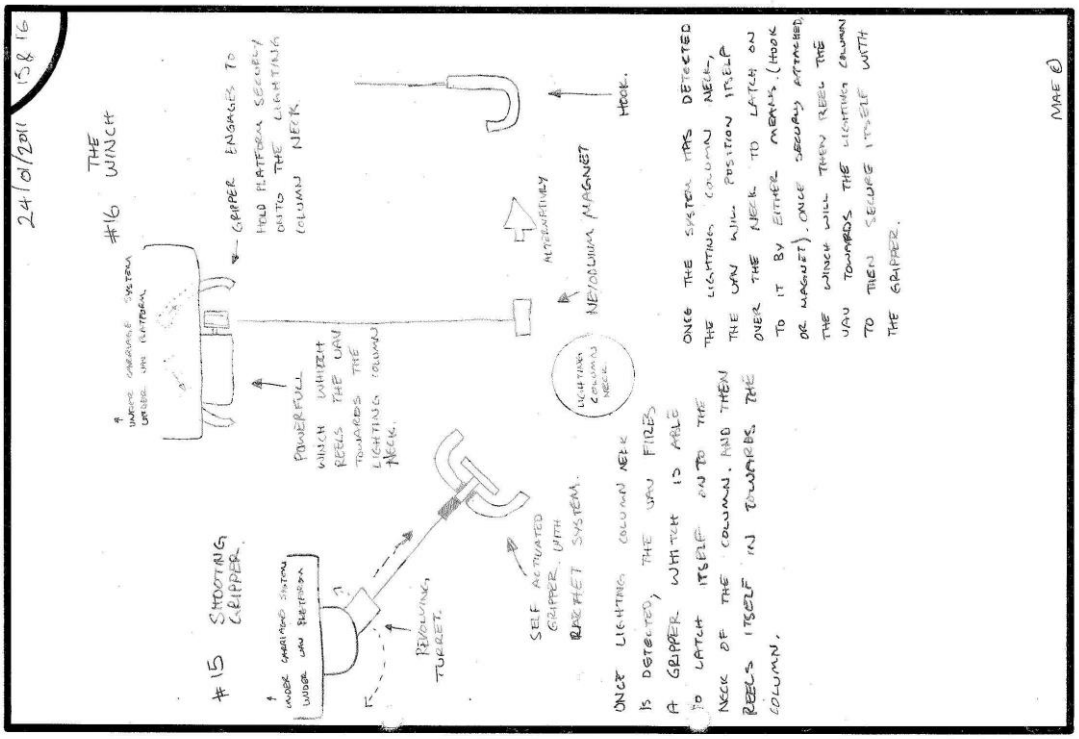
24/01/2011
15 & 16
#15 SHOOTING GRIPPER.
#16 THE WINCH
GRIPPER ENGAGES TO HOLD PLATFORM SECURELY ONTO THE LIGHTING COLUMN NECK.
POWERPULL WHICH INTERNAL REELS THE UAV TOWARDS THE LIGHTING COLUMN NECK.
PIVOTING TURRET.
SELF ACTUATED GRIPPER ARM FEET SYSTEM.
ONCE LIGHTING COLUMN NECK IS DETECTED, THE UAV FIRES A GRIPPER WHICH IS ABLE TO LATCH ITSELF AND TO THE NECK OF THE COLUMN. AND THEN REELS ITSELF IN TOWARDS THE COLUMN.
ONCE THE SYSTEM HAS DETECTED THE LIGHTNING COLUMN NECK, THE UAV WILL POSITION ITSELF OVER THE NECK TO LATCH ON TO IT BY EITHER MEANS, (HOOK OR MAGNET). ONCE SECURELY ATTACHED THE WINCH WILL THEN REEL THE UAV TOWARDS THE LIGHTING COLUMN TO THEN SECURE ITSELF WITH THE GRIPPER.
MAE ©

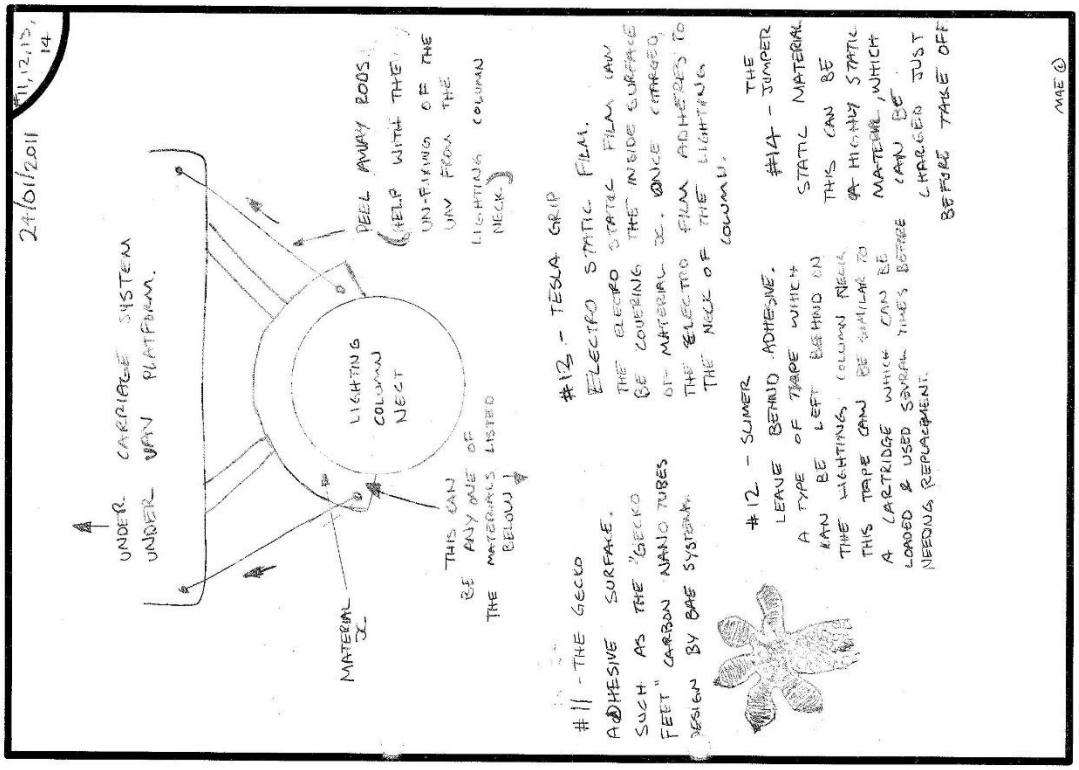
24/01/2011
11, 12, 13, 14
UNDER CARRIAGE SYSTEM
UNDER UAV PLATFORM.
LIGHTING COLUMN NECK
MATERIAL X
THIS CAN BE ANY ONE OF THE MATERIALS LISTED BELOW.)
PEEL AWAY BODS (HELP WITH THE UN-FIXING OF THE UAV FROM THE LIGHTING COLUMN NECK.)
#11 - THE GECKO ADHESIVE SURFACE. SUCH AS THE 'GECKO FEET" CARBON NANO TUBES DESIGN BY BAE SYSTEMS.
#12 - TESLA GRIP ELECTRO STATIC FILM. ELECTRO STATIC FILM CAN BE COVERING THE INSIDE SURFACE OF MATERIAL X. ONCE CHARGED, THE ELECTRO FILM ADHERES TO THE NECK OF THE LIGHTING COLUMN.
#12 - SUMMER LEAVE BEHIND ADHESIVE. A TYPE OF TAPE WHICH CAN BE LEFT BEHIND ON THE LIGHTING COLUMN NECK. THIS TAPE CAN BE SIMILAR TO A CARTRIDGE WHICH CAN BE LOADED & USED SEVERAL TIMES BEFORE NEEDING REPLACEMENT.
#14 - JUMPER STATIC MATERIAL. THIS CAN BE OF HIGHLY STATIC MATERIAL, WHICH CAN BE CHARGED JUST BEFORE TAKE OFF
MAE ©

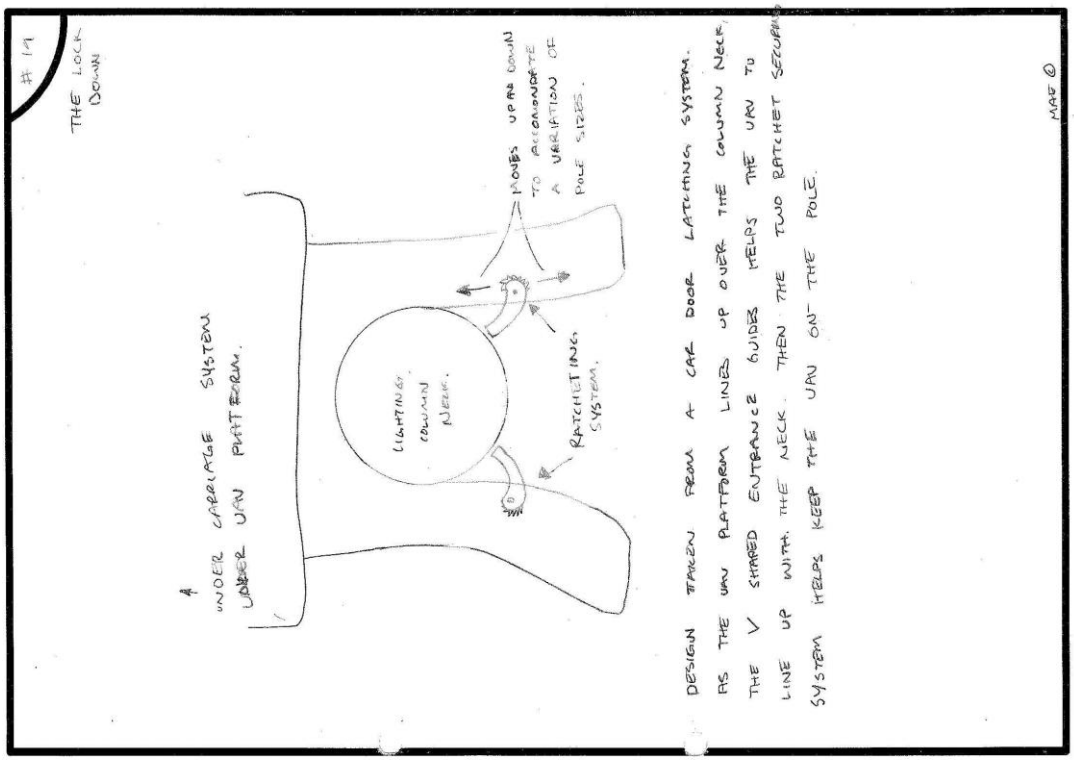
#19
THE LOCK DOWN
UNDER CARRIAGE SYSTEM
LOWER VAN PATTERN.
LIGHTING COLUMN NECK.
RATCHET ING SYSTEM.
MOVES UP AND DOWN TO ACCOMODATE A VARIATION OF POLE SIZES.
DESIGN TAKEN FROM A CAR DOOR LATCHING SYSTEM.
AS THE VAN PLATFORM LINES UP OVER THE COLUMN NECK.
THE V SHAPED ENTRANCE GUIDES HELPS THE VAN TO
LINE UP WITH THE NECK. THEN THE TWO RATCHET SECURING
SYSTEM HELPS KEEP THE VAN ON THE POLE.
MAE ©

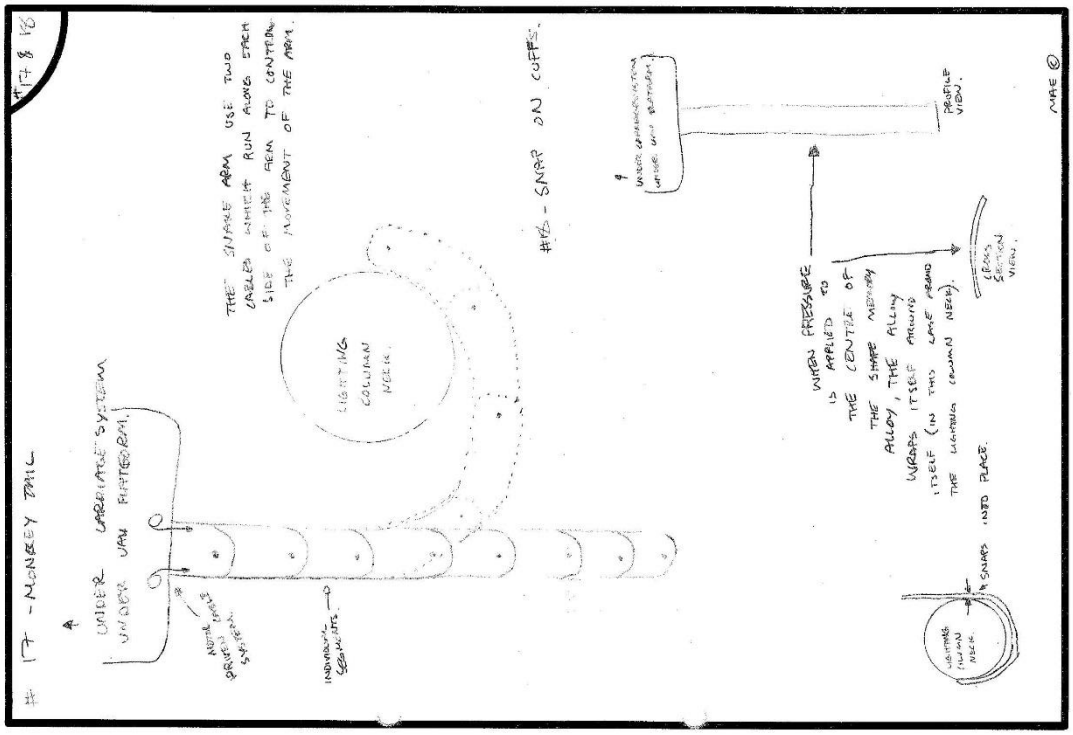
#17 & 18
#17 - MONKEY TAIL
UNDER CARRIAGE SYSTEM
VAN OVER VAN PLATFORM.
LIGHTING COLUMN NECK.
#18 - SNAP ON CUFFS.
WIPER PRESSURE IS APPLIED TO THE CENTRE OF THE SHAPE METAL ALLOY, THE ALLOY WRAPS ITSELF (IN THIS CASE AROUND THE LIGHTING COLUMN NECK).
PROFILE VIEW.
SECTION VIEW.
SNAPS INTO PLACE.
MAE ©

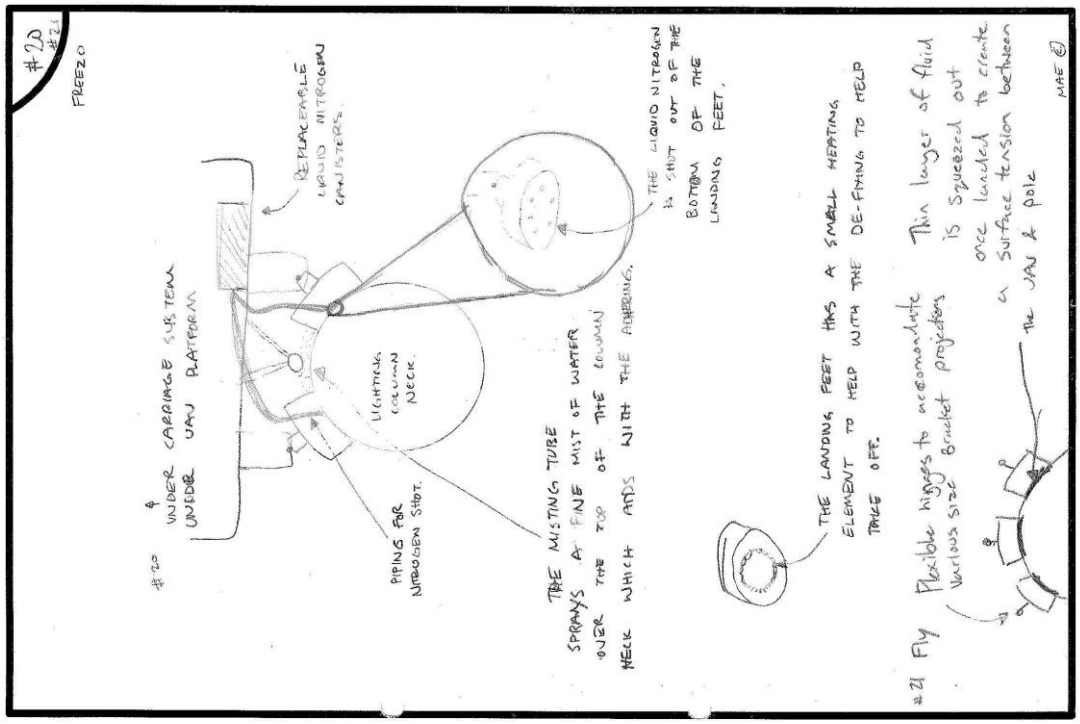
#20
UNDER CARRIAGE SUB TEAM
UNDER UAV PLATFORM
REPLACEABLE LIQUID NITROGEN CANISTERS.
LIGHTING COLUMN NECK.
PIPING FOR NITROGEN SHOT.
THE MISTING TUBE SPRAYS A FINE MIST OF WATER OVER THE TOP OF THE LIGHTING NECK WHICH ACTS WITH THE ADHERING.
THE LIQUID NITROGEN IS SHOT OUT OF THE BOTTOM OF THE LANDING FEET.
THE LANDING FEET HAS A SMALL HEATING ELEMENT TO HELP WITH THE DE-FREEZING TRIGG OFF.
#21 Fly
Flexible hinges to accommodate various size Bracket projections
Thin layer of fluid is squeezed out once landed to create a surface tension between the UAV & pole
#2D
FREEZO
MAE

Appendix C

$$F_d = \tfrac{1}{2}\rho v^2 A C_d$$

Forces acting on UAV during a set wind speed

Symbol	Description	Unit	
F_d	Drag force	N	**3.8832**
ρ	Density of air	Kg/m^3	1.2
v	Airspeed	m/s	12.5
A	Area of object which air is blowing against	m^2	0.03236
C_d	Drag coefficient	Dimensionless	1.28

Turning force due to wind

$$T=rF$$

Symbol	Description	Unit	
T	Torque	Nm	**0.2330**
r	Radius	m	0.06
F	Force	N	3.8832

Force of MK due to gravity

$$F=ma$$

Symbol	Description	Unit	
F	Force	N	**14.715**
m	Mass	Kg	1.5
a	Gravity in this case	m/s	9.81

Turning force due to wind $T=rF$

Symbol	Description	Unit	
T	Torque	Nm	**0.8829**
r	Radius	m	0.06
F	Force	N	14.7150

	Unit	
Total force to overcome at a given wind speed	Nm	**1.1159**

Determining resistive forces $f_r=F_r/N$

Symbol	Description	Unit	
f_r	Coefficient of friction	Dimensionless	0.6
F_r	Resistive force	N	**0.6695**
N	Perpendicular force	N	1.1159

Effects of the lever $F_e=F_l d_l/d_e$

Symbol	Description	Unit	
F_e	Effort force	N	**0.6677**
F_l	Load force	N	0.6695
d_e	Distance to effort from pivot	m	0.02544
d_l	Distance to load from pivot	m	0.02537

Transfering linear to roational force $F_u=F\tan(\alpha+\rho)$

Symbol	Description	Unit	
F_u	Torque	Nm	**0.1235**
F	Linear force	N	0.6677
α	Lead angle	°	10.13
ρ	Coefficient of ABS against ABS	Dimensionless	0.35

Appendix D

Projection Bracket Angle (deg)	UAV Angle (deg)	UAV Failed Wind Speed	Wind Milling Point
0°	40		10
	30	36.8	10
	20	32.2	15
	10	33.9	18
	0	38	
	-10	29.4	11
	-20	19.7	10
	-30	17.7	5
	-40	14.7	6
15°	40	34.4	12
	30	32.8	14
	20	29.4	13
	10	34.5	19
	0	28.6	
	-10	25.1	15
	-20	23.5	10
	-30	17.3	8
	-40	14.5	7
30°	40	33.6	12
	30	35.7	14
	20	36.6	17
	10	32.3	
	0	34.2	
	-10	31.2	17
	-20	27	15
	-30	24.1	9
	-40	23.9	9
45°	40	34.9	10
	30	38	10
	20	42.7	15
	10	45	
	0	34.1	34
	-10	33.6	21
	-20	30.9	11
	-30	26.7	15
	-40	20.3	8
	40		16

60º	30		
	20		
	10		
	0	34.2	
	-10	33.9	27
	-20	32.6	18
	-30	30	14
	-40	26.4	7
75º	40		22
	30		
	20		
	10		
	0		
	-10		
	-20		
	-30		40
	-40	37.9	
90º	40	-	
	30	-	
	20	-	
	10	-	
	0	-	
	-10	-	
	-20	-	
	-30	-	
	-40	-	

Appendix E

Code for Arduino Actuation Board (Arduino, 2015)

```
// pin 3 = retract 1 end stop switch - pulled up 10k
// pin 6 = retract 2 end stop switch - pulled up 10k
// pin A2 = contract 1 end stop switch - pulled up 10k
// pin A3 = contract 2 end stop switch - pulled up 10k
// pin 5 = signal from Pi - white silicone
// pin 13 = signal from Pi - yellow silicone

#include <PinChangeInt.h>
//#include <PinChangeIntConfig.h>
#include <TimerOne.h>

#define NO_PORTB_PINCHANGES //PinChangeInt setup
#define NO_PORTC_PINCHANGES //only port D pinchanges (see: http://playground.arduino.cc/Learning/Pins)
#define PIN_COUNT 1    //number of channels attached to the reciver
#define MAX_PIN_CHANGE_PINS PIN_COUNT

#define RC_RD 5
byte pin = RC_RD;
unsigned int time = 0;

byte state=0;
byte burp=0;    // a counter to see how many times the int has executed
byte cmd=0;     // a place to put our serial data
byte i=0;       // global counter for tracking what pin we are on

int STBY = 4; //standby
//Motor A
int PWMA = 11; //Speed control
int AIN1 = 2; //Direction
int AIN2 = 12; //Direction

//Motor B
int PWMB = 10; //Speed control
int BIN1 = 8; //Direction
int BIN2 = 7; //Direction

int Moto1Curr_Pin = A0;
int Moto2Curr_Pin = A1;
long Moto1Curr = 0;
long Moto2Curr = 0;
long Moto1CurrDiv = 0;
long Moto2CurrDiv = 0;

int indexM = 0;
int buffer = 100;
int bufferArray1[101];
int bufferArray2[101];
int overshoot = 20000;
```

```
int RetractCurrThr = 700; //Motor 1 //Retract current number
int ContractCurrThr = 700; //Motor 1 //Contract current number

int RetractCurrThr2 = 700; //Motor 2 //Retract current number
int ContractCurrThr2 = 700; //Motor 2 //Contract current number

byte switchStateRetracting = 0;
byte switchStateContracting = 0;

void setup() {

  Serial.begin(115200);
  for (int i=0; i <= buffer; i++){
    bufferArray1[i] = overshoot;
    bufferArray2[i] = overshoot;

//      Serial.print("index: "); // Serial commands used to analyse code during
development
//    Serial.print(i,DEC);
//    Serial.print("\t");
//    Serial.print("Motor Array 1: ");
//    Serial.print(bufferArray1[i]);
//    Serial.print("\t");
//    Serial.print("Motor Array 2: ");
//    Serial.print(bufferArray2[i]);
//    Serial.println();
  }

 delay(2000);
  Timer1.initialize(2200);    //longest pulse in PPM is usally 2.1 milliseconds,
  Timer1.stop();              //stop the counter
  iiiii

  pinMode(pin, INPUT);     //set the pin to input
  digitalWrite(pin, HIGH); //use the internal pullup resistor
  PCintPort::attachInterrupt(pin, rise,RISING); // attach a PinChange Interrupt to
our first pin

  pinMode(STBY, OUTPUT);

  pinMode(PWMA, OUTPUT);
  pinMode(AIN1, OUTPUT);
  pinMode(AIN2, OUTPUT);

  pinMode(PWMB, OUTPUT);
  pinMode(BIN1, OUTPUT);
  pinMode(BIN2, OUTPUT);

}

void loop() {
  if (time > 1600 && time < 2400){
```

```
    if (Moto1Curr < ContractCurrThr){
      digitalWrite(AIN1, HIGH);
      digitalWrite(AIN2, HIGH);
      analogWrite(PWMA, 0);
      //Serial.println("Motor Current Reached 1C");
    }
    if (Moto2Curr < ContractCurrThr2){
      digitalWrite(BIN1, HIGH);
      digitalWrite(BIN2, HIGH);
      analogWrite(PWMB, 0);
      //Serial.println("Motor Current Reached 2C");
    }
    if (Moto1Curr > ContractCurrThr && Moto2Curr > ContractCurrThr2 &&
switchStateContracting == 0){
      switchStateContracting = 1;
      //Serial.println("Contracting");
      Contract();
    }
      analogread();

  }
  if (time > 1400 && time < 1600 || time == 0){
    switchStateRetracting = 0;
    switchStateContracting = 0;
    Stop();
    for (int i=0; i <= buffer; i++){
    bufferArray1[i] = overshoot;
    bufferArray2[i] = overshoot;
  }
  }
  if (time > 900 && time < 1300){
    if (Moto1Curr < RetractCurrThr){
      digitalWrite(AIN1, HIGH);
      digitalWrite(AIN2, HIGH);
      analogWrite(PWMA, 0);
      //Serial.println("Motor Current Reached 2R");
    }
    if (Moto2Curr < RetractCurrThr2){
      digitalWrite(BIN1, HIGH);
      digitalWrite(BIN2, HIGH);
      analogWrite(PWMB, 0);
      //Serial.println("Motor Current Reached 2R");
    }
    if (Moto1Curr > RetractCurrThr && Moto2Curr > RetractCurrThr2 &&
switchStateRetracting == 0){
      switchStateRetracting = 1;
      //Serial.println("Retracting");
      Retract();
    }
      analogread();
  }

  cmd=Serial.read();
```

```
  if (cmd=='p')
  {
    Serial.print("time: ");
    Serial.print(time,DEC);
    Serial.print("\t");
    Serial.print("Motor 1: ");
    Serial.print(Moto1Curr);
    Serial.print("\t");
    Serial.print("Motor 2: ");
    Serial.print(Moto2Curr);
    Serial.println();
  }
 if (cmd=='o')
  {
    for (int i=0; i <= buffer; i++){
    Serial.print("index: ");
    Serial.print(i,DEC);
    Serial.print("\t");
    Serial.print("Motor Array 1: ");
    Serial.print(bufferArray1[i]);
    Serial.print("\t");
    Serial.print("Motor Array 2: ");
    Serial.print(bufferArray2[i]);
    Serial.println();
    }
    Serial.print("Motor current 1: ");
    Serial.print(Moto1Curr);
    Serial.print("\t");
    Serial.print("Motor current 2: ");
    Serial.print(Moto2Curr);
    Serial.println();
  }
  cmd=0;
  switch (state)
  {
  case RISING: //we have just seen a rising edge
    PCintPort::detachInterrupt(pin);
    PCintPort::attachInterrupt(pin, fall, FALLING); //attach the falling end
    state=255;
    break;
  case FALLING: //we just saw a falling edge
    PCintPort::detachInterrupt(pin);
    PCintPort::attachInterrupt(pin, rise,RISING);
    state=255;
    break;
  }
}

void rise()
{
  Timer1.restart();        //set our stopwatch to 0
  Timer1.start();           //and start it up
  state=RISING;
```

```
  //  Serial.print('r');
  burp++;
}

void fall()       //on the falling edge of the signal
{
  state=FALLING;
  time=readTimer1();    // read the time since timer1 was restarted
  //  time[i]=Timer1.read();    // The function below has been ported into the
  // the latest TimerOne class, if you have the
  // new Timer1 lib you can use this line instead
  Timer1.stop();
  //  Serial.print('f');
}

unsigned long readTimer1()      //returns the value of the timer in microseconds
{                               //remember phase and freq. correct mode counts
  //up to ICR1 then down again
  unsigned int tmp=TCNT1;
  char scale=0;
  switch (Timer1.clockSelectBits)
  {
  case 1:// no prescalse
    scale=0;
    break;
  case 2:// x8 prescale
    scale=3;
    break;
  case 3:// x64
    scale=6;
    break;
  case 4:// x256
    scale=8;
    break;
  case 5:// x1024
    scale=10;
    break;
  }
  while (TCNT1==tmp) //if the timer has not ticked yet
  {
    //do nothing -- max delay here is ~1023 cycles
  }
  tmp = (  (TCNT1>tmp) ? (tmp) : (ICR1-TCNT1)+ICR1  );//if we are counting down
add the top value
  //to how far we have counted down
  return ((tmp*1000L)/(F_CPU /1000L))<<scale;
}


void move(int motor, int speed, int direction){
  //Move specific motor at speed and direction
  //motor: 0 for B 1 for A
  //speed: 0 is off, and 255 is full speed
```

```
  //direction: 0 clockwise, 1 counter-clockwise

  digitalWrite(STBY, HIGH); //disable standby

  boolean inPin1 = LOW;
  boolean inPin2 = HIGH;

  if(direction == 1){
    inPin1 = HIGH;
    inPin2 = LOW;
  }

  if(motor == 1){
    digitalWrite(AIN1, inPin1);
    digitalWrite(AIN2, inPin2);
    analogWrite(PWMA, speed);
  }
  else{
    digitalWrite(BIN1, inPin1);
    digitalWrite(BIN2, inPin2);
    analogWrite(PWMB, speed);
  }
}

void stop(){
  //enable standby
  digitalWrite(STBY, LOW);
}

void analogread(){
  bufferArray1[indexM] = analogRead(Moto1Curr_Pin);
  bufferArray2[indexM] = analogRead(Moto2Curr_Pin);
  indexM++;
    for (int i=0; i <= buffer;){
      Moto1CurrDiv = bufferArray1[i]+Moto1CurrDiv;
      Moto2CurrDiv = bufferArray2[i]+Moto2CurrDiv;
      i++;
    }
    Moto1Curr = Moto1CurrDiv/(buffer+1);
    Moto2Curr = Moto2CurrDiv/(buffer+1);
    Moto1CurrDiv = 0;
    Moto2CurrDiv = 0;
    //Serial.print(Moto1Curr);
    //Serial.print("    ");
    //Serial.print(Moto2Curr);
    //Serial.println("");
   if (indexM-1 >= buffer){
    indexM = 0;
   }
}

void Retract(){
  move(1, 255, 1); //motor 2, full speed, Retract
```

```
  move(2, 255, 0); //motor 1, full speed, Retract
}
void Stop(){
  digitalWrite(AIN1, HIGH);
  digitalWrite(AIN2, HIGH);
  analogWrite(PWMA, 0);
  digitalWrite(BIN1, HIGH);
  digitalWrite(BIN2, HIGH);
  analogWrite(PWMB, 0);
  //digitalWrite(STBY, LOW);
}
void Contract(){
  move(1, 255, 0); //motor 2, full speed, Contract
  move(2, 255, 1); //motor 1, full speed, Contract
}


//END OF PROGRAM
```

Appendix F

Detection Program

```
# Improving the Perching Capability of a VTOL UAV through Reconfiguration - UAV Vision Algorithm

# Mehmet Ali Erbil - 2016

# Lamppost detection and navigation

#import the necessary packages

import argparse

import cv2
import time
import numpy as np
from picamera.array
import PiRGBArray
from picamera
import PiCamera
import math

## get camera ready
camera = PiCamera()
camera.resolution = (640,  480)
camera.framerate = 32
raw
Capture = PiRGBArray(camera, size=(640, 480))
time.sleep(0.1)

# warm up camera
while True: # video capture loop

# grab the current  frame and initialise the status text
image = camera.capture(rawCapture, format="bgr", use_video_port=True)
frame = rawCapture.array
status = "No Circles" #update status

#draw x screen line
cv2.line(frame, (0,240), (640,240),(0,0,0), 1)

#draw y screen line
cv2.line(frame, (320,0), (320,480),(0,0,0), 1)

#text 0,0
cv2.putText(frame, ("0,0"), (322, 250), cv2.FONT_HERSHEY_DUPLEX, 0.3, (0,0,0), 1)

#text x
cv2.putText(frame, ("X"), (625, 235), cv2.FONT_HERSHEY_DUPLEX, 0.5, (0,0,0), 1)
```

```
#text y
cv2.putText(frame, ("Y"), (322, 15), cv2.FONT_HERSHEY_DUPLEX, 0.5, (0,0,0), 1)

# convert the frame to grayscale
grey = cv2.cvtColor(frame, cv2.COLOR_BGR2GRAY)

circles = cv2.HoughCircles(grey, cv2.HOUGH_GRADIENT, 1 , 600, param1=19,
param2=20, minRadius=5, maxRadius=40)

#find the circles
for i in circles [0,:]:
cv2.circle(frame, (i[0], i[1]), i[2], (0, 255, 0), 2)

#outer circle
cv2.circle(frame, (i[0], i[1]), 1, (0, 0, 255), 2)
#inner circle
cv2.circle(frame, (320, 240), 30, (0, 0, 0), 1)
#centre zone when the Pi stops sending commands to MK - SafeLandZone
status = "Circle(s) Acquired" #update status

#x position of screen centre
centrex = 320

#y position of screen centre
centrey = 240

Tx = int(i[0]) #convert HoughCircle x into integer
Ty = int(i[1]) #convert HoughCircle y into integer
Tr = int(i[2]) #convert HoughCircle radius into integer

mx = Tx-centrex #x position of each circle in relation to 0,0
my = centrey-Ty #y position of each circle in relation to 0,0
mxf = i[0]-centrex #float version of the x postion for math equations
myf = centrey-i[1] #float version of the y postion for math equations

#split the xyr of each circle into 3 line \n
xyr = "X= %d \nY= %d \nR= %d" % (mx, my, Tr)
y0, dy = (Ty+Tr+15), 15

for i, line in enumerate(xyr.split('\n')): #this tells what to split and how
y = y0 + i*dy

cv2.putText(frame, line, ((Tx-25), y), cv2.FONT_HERSHEY_DUPLEX, 0.4,
(255,255,255), 1)
#xyr text of each circle

cv2.line(frame, (Tx, Ty), (centrex, centrey), (0,0,255), 2) #draw direction line
Stop = 30 #defines the number to stop the UAV
Slow = 75 #defines the number to slow the UAV down

checkx = mx >= -Stop and mx <= Stop #computes if the x of the circle is within
the stop zone
```

```
checky = my >= -Stop and my <= Stop #computes if the y of the circle is within the stop zone
checkslowx = mx >= -Slow and mx <= Slow #computes if the x of the circle is within the stop zone
checkslowy = my >= -Slow and my <= Slow #computes if the y of the circle is within the stop zone


if checkx and checky: #ensures the circle is within the stop zone
UAVcommands = "Signals to UAV = STOP" #display
elif checkslowx and checkslowy: #ensures the circle is within the slow down zone
UAVcommands = "Signals to UAV = Slow Down" #display

else:
UAVcommands = "Signals to UAV = Keep Moving"
#display

#This next section determines what heading needs to be sent to the UAV to get it over the safe zone
if mx >= 0 and my >= 0: # checks x,y of circle (wether it is negative or positive) and determines which quadrant it is in

Q1 = math.degrees(math.atan(mxf/myf))
Theta = "Heading = %d" % Q1
elif mx >= 0 and my <= 0:
Q2 = math.degrees(math.atan(mxf/myf))+180
Theta = "Heading = %d" % Q2
elif mx <= 0 and my <= 0:
Q3 = math.degrees(math.atan(mxf/myf))+180
Theta = "Heading = %d" % Q3
else:
Q4 = math.degrees(math.atan(mxf/myf))+360
Theta = "Heading = %d" % Q4

cv2.putText(frame, status, (10, 20), cv2.FONT_HERSHEY_DUPLEX, 0.5, (0,255,0), 1) #text output
cv2.putText(frame, UAVcommands, (10, 40), cv2.FONT_HERSHEY_DUPLEX, 0.5, (0,255,0), 1) #text output
cv2.putText(frame, Theta, (10, 60), cv2.FONT_HERSHEY_DUPLEX, 0.5, (0,255,0), 1) #text output

## show the frame and kill screen if a key is pressed
cv2.imshow("Final Output", frame)
key = cv2.waitKey(1) & 0xFF
rawCapture.truncate(0)
## if the 'q' key is pressed, stop the loop
if key == ord("q"):

break
# cleanup the camera and close any open windows
cv2.destroyAllWindow
```

References

ACUO. 2016. *What do we call them: UAV, UAS or RPAS?* [Online]. Australia: Australian Certified UAV Operators Inc. . Available: http://www.acuo.org.au/industry-information/terminology/what-do-we-call-them/ [Accessed 04/03/2016 2016].

ANDREA, R. D. 2013. The astounding athletic power of quadcopters. *In:* TED (ed.). Edinburgh, Scotland: Ted.

ARDUINO. 2015. *Example code* [Online]. Available: https://www.arduino.cc/.

ATAIR. 2014. Powered Paraglider UAVs Family of LEAPP™ UAVs.

BI, Y. & DUAN, H. 2013. Implementation of autonomous visual tracking and landing for a low-cost quadrotor. *Optik - International Journal for Light and Electron Optics,* 124**,** 3296-3300.

BLACK, R. 1996. Idea Evaluation. *Design and Manufacture: An Integrated Approach.* Macmillan Pub Ltd.

BLOSCH, M., SCARAMUZZA, D. & SIEGWART, R. Vision based MAV navigation in unknown and unstructured environments. Robotics and Automation (ICRA) 2010 IEEE International Conference, 2010 Anchorage, AK. IEEE, 21-28. 978-1-4244-5038-1.

CETINSOY, E., DIKYAR, S., HANCER, C., ONER, K. T., SIRIMOGLU, E., UNEL, M. & AKSIT, M. F. 2012. Design and construction of a novel quad tilt-wing UAV. *Mechatronics,* 22**,** 723-745.

CONTROZZI, M., CIPRIANI, C. & CARROZZA, M. C. 2010. Miniaturized non-back-drivable mechanism for robotic applications. *Mechanism and Machine Theory,* 45**,** 1395-1406.

CORY, R. E. 2010. *Supermaneuverable Perching.* Doctor of Philosophy PhD Thesis, MIT - Massachusetts Institute of Technology.

CRESWELL, J. W. 2003. *Research Design: Qualitative, Quantitative, and Mixed Methods Approaches,* Thousand Oaks, London, New Delhi, Sage Publications, Inc.

DESBIENS, A. L., ASBECK, A. T. & CUTKOSKY, M. R. 2009. Scansorial Landing and Perching. Springer Berlin Heidelberg.

DJI. 2016. *WooKong-M Waypoint-Auto Takeoff & Landing* [Online]. DJI wiki. Available: http://wiki.dji.com/en/index.php/WooKong-M_Waypoint-Auto_Takeoff_%26_Landing.

DOYLE, C. E., BIRD, J. J., ISOM, T. A. & KALLMAN, J. C. Avian-Inspired Passive Perching Mechanism for Robotic Rotorcraft. Intelligent Robots and Systems, 2011 San Francisco, CA, USA. 4975-4980. 978-1-61284-454-1.

DOYLE, C. E., BIRD, J. J., ISOM, T. A., KALLMAN, J. C. & BAREISS, D. F. 2012. An Avian-Inspired Passive Mechanism for Quadrotor Perching. *Mechatronics* 18**,** 506-517.

DSTL 2012. National PhD Programme 2012: Calling note to Doctoral Training Centres (ESRC) and Centres for Doctoral Training (EPSRC) for 2012. 5.

ERBIL, M. A., PRIOR, S. & KEANE, A. J. 2013. Design Optimisation of a Reconfigurable Perching Element for Vertical Take-Off and Landing Unmanned Aerial Vehicles. *International Journal of Micro Air Vehicles,* 5**,** 207-228.

FAA 2016. FAA Aerospace Forecast. *In:* ROGER, D. S., JR. (ed.). Washington: FAA.

FENSKE, G., ERCK, R., AJAYI, L., ERDEMI, A. & ERYILMAZ, O. 2006. Parasitic Energy Loss Mechanisms Impact on Vehicle System Efficiency. Argonne National Laboratory: The University of Chicage.

FESTO 2014. Bionic Handleing Assistant. Germany: Festo AG & Co. KG.

FINNEGAN, P. 2015. UAV Production Will Total $93 Billion. 12th ed.: Teal Group.
GENCER, C. & GEDIKPINAR, M. 2006. Modeling and Simulation of BLDCM Using MATLAB/SIMULINK. *Journal of Applied Sciences,* 6**,** 688-691.
GENTRY, N. K., HSIEH, R. & NGUYEN, L. K. 2016. *Multi-Use UAV Docking Station Systems and Methods*. US patent application.
GHADIOK, V. 2011. *Autonomous Aerial Manipulation Using a Quadrotor.* MSc Thesis Master of Sciences, Utah State University.
GHADIOK, V., GOLDIN, J. & REN, W. Autonomous Indoor Aerial Gripping Using a Quadrotor. Intelligent Robots and Systems, 2011 San Francisco, CA, USA. IEEE, 4645-4651. 978-1-61284-454-1.
GRABE, V., BULTHOFF, H. H. & GIORDANO, P. R. On-board velocity estimation and closed-loop control of a quadrotor UAV based on optical flow Robotics and Automation (ICRA) 2012 IEEE International Conference, 2012 Saint Paul, MN IEEE, 491-497. 978-1-4673-1403-9
HEHN, M. & ANDREA, R. D. 2015. Real-Time Trajectory Generation for Quadrocopters. *IEEE Transactions on Robotics,* 31**,** 877-892.
HERISSE, B., HAMEL, T., MAHONY, R. & RUSSOTTO, F. X. 2010. The landing problem of a VTOL Unmanned Aerial Vehicle on a moving platform using optical flow. *Ieee/Rsj 2010 International Conference on Intelligent Robots and Systems (Iros 2010)***,** 1600-1605.
HIGHWAYS AGENCY 1999. Trunk Roads and Trunk Road Motorways Inspection and Maintenance of Road Lighting. *Design Manual for Roads and Bridges.*
HIGHWAYS AGENCY 2004. Design of Lighting Columns: Highway structures: Design (substructures and special structures), materials. UK.
HUGHES, W. J. 2013. Global Positioning System (GPS) Standard Positioning Service (SPS) Performance Analysis Report. Washington DC, USA.
HYGOUNENC, E., JUNG, I.-K., SOUERES, P. & LACROIX, S. 2004. The Autonomous Blimp Project of LAAS-CNRS: Achievements in Flight Control and Terrain Mapping. *The International Journal of Robotics Research,* 23**,** 473-511.
KEARNEY, D. & KEARNEY, B. 2014. *Wind Urchin* [Online]. Dublin: Energy Resource Group. Available: http://www.energyresourcegroup.io/windurchin/ 2015].
KOVAC, M., GERMANN, J. & HURZELER, C. 2009. A perching mechanism for micro aerial vehicles. *Journal of Micro-Nano Mechatronics,* 5**,** 77-91.
LEA-COX, J. D., BELAYNEH, B., KIM, J. & MAJSZTRIK, C. 2012. The Value of Weather Data for Daily Nursery Management Decisions. *In:* BACHMAN, G. (ed.) *Engineering, Structures and Innovations.* Arthur R. Outlaw Convention Centre, Mobile, AL, USA: Southern Nursery Association.
LEICA GEOSYSTEMS. 2016. *Our newest take on the classic Leica DISTO™ D2.* [Online]. Leica. Available: http://lasers.leica-geosystems.com/uk/disto/d2 [Accessed Feb 2016 2016].
LEISHMAN, J. G. 2006. *Principles of Helicopter Aerodynamics (Cambridge Aerospace Series),* Cambridge, U.K, Cambridge University Press.
LENGE, S., SUNDERHAUF, N. & PROTZEL, P. 2008. Autonomous Landing for a Multirotor UAV Using Vision. *SIMPAR 2008 Intl. Conf. on SIMULATION, MODELING and PROGRAMMING for AUTONOMOUS ROBOTS* Venice, Italy: 978-88-95872-01-8
LINDSEY, Q., MELLINGER, D. & KUMAR, V. 2012. Construction with quadrotor teams. *Autonomous Robots***,** 13.
MARSHALL, D. 2015. Wind Tunnel Statistics *In:* ERBIL, M. A. (ed.). Southampton University: UoS.
MET OFFICE. 2014. *Energy trends section 7: weather; Average Wind Speed and Deviations from the Long Term Mean* [Online]. Available:

https://www.gov.uk/government/statistical-data-sets/december-2012-energy-trends-weather-data [Accessed September 2014.
MIDDENDORF, W. H. 1986. Optimum Design. *Design of devices and systems.* M. Dekker.
MIKROKOPTER. 2016. *Serial Protocol* [Online]. Available: http://wiki.mikrokopter.de/en/SerialProtocol 2016].
MILLET, P. 2010. *Vision-Based Precision Landings of a Tailsitter UAV.* MSc, Brigham Young University.
MOD 2011. Next Generation Small UAS. *In:* DSTL (ed.). MoD.
MONKMAN, G. J., HESSE, S., STEINMANN, R. & SCHUNK, H. 2006. *Robot Grippers,* Weinheim, Wiley-VCH.
MOORE, J. & TEDRAKE, R. 2009. Powerline Perching with a Fixed-Wing UAV. *American Institute of Aeronautics and Astronautics*.
MUELLER, M. W. & ANDREA, R. D. Stability and control of a quadrocopter despite the complete loss of one, two, or three propellers. IEEE International Conference on Robotics & Automation (ICRA) 2014 Hong Kong, China. IEEE, 45-52 1050-4729
MUELLER, M. W., HAMER, M. & ANDREA, R. D. Fusing ultra-wideband range measurements with accelerometers and rate gyroscopes for quadrocopter state estimation. 2015 IEEE International Conference on Robotics and Automation (ICRA, 2015 Seattle, Washington. IEEE, 1730-1736.
MUIR, A. 2011. *What do you want from motion capture?* [Online]. DIY Drones. Available: http://diydrones.com/profiles/blogs/what-do-you-want-from-motion-capture [Accessed April 2013.
ORDNANCE SURVEY. 2014. *Wind statistics for POSTCODE: WC2N* [Online]. Available: http://www.shop.ordnancesurveyleisure.co.uk/search/series/wc2n/1 [Accessed September 2014.
PAGE, L. 2008. *DARPA seeks 'perch and stare' spy-fly robot* [Online]. The Register. Available: http://www.theregister.co.uk/2008/08/21/darpa_gargoyle_mode/print.html [Accessed Nov 2012.
PAHL, G., BEITZ, W., SCHULZ, H.-J. & JARECKI, U. 2007. Selection and Evaluation Methods. *Engineering Design: A Systematic Approach.* Springer.
PARANJAPE, A., KIM, J. & CHUNG, S.-J. 2012. Closed-Loop Perching of Aerial Robots with Articulated Flapping Wings. *Robotics,* Under Review.
PEPPM. 2013. *Official Vendor Line-Item Price Submission Form - VICON* [Online]. Available: http://www.peppm.org/Products/vicon/price.pdf [Accessed April 2013.
PETER, P. 2012. *Implementing an unmanned aerial vehicle (UAV) for surveillance tasks.* Bachelor Thesis, Saarland University.
PILLAY, P. & RAMU, K. Modeling, Simulation, and Analysis of Permanent-Magnet Motor Drives, Part II: The Brushless DC Motor Drive. IEEE Transactions of Industry Applications, 1989. IEEE, 274-279.
POUNDS, P. E. I. & DOLLAR, A. M. Hovering Stability of helicopters with Elastic Constraints. Systems and Control Conference, 2010 Cambridge, Massachusetts, USA. ASME, 781-788. 978-0-7918-4418-2.
QINETIQ. 2008. *Breakthrough unmanned aerial surveillance technology* [Online]. Available: http://www.qinetiq.com/what/products/Documents/Zephyr-UAV.pdf [Accessed April 2013.
RASPBERRYPI. 2016a. *Python* [Online]. Raspberry Pi Foundation. Available: https://www.raspberrypi.org/documentation/usage/python/ 2016].

RASPBERRYPI. 2016b. *Raspberry Pi 2 Model B* [Online]. Raspberry Pi Foundation. Available: https://www.raspberrypi.org/products/raspberry-pi-2-model-b/ [Accessed 05/04/2016 2016].

REED, J. 2010. *UAV Auto Take-off and Landing Could Save Serious Money* [Online]. Defensetech. Available: http://www.defensetech.org/2010/11/12/uav-auto-take-off-and-landing-could-save-serious-money/ [Accessed Jan 2016 2016].

ROTH, F. L., DRISCOLL, R. L. & HOLT, W. L. 1942. Frictional Properties of Rubber *National Bureau of Standards,* 28**,** 439-462.

ROTORBREEZE 2006. Eagle Eye TR918 Certified. *In:* DEWEY, M. (ed.). Bell Helicopter.

SCILLITOE, A. D. 2011. *Propulsion System Design and Optimsation for the Tumbleweed Novel Autonomous Hexrotor Micro Air Vehicle.* Master of Engineering Master of Engineering, The University of Manchester.

SCOTT, D. 2008. Advanced image processing enables UAVs to fulfil their potential. *Military Embedded Systems.* GE Fanuc Intelligent Platforms.

SOUTHAMPTON, U. O. 2015. *7' x 5' Tunnel* [Online]. University of Southampton. Available: http://www.southampton.ac.uk/windtunnels/facilities/7x5tunnel.page? [Accessed 06/05/2015 2015].

TECQUIPMENT. 2013. *Motor Test Equipment* [Online]. Available: http://www.tecquipment.com/Theory_of_Machines/Motion/TM1018.aspx [Accessed August 2013.

THOMAS, M. 2011. *Euro GPS 'accurate to below 10cm'* [Online]. BBC. Available: http://news.bbc.co.uk/today/hi/today/newsid_9620000/9620148.stm [Accessed April 2013.

TTS 2010. Module 17.1 Fundamentals *Module 17 - Propeller for EASA Part-66.* Milton Keynes, UK: Total Training Support Ltd.

UAVFORGE. 2011. *Competition Course* [Online]. Available: http://www.uavforge.net/instructions.php [Accessed April 2013.

VICON. 2016. *Bonita* [Online]. Vicon Motion Systems Ltd. Available: http://www.vicon.com/products/camera-systems/bonita [Accessed 05/04/2016 2016].

VOYLES, R. & JIANG, G. Hexrotor UAV Platform Enabling Dextrous Interaction with Structures - Preliminary Work. Safety, Security, and Rescue Robotics (SSRR), 2012 Texas.

WENZEL, K. E., ROSSET, P. & ZELL, A. 2010a. Low-Cost Visual Tracking of a Landing Place and Hovering Flight Control with a Microcontroller. *Journal of Intelligent & Robotic Systems,* 57**,** 297-311.

WENZEL, K. E., ROSSET, P. & ZELL, A. 2010b. Low-Cost Visual Tracking of a Landing Place and Hovering Flight Control with a Microcontroller. *Journal of Intelligent and Robotic Systems,* 57**,** 15.

WHITEHOUSE, R. 2010. *Autoland* [Online]. UK: Roke. Available: http://www.roke.co.uk/resources/datasheets/0373-Autoland.pdf [Accessed Nov 2012.

WINDFINDER.COM. 2014. *Windfinder - Wind & weather statistic London City Airport* [Online]. Available: http://www.windfinder.com/windstats/windstatistic_london_city_airport.htm [Accessed May 2014.

WINKVIST, S. & RUSHFORTH, E. 2013. Towards an autonomous indoor aerial inspection vehicle. *Industrial Robot: An International Journal,* 40**,** 196-207.

WOLFGANG, B. 2013. Drone industry gives journalists not-so-subtle hint — don't use the word 'drones'. *In:* DOLAN, C. (ed.). Washington: The Washington Times.

YANG, C., INC., S. T. & MATEO, S. 2014. Mobile positioning via fusion of mixed signals of opportunity. *IEEE Aerospace and Electronic Systems Magazine* 29**,** 34-48.